An-Najah National University

Faculty of Graduate Studies

Vp/Vs Ratio Determined from Local Seismicity along the Dead Sea Transform for the Period 2010-2016

By

Anas Atatri

Supervisor

Prof. Jalal Al Dabbeek

This Thesis is submitted in Partial Fulfillment of the Requirements for the Degree of Master of Urban and Regional Planning Engineering, Faculty of Graduate Studies, An-Najah National University, Nablus-Palestine.

2018

Vp/Vs Ratio Determined from Local Seismicity along the Dead Sea Transform for the Period 2010-2016

By
Anas Atatri

This Thesis was defended successfully on 28/03/2018 and approved by:

Defense Committee Members	**Signature**
Prof. Jalal Al Dabbeek / Supervisor	………..........
Dr. Ayman Mohsen / External Supervisor	……………….
Dr. Radwan El-Kelani / Internal Supervisor	………………

Dedicated

To my mother, father, brothers, sisters and all of my family members.

To the souls of those who departed from us.

Acknowledgments

First of all, I would like to offer my full thanks and deep gratitude to my advisor Prof. Dr. Jallal Al dabeek to providing all his capabilities, patience and special care to finish this research.

I would like to acknowledge and express my cordial thanks to the USAID MERC project M30-023, which was sponsored my project.

I am very grateful to Dr. Radwan El-Kelani for his time, guidance and essence notes, which culminated in the completion of this work.

I would like to express my thanks to Dr. Ayman Mohsen for the support and scientific discussions during the work period on this research.

I provide the special thanks to the professional experts and my colleagues at An-Najah National University, particularly the Urban Planning and Disaster Risk Reduction center and Earth Sciences and Seismic Engineering Unit.

Finally, my thanks to a number of unknowns who contributed and provided their expertise in the study of the Levant region.

الإقرار

أنا الموقع أدناه، مقدم الرسالة التي تحمل العنوان:

Vp/Vs Ratio Determined from Local Seismicity along the Dead Sea Transform for the Period 2010-2016

أقر بأن ما اشتملت عليه هذه الرسالة إنما هو نتاج جهدي الخاص، باستثناء ما تمت الإشارة إليه حيث ما أن هذه الرسالة كاملة، أو أي جزء منها لم يقدم من قبل لنيل أي درجة أو لقب علمي أو بحث لدى أي مؤسسة تعليمية أو بحثية أخرى.

Declaration

The work provided in this thesis, unless otherwise referenced, is the researcher's own work, and has not been submitted elsewhere for any other degree or qualification.

Student's name: **اسم الطالب:**

Signature: **التوقيع:**

Date: **التاريخ:**

Table of Contents

List of Tables

List of Figures

List of Appendix

Vp/Vs Ratio Determined from Local Seismicity along the Dead Sea Transform for the Period 2010-2016

By

Anas Atatri

Supervisor

Prof. Jalal Al Dabbeek

Abstract

The Dead Sea Transform fault system (DST) is the most important tectonic structure in the Levant region as well as in the Middle East. Historically, this system caused destructive earthquakes, causing human and property losses. The systematic monitoring of the local seismicity of the DST started on 1980's, in which many different types of seismic stations are installed on both wings along the DST. These stations are operated by different local and global seismic agencies. These agencies use different parameters to locate the earthquakes. The most important ones are the Vp/Vs ratio and the velocity model, which directly has an effect on the earthquake location accuracy. More than 60 seismic stations are used to study the local seismicity of the DST and the surrounding area during 2010-2016, by using SEISAN software. While, these data are available in the global archive (GEOFON). Very broadband, broadband and short period stations are used. The Vp/Vs ratio is an important factor stressed in this study. About 190 earthquakes are used to estimate this ratio. These earthquakes have five clear of both P and S-arrival times at least. This parameter is 1.44 to 2.14 with an average 1.75 (± 0.08). Different statically analyses are used to

prove the average fitness. While, most of these earthquakes have a correlation coefficient $\geq$ 0.9. Many 1-D velocity models are tested and compared together with the average of the RMS arrival time, horizontal-location error (ERH) and vertical-location error (ERZ). These models are used by different local agencies and one of them is considered as a model reference, created by using seismic refraction method. On the other hand, the reference model is modified (initiative model) to reduce the earthquake location errors. The average of RMS and ERH are 4.1 seconds and 45.59 km, which are the lowest value compared with the tested models. While, the ERZ is about 42.26 km. The epicenter map shows the tectonic structures that mainly cause the earthquakes in the study area. The epicenters, concentrated on the DST in the northern part in the study area, are mostly very shallow earthquake focal depths ($\leq$ 10 km). While, the epicenters distributed on the southern part of the study area with a significant activity along the DST, increase the earthquake focal depth. They are mostly $\leq$ 40 km. Finally, there are additional factors that have an effect on the location accuracy. One of them is the picking error. More than 120 P-wave arrival times in our data are compared with the European-Mediterranean Seismological Centre (EMSC), which include national arrival time picking. Mostly, the difference is (-0.7 to 1) second. While, most of them are (-0.2 to 0.2) second. The second factor is the network(s) geometry. It shows the ERH and ERZ which sharply increase when the azimuth gap is above 180° and 160°, respectively.

Chapter One
General Introduction

1-1. General Background

Earthquakes are the most dangerous natural hazards that cause human and property losses (Maio, et al., 2018). While, an earthquake is defined as an unexpected strong shaking of the earth, typically causing major demolition, because of the movements within the earth's crust, volcanic action or collapse (Zhou, et al., 2017).

The Dead Sea Transform fault system (DST) is the most important tectonic structure in the Levant region as well as in the Middle East, which is considered as the keystone of the tectonic structure in the region. The movements of the DST directly affect the tectonic structures in the region (El-Isa, et al., 2015). On the other hand, these movements are the main reason for the occurrence of the earthquakes in the Levant and the surrounding region.

The main and important task of the seismology is to estimate the earthquake locations (Havskov, et al., 2011). Whereas, earthquakes help to understand the geodynamic evolution (Lucente, et al., 1999). In addition to that, the accurate location of the earthquakes is very meaningful for a wide range of scientific disciplines.

Reliable earthquake locations rely on many factors such as the seismic network geometry, the Vp/Vs ratio, the velocity model, etc... The most important factor is the velocity model. Several types of velocity models can be used to locate the earthquakes. The 1-D model is the most common among seismologists. While, improving the earthquake accuracy needs a suitable velocity model (Havskov, et al., 2011).

In this thesis, we select the DST and adjacent area in the Leaven region to determine the Vp/Vs ratio form the local seismicity during 2010 - 2016. The study area includes several national seismic networks, using different models, such as the Jordanian and Israelian velocity models (Feigin & Shapira, 1994; Al-Tarazi, et al., 2006). In addition to that, (El-Isa Z. , Mechie, et al., 1987) published other model by using the seismic method.

1-2. The objectives of this study

The seismicity map (epicenter map) as well as the earthquake catalogue are priceless. Therefore, the earthquake catalogue must continually updated to specify the seismic source hazard and understand the tectonic evolution.

The main goal of this thesis is determine the Vp/Vs ratio from local seismicity along the DST and the surrounding area during 2010 -2016.

The methodology of this thesis is based on the analysis of the waveforms of the events to estimate the earthquake locations. Therefore, this thesis can be divided into three principle steps. The first step is the data acquisition and archiving. The second step is the development of the necessary parameters to calculate the earthquake locations. These parameters are the Vp/Vs ratio, finding a suitable 1-D velocity model. The third step helps in creating an epicenter map.

1-3. The Outline of this Thesis

In addition to the general introduction in this chapter; chapter two presents the geological and tectonic structures of the study area.

Chapter three discusses the seismological and the related geophysical works in the investigated area.

Chapter four shows the data acquisition and analysis.

Chapter five presents the results of this study in terms of the Vp/Vs ratio, testing and modifying the 1-D velocity models and represents the epicenter map.

The conclusions are presented in chapter six. Additional information about the station coordinates, samples of waveforms, Wadati results, the velocity models, relocation of earthquakes and error picking are provided in the appendices 1 to 6, respectively.

Chapter Two

Geology Setting and Tectonic Structures

2-1. Geological Setting

Active tectonic structures are the main determinant of our specific study area. In addition, these structures represent natural hazards on the Palestinian community. The study area is located between latitudes (27°–35.5°) N and longitude (32°-39°) E, according to the geographic coordinated system.

Most of the geological formations in the Levant region formed during Precambrian to Holocene era (Figure 2-1). The Precambrian formation represents the oldest formation in the Levant, which is exposed in the southern part of the study area. This formation is part of the late Precambrian Arabian–Nubian Shield with crags of different igneous and metamorphic suites (Rashdan, 1988; Jarrar, et al., 2003). The Arabian–Nubian Shield covers a wide area along both sides of the Red Sea and is considered as a northern resumption of the East Africa Orogen (Pan-Africa). The movements of oceanic and back arcs have added a huge of Neoproterozoic juvenile crust (Duyverman, et al., 1982; Stern, 1994; Kröner & Stern, 2004; Stoeser & Frost, 2006; Stern, et al., 2010; Fritz, et al., 2013).

The uncovered Precambrian rocks in the southern part of the study area can be divided into two groups, the older group in Aqaba region and the youngest group in Araba region, in addition a regional unconformity (Saramuj conglomerate) between the two groups. Geological remarks, the Precambrian crags are superimposed by an incomplete Paleozoic stratigraphy with an angular unconformity, which presented the ‘Pre-Saq Unconformity’ (Rashdan, 1988; Ibrahim & McCourt, 1995). The incomplete section of the Paleozoic sequence is a result of mainly three eras of incline, uplift and erosion, which happened in pre-Carboniferous, pre-Triassic and pre-Cretaceous eras (Powell J. , 1989).

The Ram Group mostly consists of intermediate rough grained sandstones and siltstones mixed with marine carbonate/fine-grained sandstone unit. This group was deposited in an alluvial milieu on a very mild slop under a semi-dry to humid climate (Powell J. , 1989; Amireh, et al., 1994; Kolodner, et al., 2006; Powell, et al., 2014).

The Ordovician to Silurian Khreim group mostly consists of fine intermediate grained quartz arenite and micaceous siltstone with subordinate mudstone (Powell J. , 1989). The lower Paleozoic layer is superimposed uncomfortably by a stout series of Cretaceous to Eocene sediments. With reference to, Devonian to Jurassic layers are missing (Bender, 1975; Bender & Khoury, 1981; Powell, et al., 2014).

The Kurnub, the Ajloun and the Belqa Groups are the most important formations in the eastern Dead Sea Transform fault system (DST), which are known within the Cretaceous to Eocene sedimentary (Burdon, 1959; Powell & Moh'd, 2011). The Lower Cretaceous Kurnub group is mostly a thick deposit of the huge white to reddish and formation of intermediate rough grained sandstone. This formation was deposited in a sediment milieu (Bender, 1975; Powell & Moh'd, 2011).

The uncomfortably overlying the Ajlun Group composes of huge Cenomanian and Upper Coniacian shallow carbonated deposited marine. This formation was created to hold cliff to pelagic slop (Radaideh, et al., 2016).

The Balqa Group composes of the youngest mega-series. It was the last marine stage. The chalk, chert and phosphorite mainly form this structure. It is formed in the surface (or) semi-pelagic slop setting (Powell & Moh'd, 2011).

Quaternary deposits are another important formation in our region. It is mainly made up of lacustrine and alluvial sediments, fluviatile sand, gravel, and conglomerate (Bender, 1975).

This section presents the general geological formation in the study area (Figure 2-1). However, the geological formations in the Levant are very complicated on the microscale due to multiple superimposed tectonic systems, which the rocks are influenced by them, including Red Sea evolution, early Miocene rifting and the Turonian to Neogene Syrian Arc deformation (Zain-Eldeen, et al., 2002; Radaideh & Melichar, 2015).

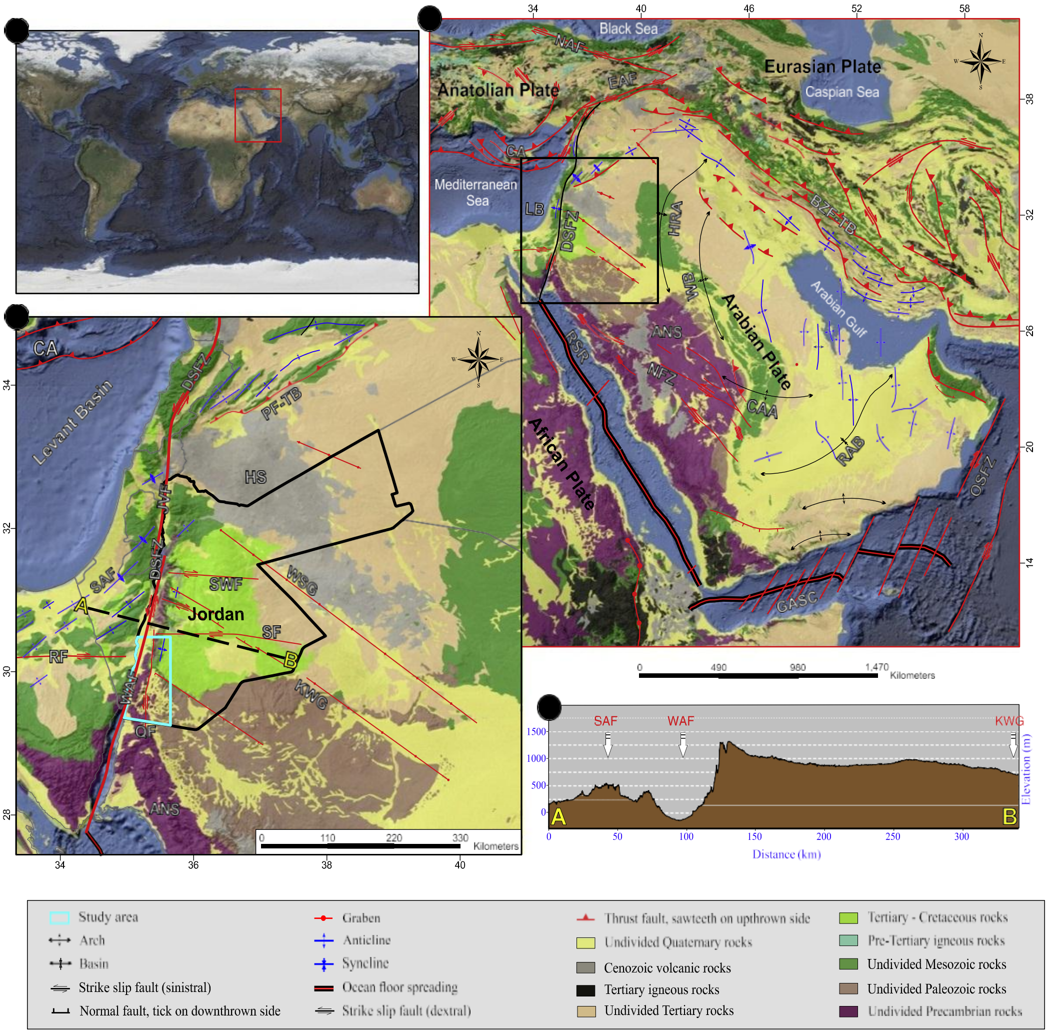

Figure 2-1: The main geological formation in the Levant region. (a) Index map showing the location of EMDR. (b) Generalized geological map of the EMDR complied from (Beicip, 1981; Alavi, 1991; Taymaz, et al., 1991; Fox & Ahlbrandt, 2002; Dilek, 2009). (c) Magnification of black-rectangle area in (b). (d) Vertical change in surface elevation along transect A–B, dashed black line in (c). The USGS provided the geological information of the EMDR. ANS: Arabian-Nubian Shield. BZF-TB: Bitlis-Zagros Fold and Thrust Belt. CA: Cyprian Arc. CAA: Central Arabian Arch. DSFZ: Dead Sea Fault Zone. EAF: East Anatolian Fault. GASC: Gulf Aden Spreading Center. HRA: Ha'il-Rutbah Arch. HS: Harrat Ash Shaam Basalts. JVF: Jordan Valley Fault. KWG: Karak-Wadi Al Fayha Graben. LB: Levant Basin. NAF: North Anatolian Fault. NFZ: Najd Fault Zone. OSFZ: Owen Sheba Fracture Zone. PF-TB: Palmyra Folds and Thrust Belts. QF: Quwayra Fault. RAB: Rub Al Khali Basin. RF: Ramon Fault. RSR: Red Sea Rift. SAF: Syrian Arc Folds. SF: Salwan Fault. SWF: Suwaqa Fault. WAF: Wadi Araba Fault. WB: Widyan Basin. WSG: Wadi Sirhan Graben; After (Radaideh, et al., 2016).

2-2. Tectonic Structures

The Levant region includes three tectonic plates. These plates are the African, Eurasian and Arabian Peninsula plates. While, the DST forms the boundary between the Arabian and Sinai plates as well as the African plate (Quennell A. , 1959; Freund, et al., 1970; Garfunkel , 1981).

The study area has a special tectonic structure. It includes an extremely complex tectonic environment. In addition to that, it allows researchers to understand the fundamental tectonic evolution such as continental rifting, collision, etc. The DST is a keystone of tectonic feature, which controls the tectonic evolution of the Middle East region since the Miocene era.

The DST is the most important geological structure in the Levant, because it controls the regional tectonic structures (Quennell A. , 1958; Dewey & Şengör, 1979; Garfunkel , 1981; Abou Karaki , 1987).

(Quennell A. , 1959), first estimated that the 107 km left lateral movement of the plates bordering the DST since (18-22) Ma years ago with N-NNE direction. It extends over some 1100 km from the Red Sea to the continental collision zone in the Taurus Zagros mountainous belt.

According to (Abou Karaki, 1994), the Arabian and Sinai plates are both moving to the northward within general context of African-Eurasian convergence. Whereas, the Arabian plate is faster than Sinai plate.

The study area includes three major deformational phases: Figures (2-1 and 2) (Quennell A. , 1958; Freund, et al., 1970; Garfunkel , 1981). The phases are as follows:

2-2-1. The Levant Arc Fold Belt

(Krenkel, 1924) pointed that this formation expands from Syria, Palestine, Jordan to Sinai. It has (S) shape. The Arabian plate, which is an anti-clockwise rotation, is the main reason to create this deformation.

This phase represents the oldest tectonic structure in the Levant region. The geological ages of these folds affected by three main phases: Pre-Jurassic, Late Mesozoic-Early Cenozoic era and Late Eocene-Oligocene era (Quennell A. , 1958).

2-2-2. The Erythrean Fault System

This phase consists of northwest-southeast and east-west directions, which are normal and strike-slip faults from the Late Miocene-Early Pliocene era. This formation crosses the DST. It is more recent than the Syrian Arc folds System. In addition to that, the Erythrean system associated with most of the Gulf of Suez faulting and considered as the elementary stage of the sea-floor spreading in the Red Sea (Eyal, et al., 1981; Girdler R. , 1985). During this phase, relief was acquired by fractures and many major structural formations were created, such as Wadi Sirhan rift, the Karak-Fayha fault and Carmel-Wadi el Faria Graben system seems to have connected the transform with the Mediterranean Sea.

2-2-3. The Dead Sea Transform fault system (DST)

It was created in the Cenozoic era as a result of the breaking off of the Arabian plate from the African plate. Geological observations, estimated the cumulative left-lateral movement along the DST, which is about 107 ± 4 km, started since the Post-Cretaceous era (Quennell A. , 1958, 1959, 1984; Freund, et al., 1970; Garfunkel , 1981; Walley , 1988; Girdler R. W., 1990).

The movement of this formation strikes in N-NNE and extends about 1100 km from the Gulf of Aqaba northward along Wadi-Araba, the Dead Sea, the Jordan Valley, Lake Tiberias and central Lebanon arriving to the continental collision zone in the Taurus-Zagros mountainous belt. It mainly has a left-lateral motion with minor components of the extension, compression and up-warping (Quennell A. , 1958, 1959, 1984; Freund, et al., 1970).

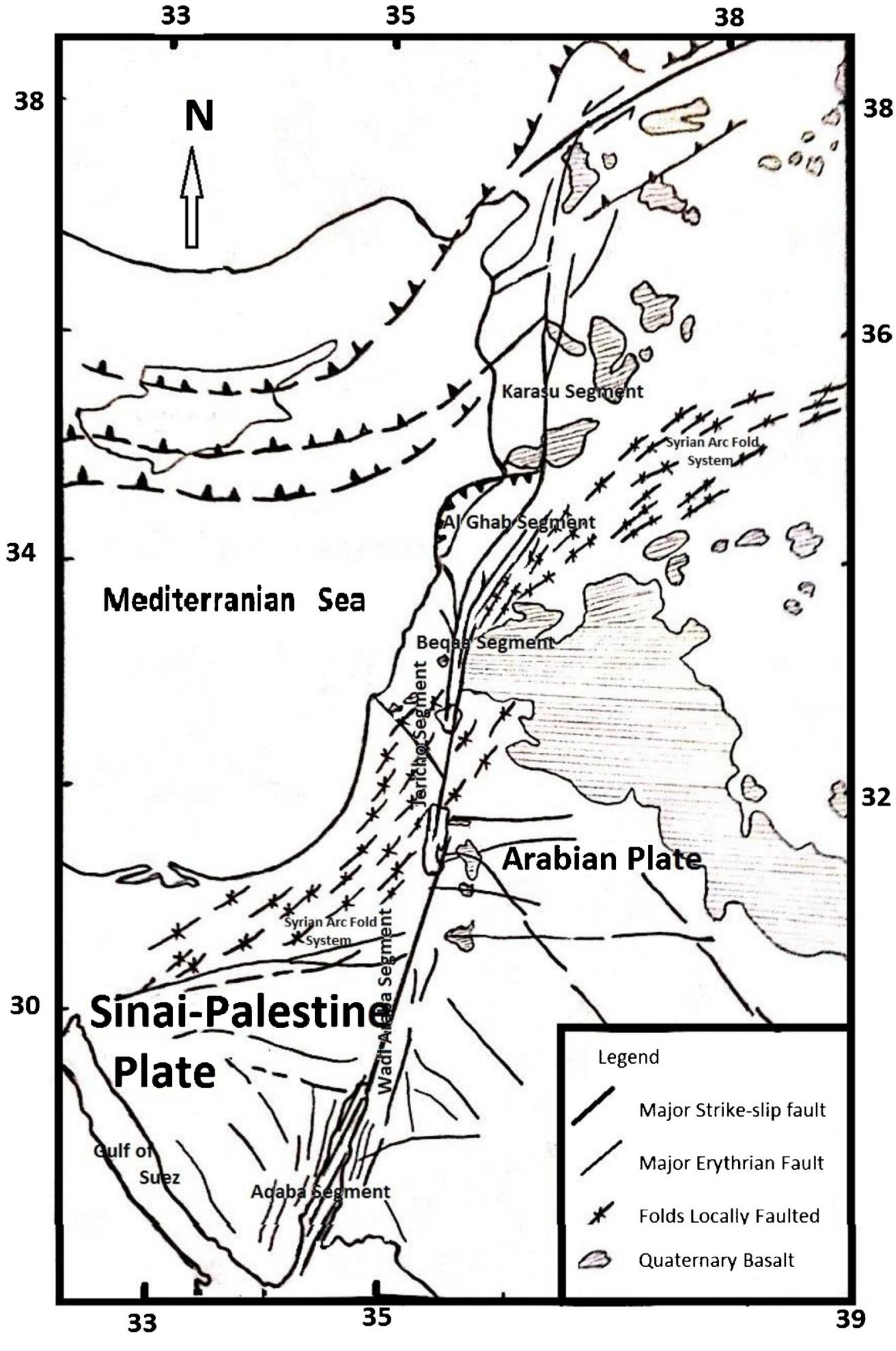

Figure 2-2: Regional tectonics of the study area (Garfunkel , 1981).

Chapter Three

Seismicity, Seismotectonics and Crustal Structure of the Study Area

3-1. Seismicity

The local instrumental seismic activity monitoring in the Dead Sea Transform region started in 1954. Mostly, the earthquakes with magnitude more than 4 were recorded in the Helwan station (Egypt), Kasra (Lebanon) and Istanbul (Turkey) (Garfunkel, et al., 2014).

In Palestine, west of the DST, the monitoring of the local instrumental seismic activity initiated by two seismograph stations installed in Jerusalem (JER) and Safad. In Jordan, east of the DST, a short-period seismograph station has three components, which was installed in the Jordan University area about 10 km NW of Amman in 1981. After that, many seismological stations were installed in the region to monitor the transform seismic activity (Mohsen, 2004; Garfunkel, et al., 2014).

The Dead Sea region is one of the unique geological features that attracts the attention of researchers in the world, where important evidences as well as the earthquake activity have been documented since many centuries. The Islamic and Arabic manuscripts and writings described and illustrated the material damage and featured deformations due to seismic activity. These documents have been used to create catalogues of local seismicity and assign epicentral maps and intensity distribution. As-Soyouti was one of the first scientists who documented the historical earthquakes in the Middle East area during the period from the seventh to eighteenth centuries in his book “Kashf As-Salsala a’n wasf Az-zalzla” (Al-Sa'adani, 1971). Many of the compilations and studies of the seismicity of this region have been done in the last decades (e.g. (Willis , 1928; Abou Karaki , 1987; El-Isa Z. , 1992, 2017; Meghraoui, et al., 2003; Hofstetter, et al., 2007; etc.…).

A summarized account of the most relevant conclusions from these studies is as follows:

3-1-1. Historical Seismicity

A number of destructive earthquakes are documented in our study area during the last twenty centuries (figure 3-1). Significant destruction in archeological sites situated within the studied area has been reported by many studies such as (El-Isa & Mustafa, 1986; Abou Karaki , 1987), with the most noticeable deformation at sites located along the DST and the surrounding area in the Levant region. Many studies and compilations of the historical seismicity in our study area have been accomplished during the last few decades (e.g. (Willis , 1928; Ambraseys N. , 1978; Abou Karaki , 1987; Ambraseys, et al., 1994; Meghraoui, et al., 2003; Sbeinati, et al., 2005)).

The maximum magnitude of these earthquakes within our study area is 7.6 with an average recurrence period of 1,000 years. While, the earthquake magnitudes of $M \geq 6$ and 7 had an average recurrence period of about 21 and 63 years, respectively (El-Isa, et al., 2015).

Some of these earthquakes occurred in the form of sequences and swarms, which were related to possible subsurface volcanic activities (Al-Qaryouti, 1990; El-Isa Z., 2012; El-Isa, et al., 2015). In addition to that, the historical earthquake epicenters have a good correlation with the tectonic structure phases in the Levant region.

Studies of historical seismicity such as (Ambraseys N. , 1978; Abou Karaki, 1987; Ambraseys, et al., 1994; Klinger, et al., 2000) and others proved that the strong earthquakes have relatively large intensities about VI, magnitudes ≥ 6. Whereas, the earthquakes, occurring along the DST affected some or all cities and towns located within the Levant region such as Aqaba, Karak, Hebron, Jerusalem, Jericho, Damascus, Beirut, Hems, other cities and smaller villages. Historically, the Levant region, which has a high population density, suffered from human and property losses due to these earthquakes.

On the other hand, the documents and studies proved some of the earthquakes, (such as the earthquakes occurring in 115, 746, 1033, 1202 and 1759), generated tsunamis along the southern and northern Palestinian and Red Sea coasts. These tsunamis are classified into two kinds: local and moderate ones (Salamon, et al., 2007; Ambraseys & Synolakis, 2010).

3-1-2. The Instrumental Seismicity

The Helwan seismic station (HLW) was the first station installed in our study area in 1899. After that, a number of stations were installed in Ksara (Lebanon) and Istanbul in 1910 and 1935, respectively. While, the

Jerusalem station (JER) was installed in 1954 to monitor the local seismicity of the Dead Sea basin. However, two relatively large systematic seismic networks were installed in 1982-1983 on both sides of the DST. Since that time, these networks have allowed researchers to continuously monitor the DST seismicity (Garfunkel, et al., 2014).

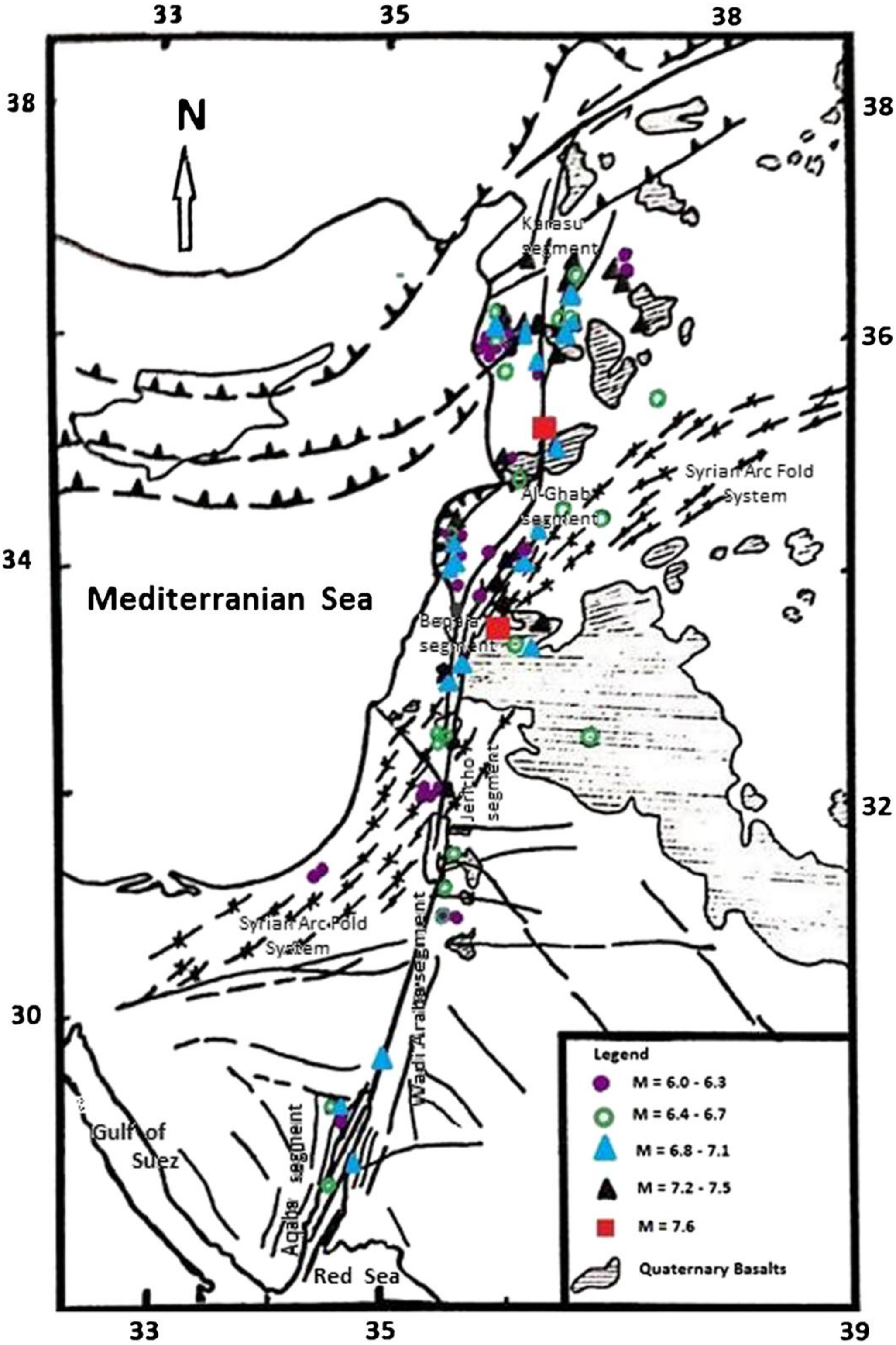

Figure 3-1: The regional tectonic structures of the Dead Sea Transform region and epicentral distribution of 96 historical earthquakes of magnitude ≥ 6 (El-Isa, et al., 2015).

Many efforts have been made on the instrumental seismicity of our investigated area during the last decades, such as (El-Isa & Al Shanti, 1989; Ambraseys, et al., 1994; Klinger, et al., 2000; Hussein, et al., 2008; Salamon, 2010; Meghraoui, 2015; Sawires, et al., 2016; El-Isa Z. , 2017). While, these studies estimated the maximum of the expected magnitude M = 7.5 along the transform (figure 3-2).

Several major earthquakes occurred along the DST region during the instrumental period. The largest recorded earthquake (Dead Sea (Jericho) earthquake and the Gulf of Aqaba earthquake) occurred in 1927 and 1995, respectively. These events had a magnitude of about 6.25 and 7.1, respectively (Ben-Menahem, et al., 1976; Abou Karaki, 1999; Al-Tarazi E., 2000; Zohar & Marco, 2012; Zohar, et al., 2014, El-Isa Z. , 2017).

In addition to strong earthquakes, the swarm and sequences are other important forms of energy release within our study area. The most important of these swarms occurred in 1983, 1990 and 1993. Many of these swarms and sequences are situated close to outcropping Quaternary volcanic regions and thus are properly volcanic-related ones. The major magnitude of these swarms ranged 3.5 to 5.5 (El-Isa, et al., 1984; Al-Amri, et al., 1996; Al-Qaryouti, 2002; Al-Tarazi E. , 2005; Al-Qaryouti & Al-Tarazi, 2007; El-Isa Z. , 2013).

Both of the Levant Arc and Erythrean fault systems had the largest seismically active with magnitude $M \leq 5$. While, the largest earthquakes with magnitude M ≥ 5 have occurred along the DST, which represents the regional major source of seismic hazard (figure 3-2), (El-Isa Z. , 2017).

According to (El-Isa Z. , 2017), the seismicity along the DST has a specific spatial distribution. The focal depth is very shallow. While, the seismic moment calculation improves that the southern part has been nearly 100 times more active than the northern part during the last decades. The Aqaba segment released more than 93% of the seismic energy. The central segment that includes the Deas Sea basin accounts more than 5% of the released energy. While, the northernmost segment (Karasu segment) released less than 1% of the seismic energy.

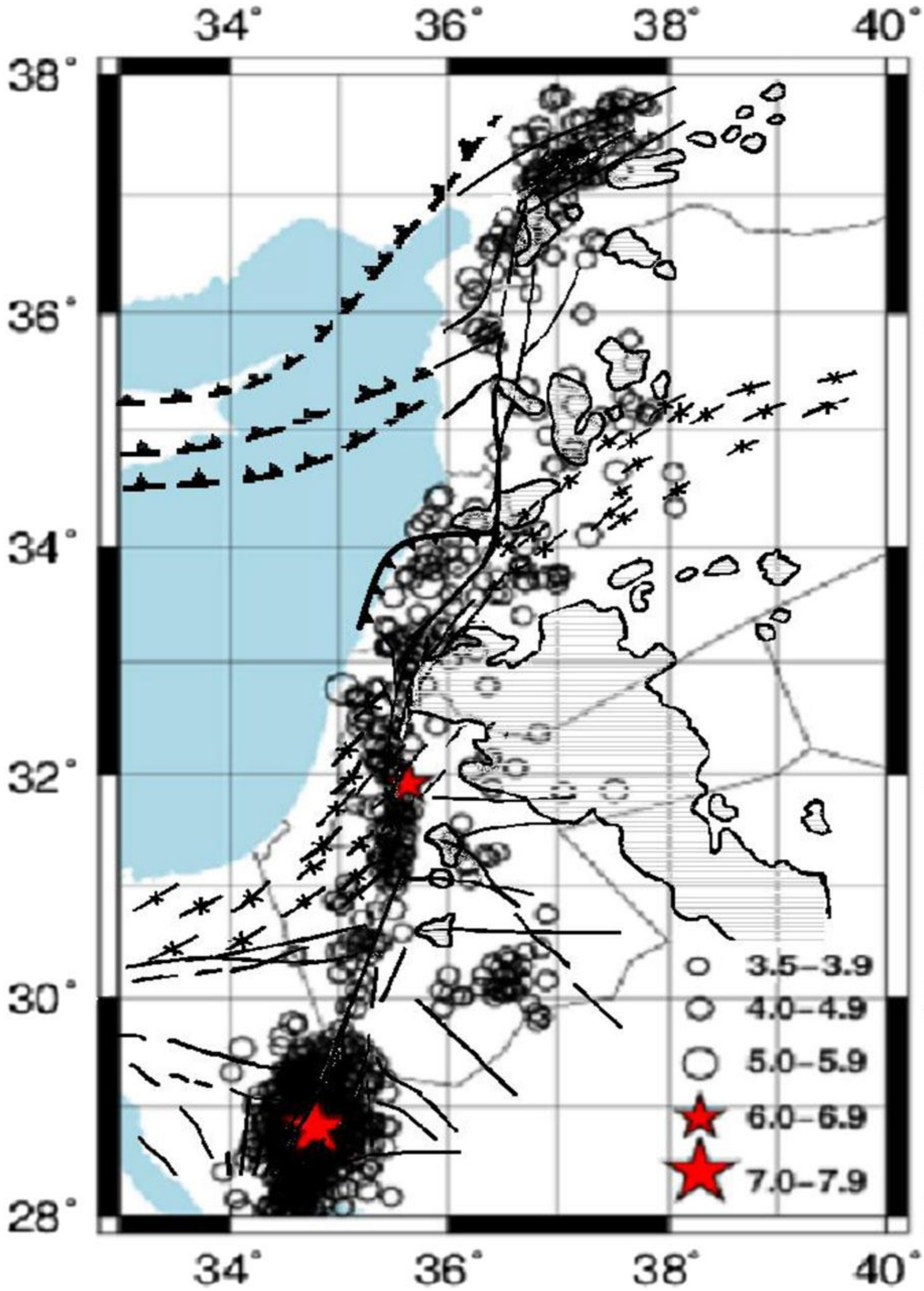

Figure 3-2: The epicentral distribution of the instrumental seismicity of (M ≥ 3.5) that occurred during the period 1900–2014 (El-Isa Z. , 2017).

3-2. Seismotectonics

The DST is the major tectonic structure that separates Arabian and Sinai-Palestine plates. The geological, geophysical and tectonic proofs improve that the Arabian plate is moving generally in the north-northeasterly trend, making a major collision zone in the part of the northern Mediterranean, Turkey and Iran (Quennell A. , 1959; Freund, et al., 1970; Ben-Menahem, et al., 1976; Garfunkel , 1981). According to this movement, shear stress-accumulation will be created, affecting the whole crust and perhaps the upper mantle of the DST region.

Recent geophysical studies improve that faulting along the transform is still active until this time (Quennell A. , 1958, 1984; Freund, et al., 1968; Girdler R. W., 1990; El-Isa, et al., 2015; El-Isa Z. , 2017). The major NW-SE and E-W faults and secondary branching segments (Erythrean deformational phase) (figure 3-1 and 2) related to the major transform; while, crustal masses moving along the transform such as, the Zarqa Mai'n zone in the southeast zone of the Dead Sea, Karak-Fayha fault zone in the southeastern side of the transform and Wadi el Faria-Karmel fault system, which strikes in a NW trend north of the Dead Sea, appears to be high stress accumulation (Ben-Menahem & Aboodi, 1981).

In 1984, (Abou Karaki , 1987) relocated a number of earthquakes in Wadi el Faria-Karmel micro-seismic activity. He remarked that there is a jump in the seismic activity from one segment of the fault to the other. On the other hand, he noted that the distribution of epicenters fits very well with the tectonic structural within the area as concluded from the analysis of the satellite images.

(Garfunkel et al., 1981) studied the active faulting in the region. They noted that the active faults can be divided into two types: the strike-slip faults, which are more obvious, and normal faults. The strike-slip faults are more common features than the normal faults. The length tectonic structures may be linked with most of the seismic activity and the high earthquake magnitudes, taking into consideration most of the relative motion between crustal blocks on both sides of the transform. In addition to that, they estimated that a seismic slip between 0.15 to 0.35 cm per year during the last 1000-1500, while the calculations of the average Pliocene-Pleistocene rate are 0.7-1.0 cm per year.

The average slip of motion along the DST was estimated a 3-7 mm per year by (Freund, et al., 1968). They estimated a 7-10 mm per year of the average slip rate, while a 1.5-3.5 mm pear year of the seismic slip rate estimated during the last 1000-1500 year, which used the historical and instrumental data. (El-Isa & Mustafa, 1986) calculated a 6.4 mm per year of the seismic slip, using pre-historic earthquake information. (Ben-Menahem, 1981) remarked that the Arabia region proves that there is a relatively high seismic slip probably caused by the lowest resistance of the plate motion because of the low rigidity and thin crust. On the other hand, he proposed that the seismic slip only forms a 1/3 of the plate motion significantly, which increases from south to the north of the transform.

In the framework of a general revision of the seismicity of the DST, (Abou Karaki , 1987) noted that the above-mentioned seismic slip rates are too low due to the bad suffer from the mislocation of some of the largest historical and some instrumental earthquakes, which were rather systematically shifted from the transform.

3-3. The Crustal Structure

Two deep seismic sounding experiments have been conducted in the DST region. The first experiment, in 1977, explored the Dead Sea rift proper and its western flank (Ginzburg, et al., 1979; Ginzburg, et al., 1981). The second one was in 1984, explored the eastern flank of the rift (El-Isa Z. , Mechie, et al., 1987). The results of these studies revealed that the crustal structure and its physical properties at the Dead Sea rift and the surrounding area.

In the eastern wing of the transform, the 1984 experiment found that much of the region is underlain by a continental crust. It is 32-35 km thick. It is the normal uppermost mantle with a velocity of 8.0-8.2 km/s. The two transitional zones were recognized throughout the crust of that study area. The first experiment found that the depth was between 18 and 20 km and separated between the upper crust, where the P-velocity is within 5.8-6.5 km/s and the lower crust is around 6.65 km/s (Ginzburg, et al., 1979; Ginzburg, et al., 1981). The other one exists between the lower crust and the uppermost mantle with an average thickness of about 8 km. Under the rift proper, with a possible exception of the southern Gulf of Aqaba, the crust is 33-36 km thick. Towards the southeast of Jordan, the crust thickens increases to more than 37 km in what is probably the transition towards the thick crust of the Arabian Shield (El-Isa Z. , Mechie, et al., 1987).

Under the western wing of the Dead Sea transform, the 1977 experiment found that there is a 35-km thickness of normal continental crust along the transform with a considerable thin to the southward, about 27 km along the Gulf of Aqaba. The thickness of the crust in the region between the Mediterranean, the Dead Sea and the Red Sea is estimated about 40 km. While, the north trend of the crust is about 30-33 km thick. The 1977 experiment data also estimated that there is a maximum sedimentary thickness of about 5.5 km within the transform proper.

Moreover, the west wing of the DST towards the Mediterranean Sea is the transition trend of a thin oceanic crust with gradually thickening sediments, interpreted by the authors (Ginzburg, et al., 1979) as a Pre-Jurassic crustal deformation. A crust-mantle transition zone is about 8 km thick, occurring along the Dead Sea transform, but further west the crust-mantle boundary is about 5 km thick.

(El-Isa Z. , Mechie, et al., 1987) presented a Poisson’s ratio model of the crustal structure using seismic data. The model estimated an average Poisson’s ratio of around 0.25, except beneath the NW zone of Jordan, where the sediments have a high ratio about 0.32. However, the low crust thickness about 20 km depth has high Poisson’s ratio, ranging from 0.29 to 0.32. The highest Poisson’s ratios were interpreted based on the terms of mineralogy as high feldspar and low quartz content in the rocks (e.g.

Gneiss, Amphibolite) of the lower crust or fluid phases in the form of separated penny-shaped inclusions.

(Mohsen, 2004) studied the crust and upper mantle beneath the south of the transform and the surrounding area using receiver function methods. He noted the crustal thickness increases smoothly from about 30 to 34–38 km towards the east across the transform, with significant north–south variations east of the transform. One of the important results of this study is that the internal crustal structure east and west of the transform is different. In addition to these results, he calculated that the V_p/V_s ratio, in which the ratio, ranging from 1.73 to 1.77. While, the ratio increases in the western direction (in the Mediterranean direction).

(El-Kelani, 2005) used the gravity method to study the geological structure beneath the surrounding area of the southern part of the DST. He presented a three-dimensional of the Bouguer anomaly model. The model, constrained by the seismic results, was used to explore the crustal thickness and density distribution beneath the Rift. The interpretation of the negative Bouguer anomalies along the axial portion of the Rift floor are mainly gave rise to deep-seated basins of the light sediments about 10 km thick. The minimum thick of the crust (≤30 km) is located in the western sector at the Mediterranean. While, the maximum thickness of the crust, about 38-42 km, is located in the southeastern of that study area. Considering the thickness and densities of the crust, the model suggests that the transform underlain by a continental crust.

Chapter Four
Data Acquisition and Analysis

4-1. Introduction

This chapter explains the data acquisition and the practical application. It uses different seismic networks, as well as, different seismic station types.

This work aims mainly to determine the Vp/Vs ratio from local seismicity along the DST and surrounding area, where the systematic monitoring in this area started in 1980's. The first two networks installed to monitor the local seismicity along the Transform are the Jordan Seismic Network (JS), operated by Jordan Seismo Obs & Geo Studies / Natural Resources Authority (NRA Jordan) and Israel National Seismic Network (IS), operated by the Geophysical Institute of Israel (GII Israel). Besides these networks, the GEOFON operated by the GEOFON Program (GFZ-Potsdam, Germany) are considered as a global seismic network. In addition to that, two seismic stations (UJAP and SALP) were installed in Palestinian territory, which are considered as a part of the GEOFON network.

SEISAN is the main software package used to read and pick the seismic waveforms. This package includes a large number of programs that are used in seismology, such as HYPOINVERSE. As well as, it is a compatible with the Windows environment. In addition to these features, the program developers provide a large number of converters, which helps to use one database for different programming environments.

4-2. Data selection

4-2-1. Seismic Global and National Networks

Over the past years, the International institutions have been trending to create global seismic waveforms banks, containing earthquakes waveforms. These banks contain data acquisition waveforms from national and global seismic networks. The GEOFON is the global seismological broadband network started since 1993. The GEOFON network is engaged jointly with more than 50 global partners. In 2017, it consisted of 115 seismic stations (Hanka & Kind, 1994; Helmholtz-Zentrum Potsdam, 2017). However, most of these stations installed in the following regions: Europe, the Mediterranean and Indian Ocean (Figure 4-1).

The DST has a special attention from geologists and geophysicists, as well as, the GFZ researchers have revealed that attention. Therefore, the GFZ installed many seismic stations around the Transform, including two seismic stations in Palestinian territory (al-Auja and Salfit) (Figure 4-1). These stations include different types of seismic sensors, especially the broadband type. The GFZ provides online data for the GEOFON stations and a large number of stations for the national networks.

In addition to the GFZ network, two local seismic networks (JS and IS networks), was used to studying the seismicity of the Transform. The (JS) has monitored the local seismicity in the east of the Transform Fault. This network has 19 broadband and short-period seismic stations. The (IS) has monitored the seismicity in the west part of the Transform. The IS consists of 43 broadband seismic stations. The figure (4-2) represents the distribution of the JS and IS seismic stations, which illustrated in this study.

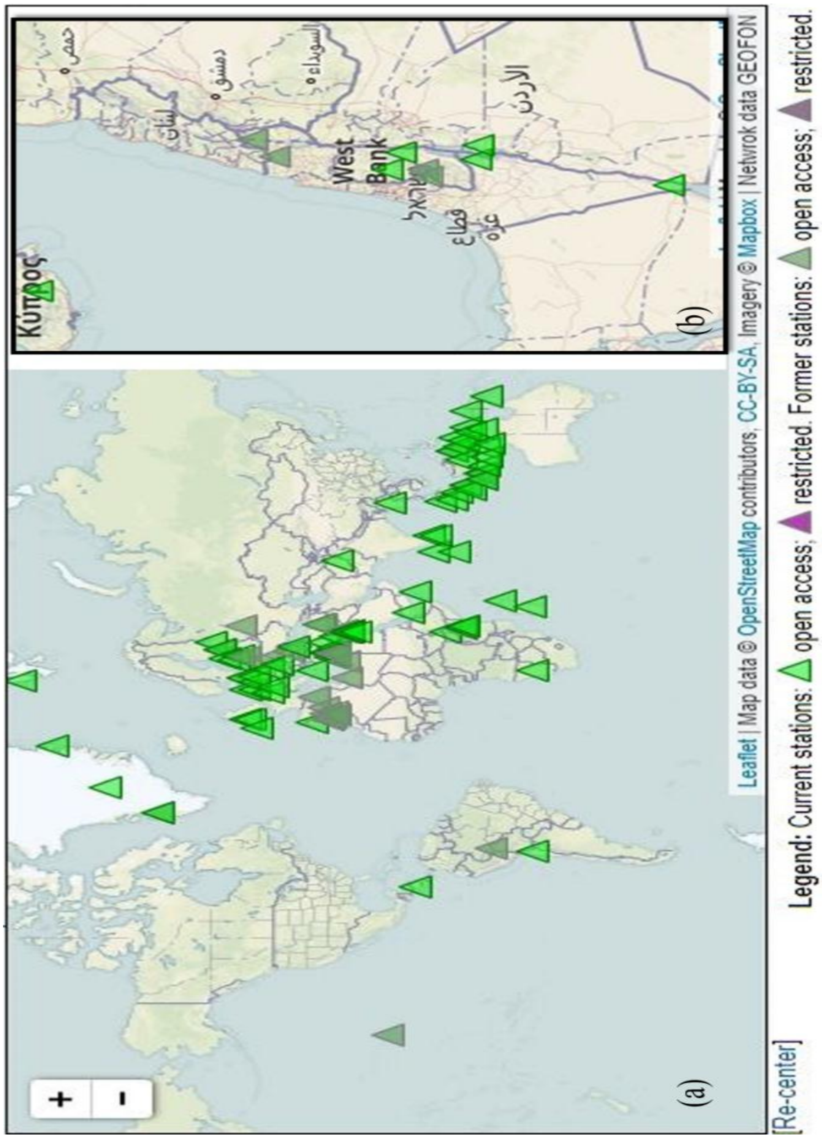

Figure 4-1: (a) The distribution of the GEOFONE (GE) Network Stations and (b) The distribution of GEOFONE Stations along the Dead Sea Transform fault system.

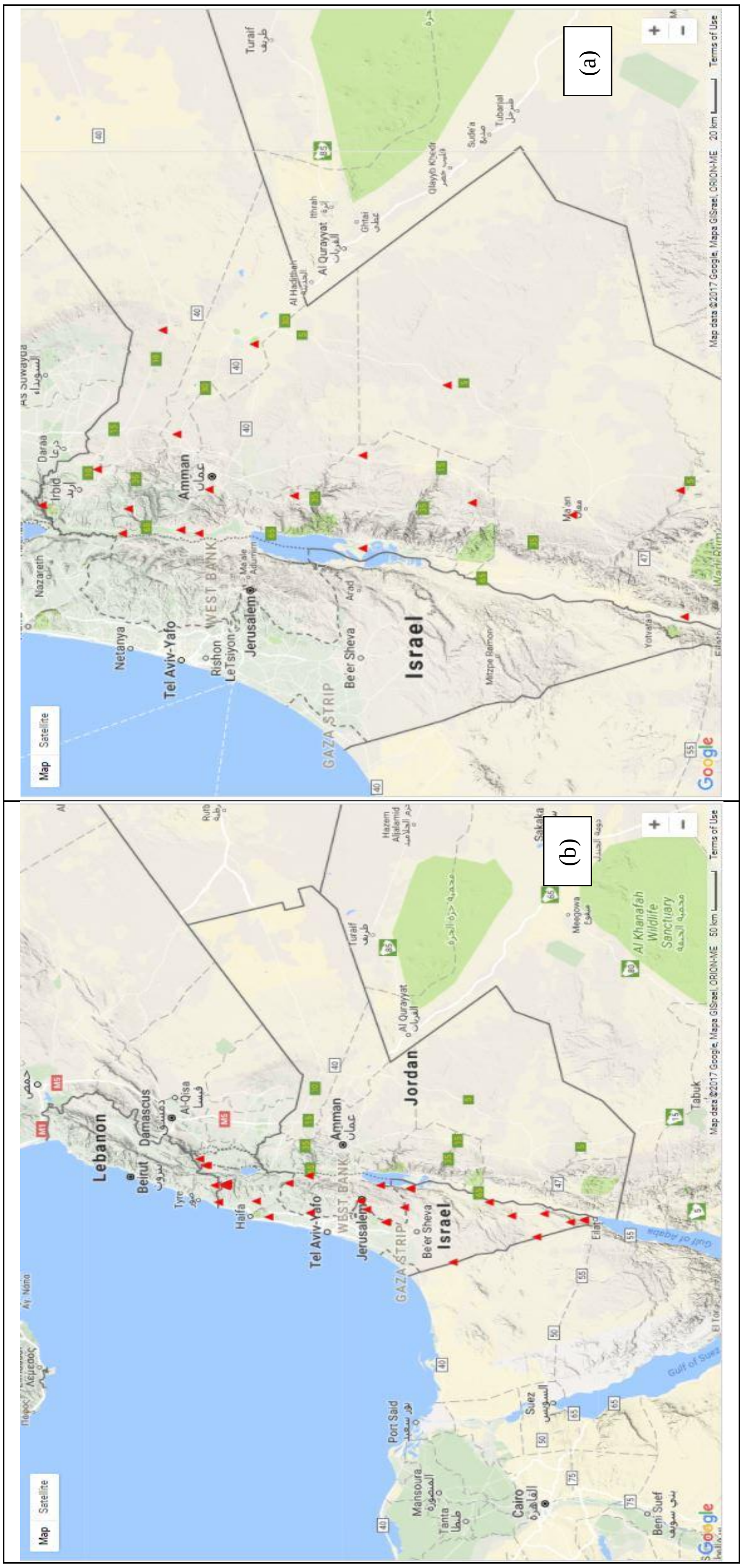

Figure 4-2: (A) The Jordan seismic network (JS). (B) The Israelian National Seismic Network (IS). Source: http://www.fdsn.org.

4-2-2. Seismic stations and channels characteristics

It is common to use several sensors of different types of earthquake stations, especially for permanent installed seismic stations. Hence, they are important to highlight the naming seismic channels (channel code) and accurately identifying the data we need to analyze. Whereas, the seismic stations and channels have a global uniform codes, which lead to the knowledge of the characteristics of these stations and channels.

Seismic sources create elastic waves, which break through the earth. The surface wave has a frequency range from less Milli-hertz (the eigenfrequency is 0.31 mHz) to about 30 Hz. The seismic sources are various and can be divided into two main types; natural sources such as the earthquakes and man-made ones such as explosion and human activity in the urban area. Seismic noise produced by an earthquake is mostly characterized by constant randomness, unlike other seismic sources such as wind, ocean waves, and cultural activities. The seismic dynamic spectrum ranges from the level of environmental noise to the largest seismic signal. Both limits depend on the frequency. While, the signal levels are mainly dependent on the distance between seismic source and receiver. The study of the seismic spectrum takes into account both the natural source and the distance between the source and the sensor, which can identify the nature of it. Table (4-1) is an example, which illustrates the frequency ranges, the distance between the sources and the seismometer and the nature of seismic sources (Ingate & Berger, 2004).

Table 4-1: The frequency range of the seismic sources, considering the distance between the source and the seismometer (Ingate & Berger, 2004).

Seismic sources	Distance	Frequencies	RMS Amplitudes
Local earthquake	up to ~30 km	0.3 to 30 Hz	to ~ 10 ms^{-2}
Reginal earthquake	~ 1000 km	~10^{-1} to ~10 Hz	to ~10^{-1} ms^{-2}
Teleseismic	~ 10,000 km	~10^{-2} to ~1 Hz	to ~10^{-3} ms^{-2}
Normal Modes	Whole Earth	$3x10^{-4}$ to ~10^{-2} Hz	to ~10^{-5} ms^{-2}

Earthquake magnitude is a very important characteristic, which has a direct correlation between the quantity and quality of the wave emitter. Figure (4-3) represents the earthquake spectra, recorded for different distances (considered as local, regional and teleseismic ones) for a domain of the earthquake magnitudes. To have more significant comparisons between deterministic signals and random noise, the spectral unit uses a root-mean-square (RMS) acceleration in the frequency bands with a width of one octave (Ingate & Berger, 2004).

Naming stations and channels of seismic is important. If the station and channel names are not correct or similar leading to confusion, there is inability to use the data directly. The Standard for Exchange of Earthquake Data (SEED) developed the channel naming, which is universally accepted. The station code must be 3-5 characters long, in which each station should have a special code, at least in the same network.

In addition to it, the channel code provided enough information about the kind of system used. Several years ago, naming the channel coded two characters such as BZ, LZ and SZ was enough to understand that system.

The evolution of seismology during the last period has produced a large number of sensors and digitizers, which becomes necessary to determine the channel codes accurately in accordance with the systems currently used. The International Federation of Digital Seismograph Networks (FDSN) provide the set up a recommendation for channel naming compatible with SEED format. The SEED component code for channel naming consists of three letters: A frequency band code (the sensor-digitizer type), an instrument code (sensor type (family)) and the third code is the channel orientation (usually Z, N or E). Tables (4-2, 3 and 4) represent the most common codes used according to SEED format (SEED, 2012; Havskov & Alguacil, 2016).

Finally, the data were recorded by the short period (SH) and broadband (HH and BH) stations will be used in our analysis. The short period stations and the channels belonging to them have coded SHZ. These channels can be a 1 Hz sensor with a 50 Hz sample rate. In addition, the broadband seismometers have HHZ coding with sample rate of 100 Hz (Havskov & Alguacil, 2016). These kinds of sensors can study the local and regional seismicity form low to medium earthquake magnitude. On the other hand, the seismicity in the study area can be classified as a local seismicity. The features for the seismicity in the study area are fully compatible with figure (4-3).

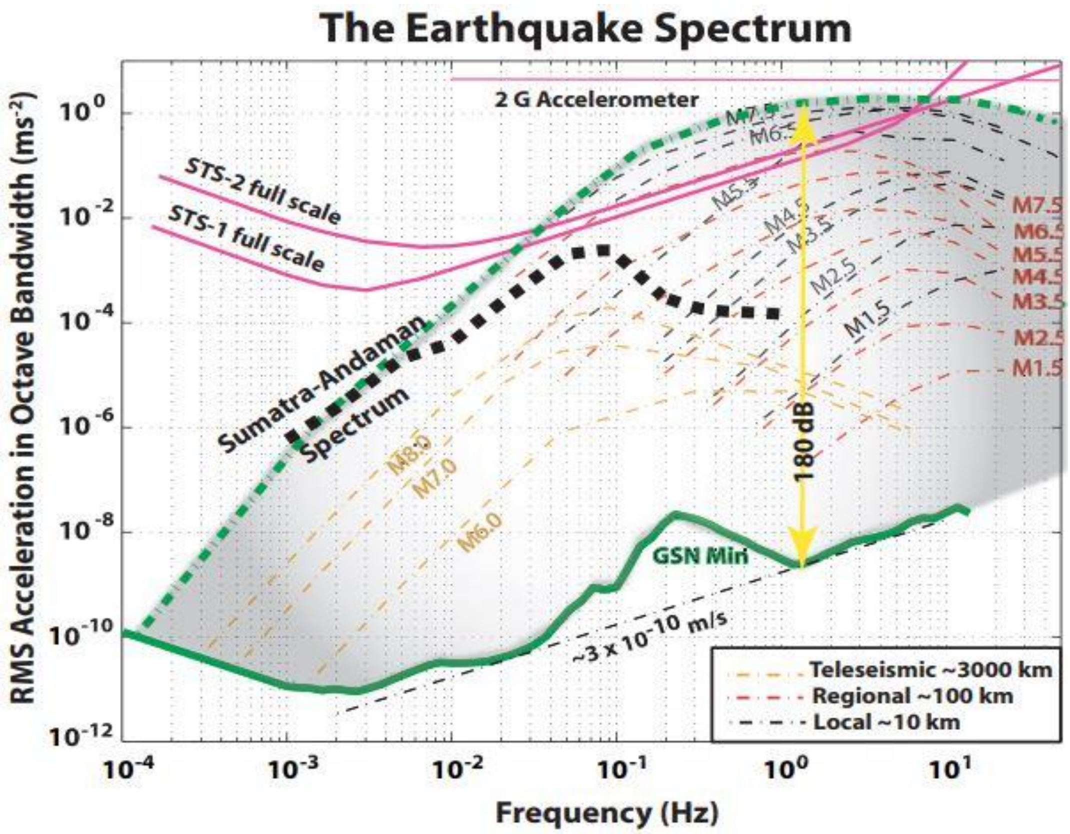

Figure 4-3: Representative earthquake spectra as recorded at different source distances and for a range of magnitudes. The shaded area signalizes the spectral range of earthquake signals and includes the signals on December 26, 2004 Sumatra-Andaman earthquake observed at the closest stations (1585 km to 2685 km). The lower green line indicates the minimum noise observed on the GSN stations (Berger, et al., 2004). The pink lines illustrate the full-scale dynamic range of the principal GSN sensors. Figure courtesy of (Berger, et al., 2004) and others, after (Clinton & Heaton, 2002).

Table 4-2: The most common band codes for Channel Naming (The first letter).

Band code	Band type	Sample rate (Hz)	Corner period
E	Extremely short period	≥ 80 to < 250	< 10 s
S	Short period	≥ 10 to < 80	< 10 s
H	High broadband	≥ 80 to < 250	≥ 10 s
B	Broadband	≥ 10 to < 80	≥ 10 s
M	Mid period	> 1 to < 10	
L	Long period	≈ 1	
V	Very long period	≈ 0.1	
U	Ultra-long period	≈ 0.01	

*There is no corner period specified in the SEED manual for sample rates lower than 1 Hz; however, it is assumed more than 10 s.

Table 4-3: The most common Instrument codes used (The second letter).

Instrument code	Description
H	High gain seismometer
L	Low gain seismometer
G	Gravimeter
M	Mass position seismometer
N	Accelerometer

Table 4-4: The Orientation code commonly used (The third letter).

Orientation code	Description
Z, N and E	Traditional (Vertical, north-south, east-west)
A, B and C	Triaxial (Along the edges of a cube turned up on a corner)
T and R	For formed beams (Transverse, Radial)

4-2-3. Data selection from GEOFON archive

The GEOFON project aims to simplify the cooperation in seismological research and earthquake and tsunami hazard mitigation, despite the international border access to seismological data and source parameters of earthquakes, through creating a databank, which contains the earthquakes waveforms accessible in the long term. The GFZ developed interactive tools to facilitate the selection of seismic data from that archive. The most important tool that helps to select the seismic data is WebDC3 (Figure 4-4). The WebDC3 (http://eida.gfz-potsdam.de/webdc3/) is an interactive website based on SeisComP3 software. This section will be described a mechanism to select and download the seismic data that used in this thesis.

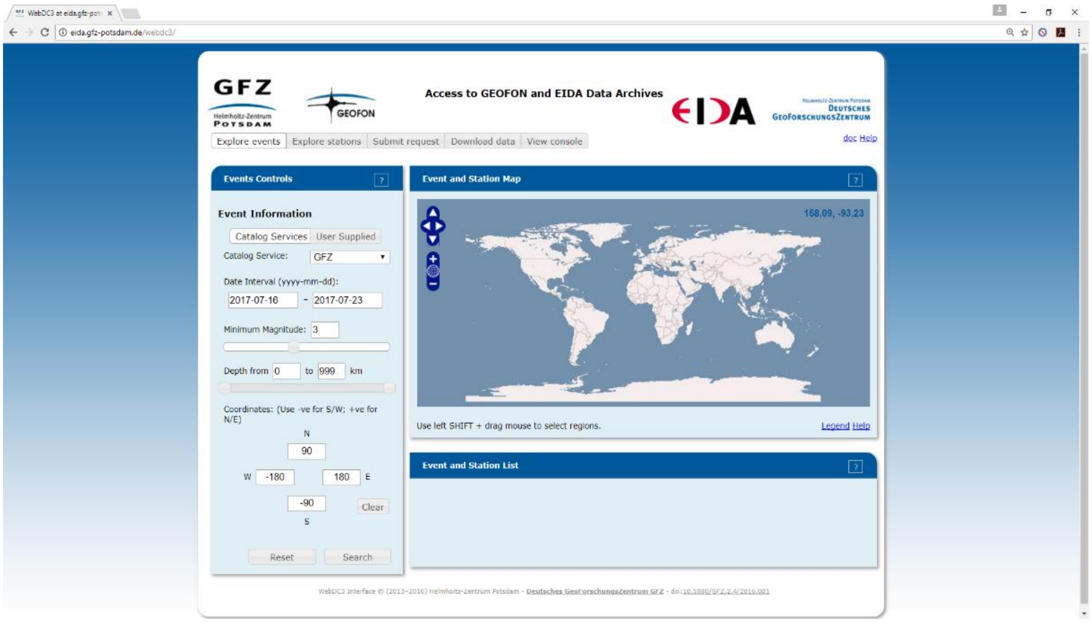

Figure 4-4: The WebDC3 interface (http://eida.gfz-potsdam.de/webdc3/).

The seismic data was selected from the GEOFON archive by using interface the following steps:

a- The first step:

The first step is to explore the events within the study area from the interactive website WebDC3 (Figure 4-5), based on the following procedures:

1- The selection catalog service, GFZ, ISC via IRIS, USGS and EMSC:

All available data in these catalogs have been used.

2- Determine the date interval:

The date period chosen for studying the seismic activity along DST and the surrounding area is between 2010 to the end of 2016.

3- Determine the minimum magnitude:

A seismic feature of the study area is characterized by weak to medium earthquakes' magnitude, to have enough waveforms from a reasonable number of stations; the earthquakes have a selected magnitude (≥ 3).

4- Selection the depth interval:

Generally, the epicenters depths in the study area are less than 50 km. Therefore, the interval depth used includes all depths.

5- Determine the geographic boundary:

The geographical boundaries of the study area are within (27°-35.5°) N and (32°-39°) E, which include the west part of the Levant region.

After defining the event properties, the global databases available through WebDC3 have 1529 events. These events include the events in the Cyprus area, which will be removed. Table (4-5) provides the number of events for each catalog service. The WebDC3 web interface provides the essential information for the events, which are the original time, magnitude, magnitude type, latitude, longitude, depth and region (epicenter region name). Mostly, these information results are automated analysis. The automated analysis is useful to demonstrate rapid information, but undoubtedly, these results cannot be used or relied on in most seismic studies.

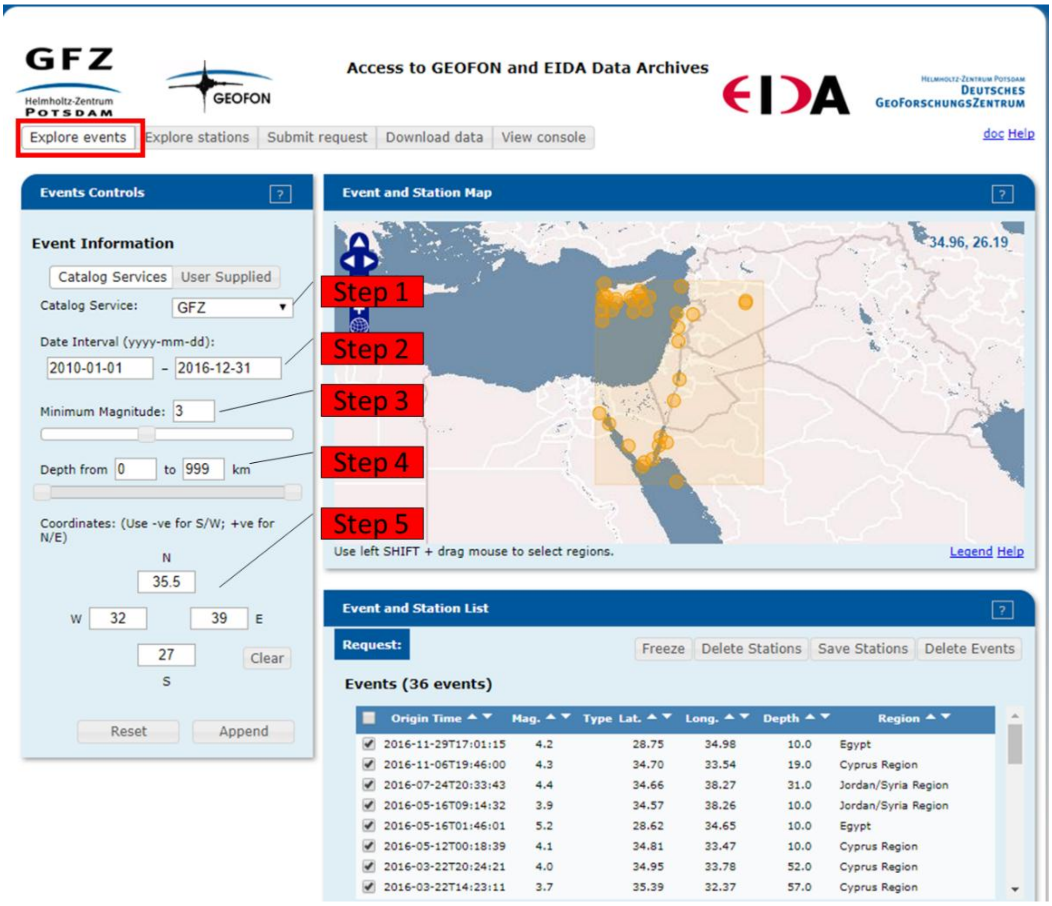

Figure 4-5: Explore events from webdc3 (http://eida.gfz-potsdam.de/webdc3/). The steps to select earthquakes on our area study are step 1: selection catalog service, step 2: the date interval, step 3: the minimum magnitude, step 4: the depth interval and step 5: determine the geographic boundary. The orange circles represent the initial location of the events**.**

Table 4-5: The numbers of events for catalog services available at WebDC3, taking into account the seismic characteristics identified for this study.

Catalog Service	Numbers of events
GFZ	36
ISC via IRIS	801
USGS	46
EMSC	646
Total	**1529**

b- The Second Step

The second step is to explore networks and stations (figure 4-6), based on the following procedures:

1- Selection Network type:

This option allows us to choose between permanent and temporal networks.

2- Network code:

The Jordanian (JS) and Israelian (IS) networks used to calculate the hypocenter location of the events.

3- Geographical location of the stations:

All the seismic stations of within the JS and IS seismic networks were selected. All of these stations located within the geographic boundaries of the study area.

4- Select seismic station channels:

Seismic data analyzed that recorded by very broadband, broadband and short period stations, which have codes as HH, BH and SH. The choice of this type of stations depends on several factors; the most important one is the earthquake magnitude in the study area.

The selected seismic stations are 61. The (JS) and (IS) seismic network consist of 19 and 42 seismic stations, respectively. The basic information (Network code, station name, latitude, longitude, operation status (O:

operating and R: repair) and the streams for the stations represented in the figure (4-6).

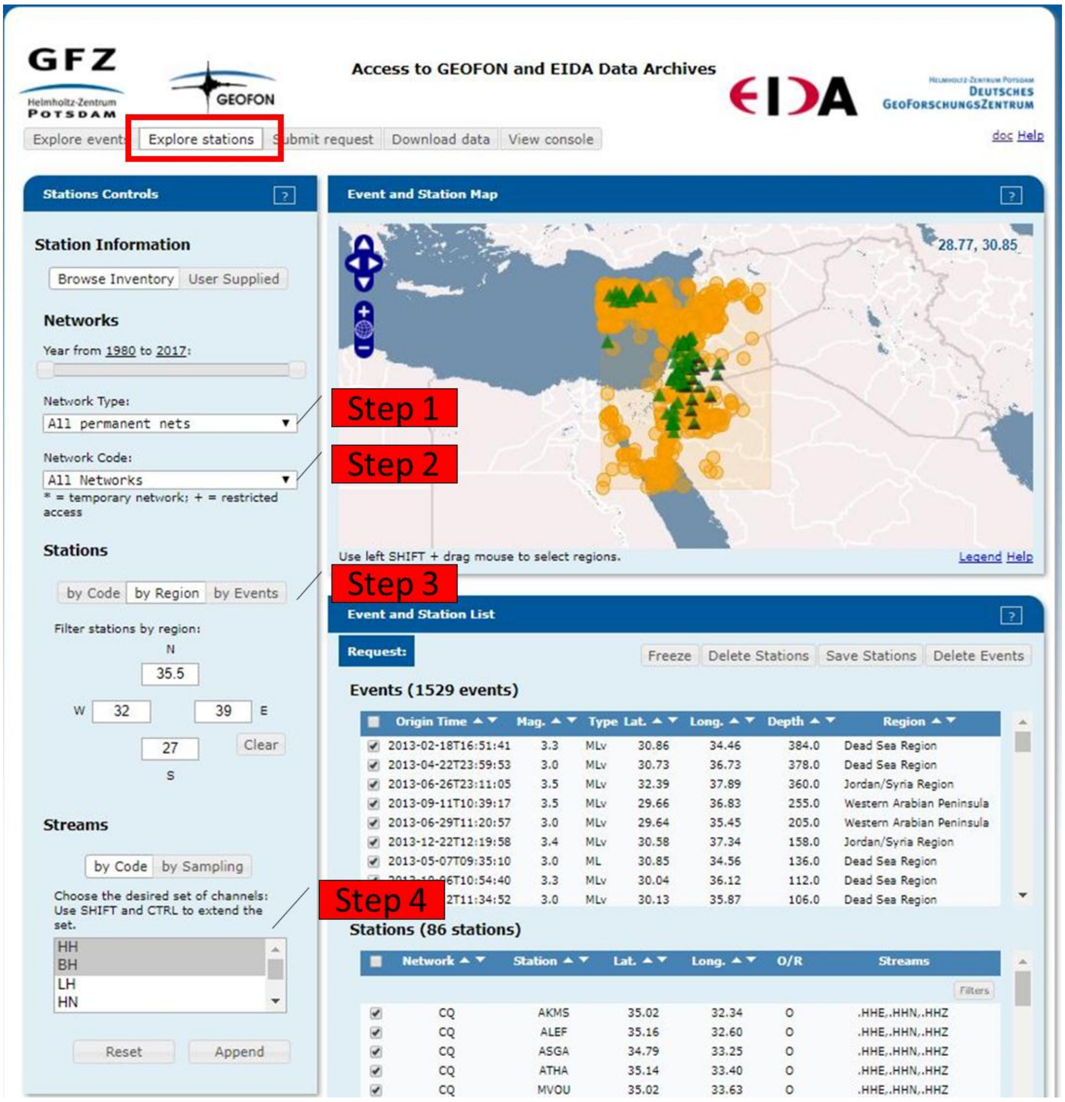

Figure 4-6: Explore networks and stations. The options adopted to determine seismic waveform consist of the following steps; selection network type, network code, geographical location of the stations and select seismic station channels, respectively. The orange circles represent the epicenter location for the events. Green triangles represent the location of seismic stations, while green and black triangles are under maintenance.

c- The Third Step:

The third step is the data request and the format of the earthquake waveform (submit request), which can identify the seismic waveform standers (figure 4-7). The starting time relates to the origin time of the event. The third step can be done by the following procedures:

1- It is important to identify the software analysis used to analyze the seismic data. The mini-seed format is one of the most famous seismic wave format and SEISAN matches with this format.

2- Writing the E-mail address is one of the requirement to GFZ.

d- The Fourth Step:

The fourth step is the download data. Figure (4-8) shows download window, selected on the previous window, considering, the events selected under the submit request window (previous step). Therefore, we always download the events one by one to facilitate the analysis.

The selected events are downloaded one by one for all the stations to get the waveforms from the largest number of surrounding seismic stations. These waveforms were archive monthly for each year. This pattern of archiving helps prevent error and confusion during the analysis process.

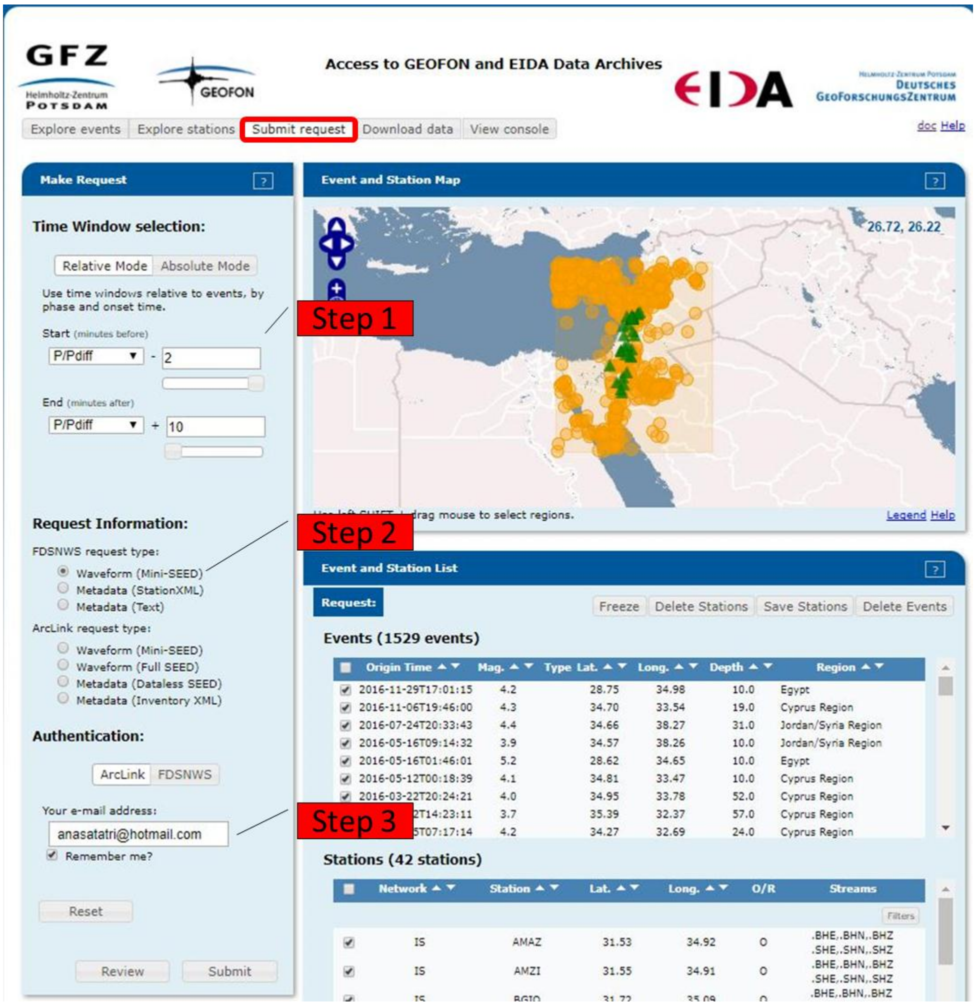

Figure 4-7: Submit request window.

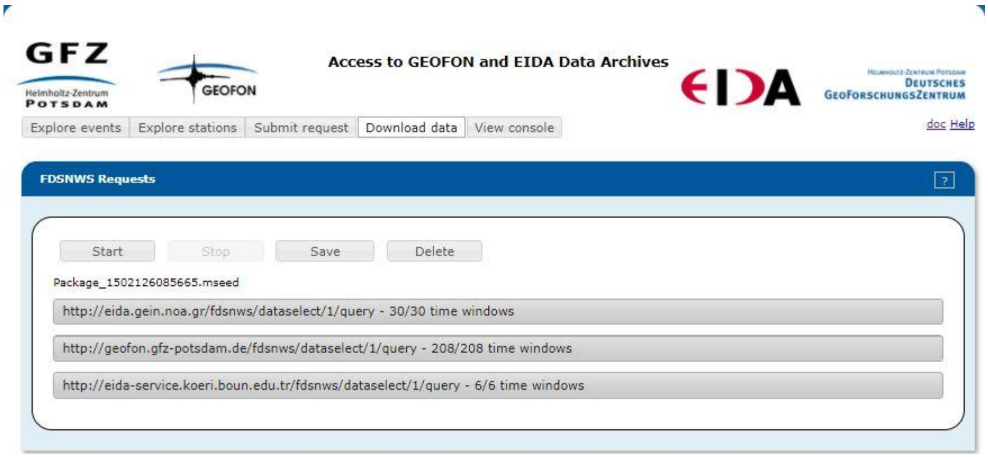

Figure 4-8: Example for download data window for an event. Start and stop button are functioning possess in severs that save waveform archive. To download selected query data click save button.

4-3. The Data Analysis (Preparation of data and location of hypocenter)

The analysis data and preparing input file that needs to locate the hypocenter will be presented in this part. The data analysis was done by using the SEISAN software (SEISAN EARTHQUAKE ANALYSIS SOFTWARE FOR WINDOWS, SOLARIS, LINUX and MACOSX Version 10.5).

4-3-1. SEISAN (Version 10.5)

The SEISAN seismic analysis system is a complete set of packages programs and a simple database for analyzing earthquakes both of analog and digital seismic data (Ottem¨oller, et al., 2016).

4-3-2. Structure of SEISAN

The SEISAN system consists of subdirectories, established under the main directory SEISMO (Figure 4-9). The SEISAN system includes the following principal subdirectories (Ottem¨oller, et al., 2016):

REA: Earthquake readings and full epicenter solutions in a database

WOR: The users work directory, initially empty

TMP: Temporal storage of files, initially empty

PRO: Programs, source code and executables

LIB: Libraries and subroutines

INC: Include files for programs and subroutines in PRO and LIB

COM: Command procedures

DAT: Default and parameter files, e.g. station coordinates

WAV: Digital waveform data files

CAL: System calibration files

INF: Documentation and information

ISO: Macroseismic information

SUP: Supplementary files and programs

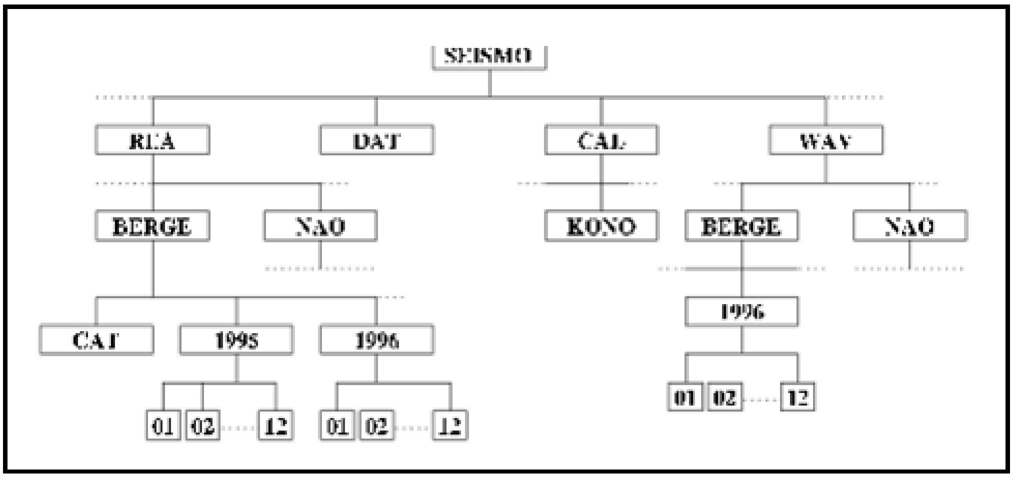

Figure 4-9: The Tree structure of the subdirectory of SEISAN.

4-3-3. Creating Database

The first step creates a specific project database, when we start a signal analysis, using SEISAN system. MAKEREA is the command (program) that allows creating a new database. The new database will be created within the REA and WAV subdirectories. MAKEREA requests the name of the new database, consisting of 1 to 5 letters, as well as the start and end date of the period (year and month) (Figure 4-10).

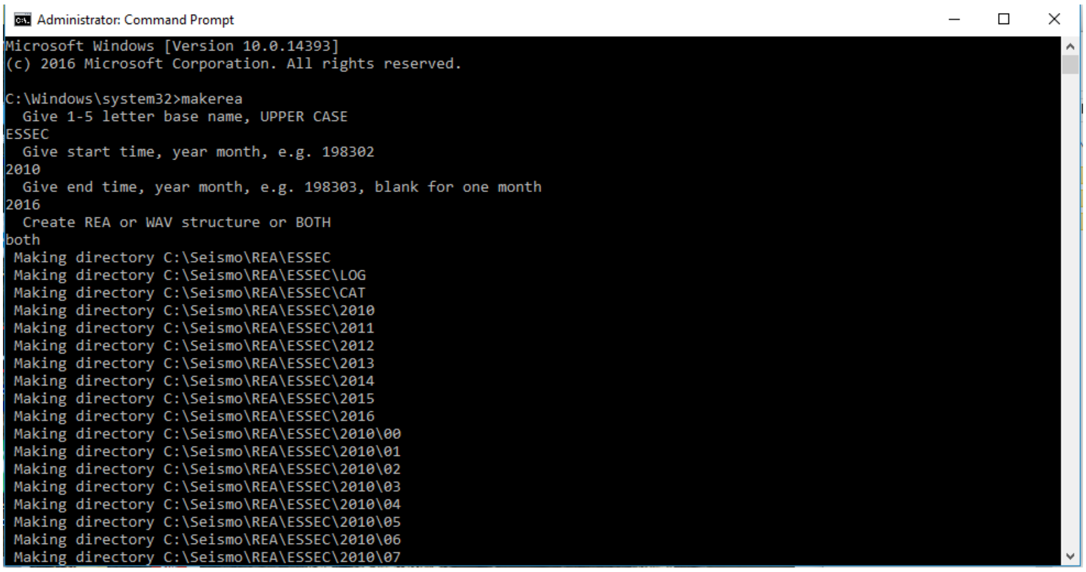

Figure 4-10: Creating a database with the MAKEREA command in a DOS window.

4-3-4. Configuration

The following configuration will be done before starting the analysis:

A- SEISAN.DEF File (SEISAN default settings)

The subdirectory (DAT) includes the SEISAN default-setting file (SEISAN.DEF). The DA command in a DOS window was used to edit the file. We introduce the name of our database (ESSEC) in the box of COPY_WAV_DIR. In addition, the file is modified to be compatible with the Windows operating system (Figure 4-11).

```
SEISAN.DEF
This file is for defaults for SEISAN and called SEISAN.DEF. The name must
be in upper case on Sun. The following shows the parameters which can be set.
The file can contain any lines in any order, only the lines with
recognized keywords and a non blank field under Par 1 will be read. The
comments have no importance.

*********NEVER USE TABS IN THIS FILE, IT WILL NOT WORK*****************

KEYWORD............Comments.............Par 1.....Par 2
WAVEFORM_BASE       Waveform base name   NSS
WAVEFORM_BASE       Waveform base name   RUND
WAVEFORM_BASE       Waveform base name   JMI
WAVEFORM_BASE       Waveform base name   TEST
WAVEFORM_BASE       Waveform base name   ESSEC
#
#   seisan cont dat abase
#
CONT_BASE           REA continuous base  RUND
CONT_BASE           REA continuous base  JMI
CONT_BASE           REA continuous base  NSS
CONT_BASE           REA continuous base  ESSEC
CONT_BEFORE         start min before     20.
CONT_AFTER          start min after      1.

WAVEFORM_DIRS       Waveform drectory    C:\Seismo\WAV\ESSEC
MERGE_WAVEFORM      Code for merging wa  NSN
MAP_LAT_BORDER      dist from center       3.0
MAP_LON_BORDER           "                 6.0
EPIMAP_STATIONS     plot stations
EPIMAP_MAP_FILE     name of map          EUROPE
EEV_COMMENT         comment for EEV      Depth has benn fixed to 10 km
EEV_COMMENT         comment for EEV      Depth has been fixed to 20 km
EPIMAP_PROJECTION   number                  3.
SPECTRAL GEO_DEPTHS                      10.0       14.0
HERKIJ_DISTANCE                          100.0
REG_KEEP_AUTO       keep phases when reg    1.
COPY_WAV_DIR        copy when register

TEXT_PRINT                Unix example   nenscript -Psps
OUTPUT_DIR                               ./
INIT_IMGMAP_FILE          PC example     c:\seismo\DAT\IMGWORLD.gif
MAP_SERVER                               0
IMGMAP_PATH               PC example     c:\seismo\DAT\IMGMAP
INIT_MAP_LOWER_LATITUDE                  -90.0
INIT_MAP_UPPER_LATITUDE                  90.0
INIT_MAP_LEFT_LONGITUDE                  -180.0
INIT_MAP_RIGHT_LONGITUDE                 180.0
INTERNET_BROWSER          Unix example   /prog/netscape
ACROBAT_READER            PC example     C:\Program Files (x86)\Adobe\Acrobat DC\Acrobat\Acrobat.exe
HELP_DIR                  PC   example   c:\seismo\INF
WEBMAPSERVER2                            http://pcseis6.ifjf.uib.no:7001/getImageMap?ACTION=2&
WEBMAPSERVER3                            http://demo.cubewerx.com/demo/cubeserv/cubeserv.cgi?

# order to select magnitudes as given here from top (high priortiy) to bottom (low priority)
MAGNITUDE_ORDER                          WGCM
MAGNITUDE_ORDER                          LBER
MAGNITUDE_ORDER                          WBER

# parameters for gmap used within eev
GMAP_DIR                                 c:\seismo\WOR
GMAP_TYPE                                MAP          [MAP, SATELLITE, HYBRID, TERRAIN]
```

Figure 4-11: SEISAN.DEF file parameters

B- STATION0.HYP File (Configuration of the station coordinates file)

STATION0.HYP is the second file in SEISAN system, modified to locate the events, which include the stations coordinates, location parameters, and the model of the earth's crust (velocity model). This file (STATION0.HYP) is located in the subdirectories DAT. To modify this file, we go to the subdirectories DAT or use the DA command, using DOS window and edit it. Appendix (1) includes the seismic stations that added into this file. The coordinates of the stations are added as in the following form:

The name of the station composes of 4 letters (4 cases), then the longitudinal component occupies 8 letters: 2 letters for the degrees, 2 letters for the minutes, 1 letter for the decimal point, 2 letters for the decimal degree and 1 letters for direction N or S. Then, the latitude component occupies 9 letters: 3 letters for the degrees, 2 letters for the minutes, 1 letter for the decimal point, 2 letters for the decimal degree and 1 letter for the direction E or W and 4 letters for the altitude in meter [m]. Note that each empty box is considered as a zero (Figure 4-12).

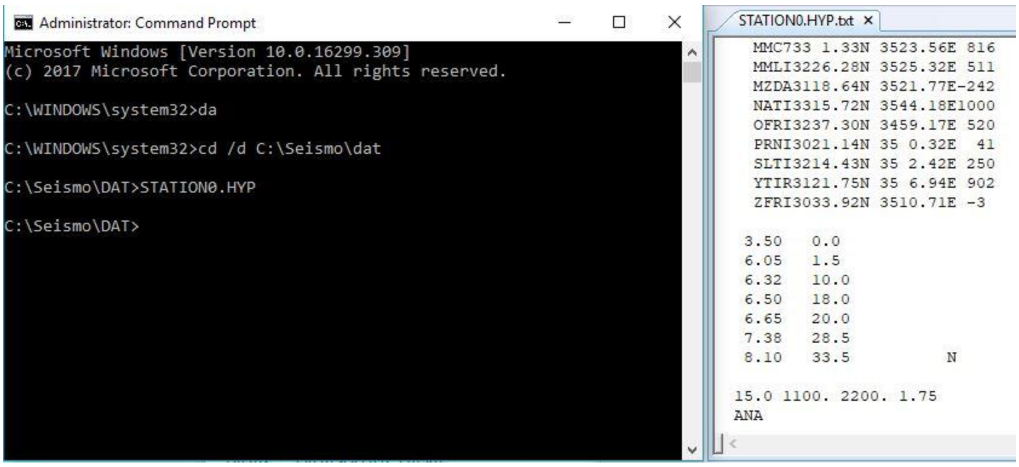

Figure 4-12: Configuring the station0.hyp file.

4-3-5. Exploitation of SEISAN

4-3-5-1. Integration Data into the Database

Mostly, the data is identified the characteristics in this chapter are digital waveforms for earthquakes. Therefore, the data are copied into subdirectory WOR. Then, using the DIRF command to create file list (filenr.lis) for all the data into the subdirectory WOR.

The MULPLT command is the tool needed to integrate the data into our database (ESSEC). The MULPLT command launches a window (figure 4-14), which allows us to view the signals and to integrate or not integrate the desired signals into the database by a simple process. AUTOREG command (program) is the second tool that enters all waveform files directly into the database.

The SEISAN system will copy the selected data needed to integrate into our database as; copying the waveform format into subdirectory WAV and create a format file called S-file into subdirectory REA for each waveform under our database (ESSEC). Each earthquake (or single(s)) has (have) unique S-file into REA. The S-file contains all information, relating to the signal recorded by one station or multi-stations.

4-3-5-2. Picking and organization waveform files

The idea of SEISAN for the interactive work is what the user can pass easily from one event (earthquake) to another and run several different programs with an event without having to restart each time the different applications. This is done using the EEV application (Figure 4-13). In this interactive mode, events are resumed, modified, located, moved, deleted etc., until a satisfactory solution is achieved. Appendix (2) represents samples of waveforms for different stations.

Figure 4-13: The EEV application in a DOS window.

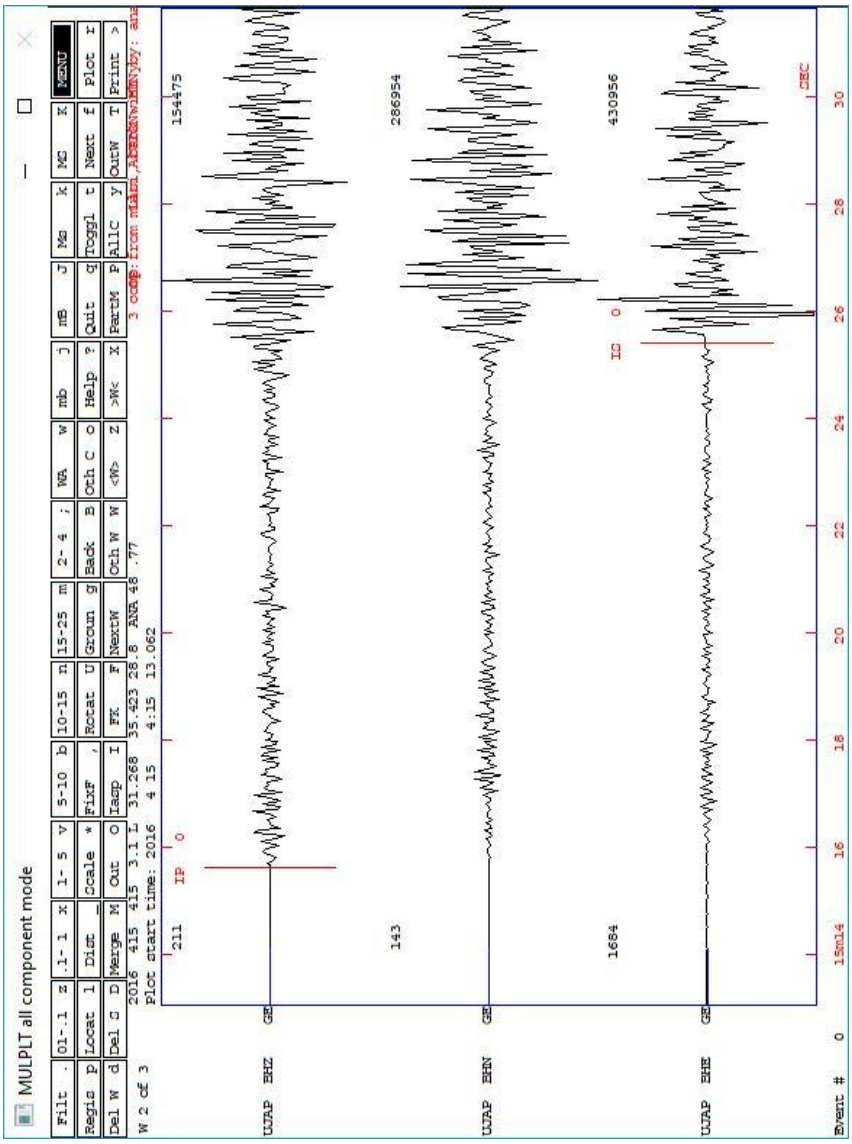

Figure 4-14: Window showing the various signal components of the earthquake (multi-trace graph) recorded by the UJAP (DESERVE Station Al Uja, Palestine Territories) on April 15, 2016.

To pick the phases, it is necessary to enter the PO command under EEV. After executing this command, the software displays a new window Figure (4-14).

Figure (4-14) and appendix (2) show the different components of the signal: Z (or number 1), the vertical component, N (or the number 2), the component of the north-south and E (or number 3), the component of the east-west, after the station name. Usually, the first arrival of the signal (p-wave) and the second (S-wave) are recorded in the Z-component and the horizontal components, respectively.

In REA, the events are organized according to the arrival time of the P-waves. The command <a> in EEV is responsible for grouping the different signals for one event. Figure (4-15) is an example for grouping signals from different stations.

4-3-5-3. Location of hypocenter by using the HYPOINVERSE (2000) program

The fundamental problem to study the seismicity is to locate the hypocenter parameters. Four basic parameters are needed to determine the focus of the earthquakes location X, Y, Z and T (longitude, latitude, depth and origin time, respectively) (Akbar, et al., 2015). Indeed, the good localization of hypocenters depends on the success of other studies such as the focal mechanism or tectonics setting studies. Few hundred meters to kilometers of hypocenter geographical coordinates accuracy are acceptable when studying the local seismicity.

To obtain, the acceptable accuracy, we require the respect of the following conditions:

- Implementation a program has a strong calculation technique to determine the hypocenters.

- A good knowledge of the speed law of the waves is needed to estimate the velocity model, especially if we do not have one.

- A judicious distribution of the seismological stations in the epicentral zone.

- Finally, good data are needed in sufficient numbers from different stations for each earthquake.

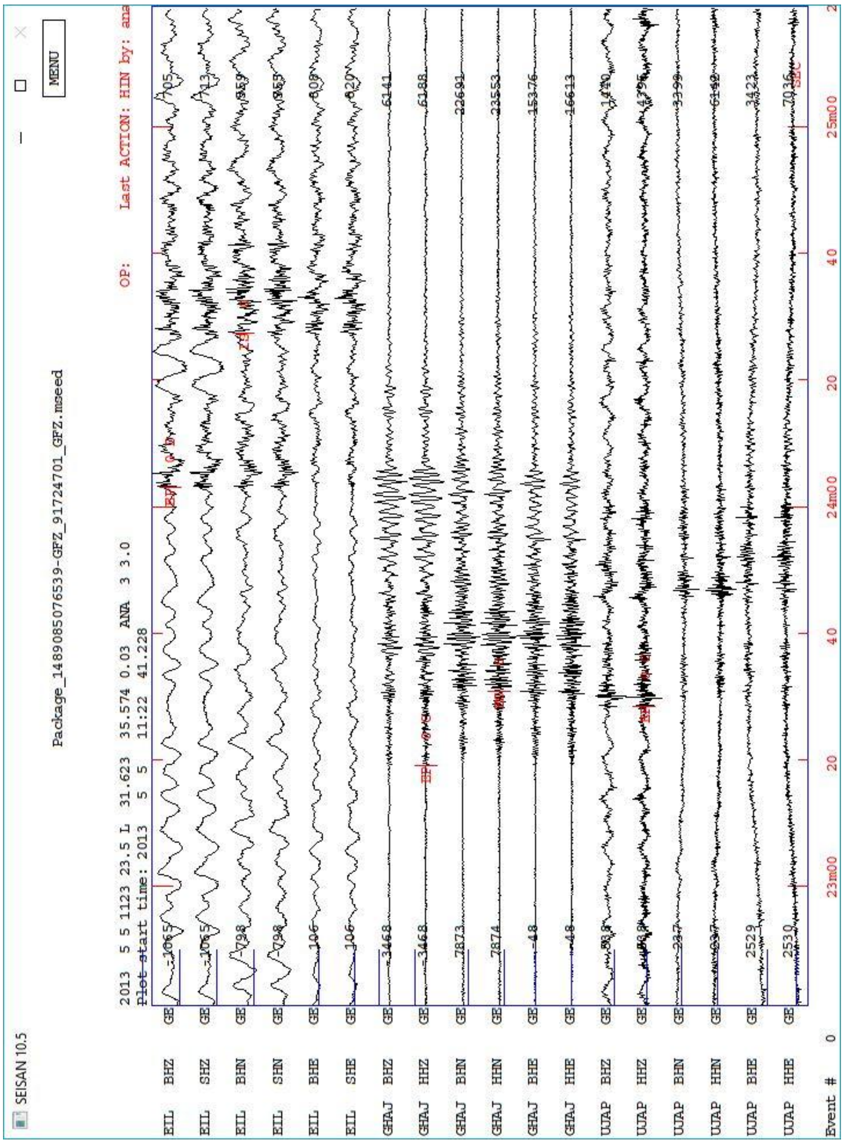

Figure 4-15: Window showing the different components of the earthquake signals (multi-trace graph).

➢ ***The HYPOINVERSE (2000) program***

The program (HYPOINVERSE) is used to localize earthquakes. The HYPOINVERSE (Klein, 1978) is derived from HYPO71 (Lee & Lahr, 1975) program. This program uses the [Geiger, 1912] method to determine the four hypocentral parameters (t, x, y, z). Neglecting the curvature of the earth over an arc of a 400 Km, the horizontal error is 30 m, the vertical is 3 Km at the extremities (Besnard, 1984). Usually, the Cartesian coordinates are used if the network dimension does not exceed several hundred kilometers.

The program principle is as follows: each station has a variable "i" and each phase "j", the arrival time available is "t_i^j", the routine calculation estimates the average for the trace of the wave way with flat, horizontal and homogeneous layers to calculate time "t_i^J" from a test hypocenter (t ', x', y ', z'). The residue of this phase will be as:

$R_i^J = t_i^j - t_i^J$ --------------- Equation (4-1)

The term (t_i^j) can be solved by using the Taylor series method as:

$t_i^j = t_i^J + dt + \frac{\partial t_i^J}{\partial \mathrm{x}} dx + \frac{\partial t_i^J}{\partial \mathrm{y}} dy + \frac{\partial t_i^J}{\partial \mathrm{z}} dz + e_i$ --------- Equation (4-2)

Considering e_i is an error that we are trying to minimize.

In order to run this program, we must modify the information contained in the following input files:

- *. STA, which lists the stations of the network operated (used) (Figure 4-16).

- *. Mod, which represents the estimated velocity model (Figure 4-17).

- PHASALT (Picking) file, which includes the arrival time phases (Figure 4-18).

The file that lists the stations (Figure 4-16) contains the code (name) of each station, their coordinates, their altitudes and their corrections if necessary.

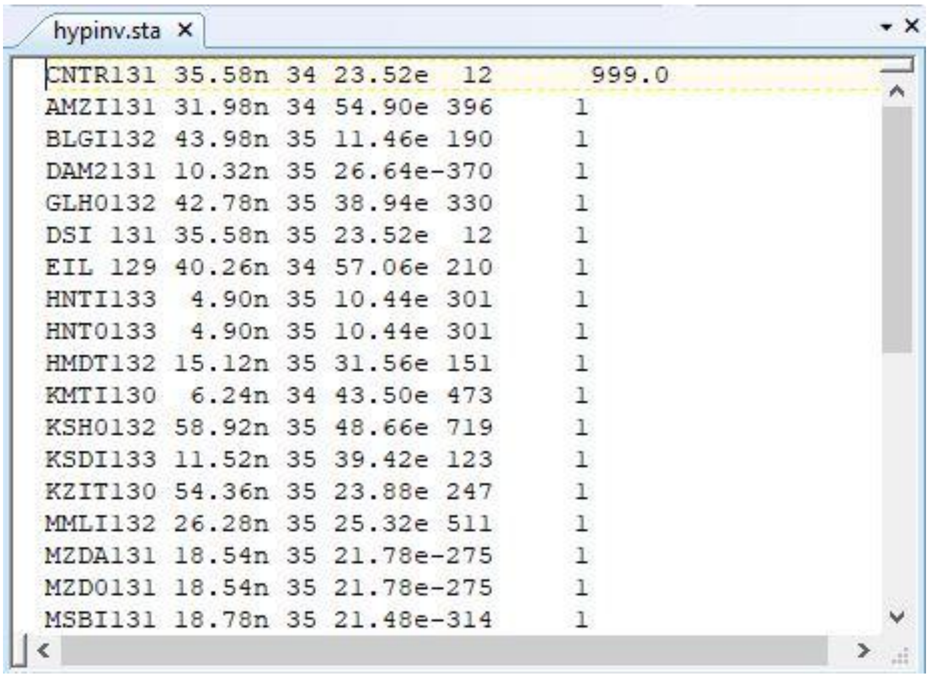

```
hypinv.sta
CNTR131 35.58n 34 23.52e  12       999.0
AMZI131 31.98n 34 54.90e 396     1
BLGI132 43.98n 35 11.46e 190     1
DAM2131 10.32n 35 26.64e-370     1
GLH0132 42.78n 35 38.94e 330     1
DSI 131 35.58n 35 23.52e  12     1
EIL 129 40.26n 34 57.06e 210     1
HNTI133  4.90n 35 10.44e 301     1
HNT0133  4.90n 35 10.44e 301     1
HMDT132 15.12n 35 31.56e 151     1
KMTI130  6.24n 34 43.50e 473     1
KSH0132 58.92n 35 48.66e 719     1
KSDI133 11.52n 35 39.42e 123     1
KZIT130 54.36n 35 23.88e 247     1
MMLI132 26.28n 35 25.32e 511     1
MZDA131 18.54n 35 21.78e-275     1
MZD0131 18.54n 35 21.78e-275     1
MSBI131 18.78n 35 21.48e-314     1
```

Figure 4-16: The input file for our seismological stations used The first line represents the coordinates of the test hypocenter. The rest of the lines represents the coordinates of the stations of the local seismological networks used. Coordinates are Latitude (degree, minute), Longitude (degree, minute), and Elevation (Altitude in meters). Number 1 is the default Period (in seconds).

The estimated velocity model is represented in the file *. Mod as shown on the (figure 4-17).

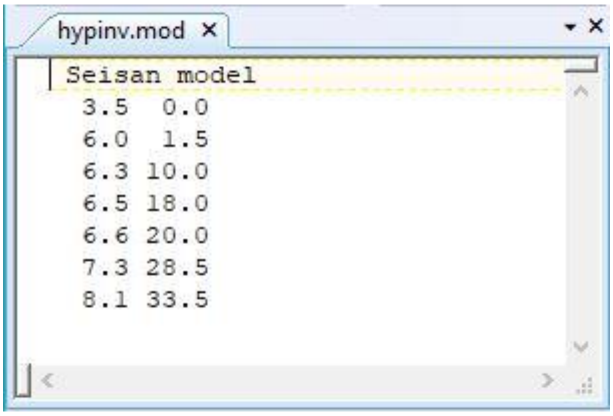

Figure 4-17: The velocity model used The first column corresponds to the velocities of the flat layers and the second column corresponds to the depths of same layers.

The PHASALT file includes all the information relating to the arrival time of the waves, the quality of the readings, the coda and even the amplitude of the phases when this is available. Figure (4-18) shows a portion of the input PHASALT file.

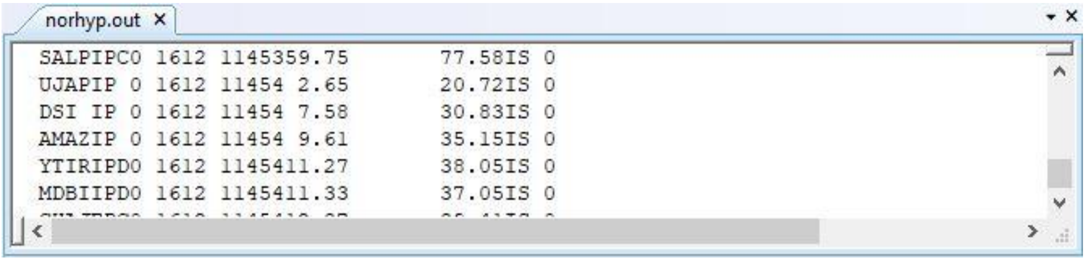

```
norhyp.out
SALPIPC0 1612 1145359.75       77.58IS 0
UJAPIP 0 1612 11454 2.65       20.72IS 0
DSI IP 0 1612 11454 7.58       30.83IS 0
AMAZIP 0 1612 11454 9.61       35.15IS 0
YTIRIPD0 1612 1145411.27       38.05IS 0
MDBIIPD0 1612 1145411.33       37.05IS 0
```

Symbol	SALP	IPC0	16	12	1	14	53	59.75	77.58	IS	0
Significance	1	2345	6	7	8	9	10	11	12	13	14

Figure 4-18: The PHASALT file extract (the seismic signal arrival time) 1: The station codes.

- 2: I for the clear beginning of the direction of the first movement, E for the doubtful beginning of the sense of the first movement.
- 3: The nature of the initial phase (P: primary).
- 4: C denotes compression (direction of first movement upwards), D denotes dilation (sense of the first movement downwards), Empty: uncertain start.
- 5: The weight denotes the quality of the P wave (0 for net, 4 for poor quality).
- 6, 7, 8, 9, 10 and 11 shows the year, month, day, hour, minute and seconds (Tenth and hundredths of a second), respectively.
- 12: The beginning of the second phase in minute and second (tenth and hundredth of a second).
- 13: Indicates the nature of the second phase (the S phase).
- 14: The weight that denotes the quality of the S wave (0 for net, 4 for poor quality).

The program generates several output files. The most important files are the summary file and the report file.

The summary file summarizes information about location, the origin time of each event and the various errors committed during the calculations (figure 4-19), where the information is presented in rows and columns.

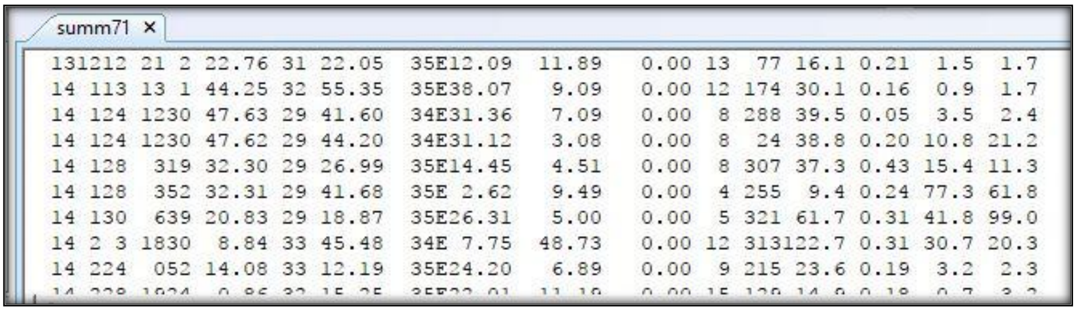

```
summ71
131212 21 2 22.76 31 22.05  35E12.09  11.89   0.00 13  77 16.1 0.21  1.5  1.7
14 113 13 1 44.25 32 55.35  35E38.07   9.09   0.00 12 174 30.1 0.16  0.9  1.7
14 124 1230 47.63 29 41.60  34E31.36   7.09   0.00  8 288 39.5 0.05  3.5  2.4
14 124 1230 47.62 29 44.20  34E31.12   3.08   0.00  8  24 38.8 0.20 10.8 21.2
14 128  319 32.30 29 26.99  35E14.45   4.51   0.00  8 307 37.3 0.43 15.4 11.3
14 128  352 32.31 29 41.68  35E 2.62   9.49   0.00  4 255  9.4 0.24 77.3 61.8
14 130  639 20.83 29 18.87  35E26.31   5.00   0.00  5 321 61.7 0.31 41.8 99.0
14 2 3 1830  8.84 33 45.48  34E 7.75  48.73   0.00 12 313122.7 0.31 30.7 20.3
14 224  052 14.08 33 12.19  35E24.20   6.89   0.00  9 215 23.6 0.19  3.2  2.3
```

131212	2102:22.76	31 22.05	35E12.09	11.89	0.00	13	77	16.1	0.21	1.5	1.7
Date	**Origin Time**	**Latitude (N)**	**Longitude (E)**	**Depth (km)**	**FMAG**	**NWR**	**GAP (°)**	**DMIN (km)**	**RMS (s)**	**ERH (km)**	**ERZ (km)**

Figure 4-19: An overview of the summary output file from the HYPOINVERSE program.

The report file is the most important output file generated by the HYPOINVERSE program, containing the details of all calculations, errors, residuals, weights assigned to each phase of the calculation and the number of iterations (Figure 4-20).

```
print.out
1 16 DEC 2016, 17:12  SEQUENCE NO.    1, ID NO.1216170654
 ERROR ELLIPSE: <SERR AZ DIP>-<   1.07 139 74>-<   0.83 308 15>-<   0.68  39  2>
 ---------------------------------------------------------------------------------
 YEAR MO DA  --ORIGIN--  --LAT N-  --LON W--  DEPTH-M RMS   ERH   ERZ  XMAG1 FMAG1 PMAG GEOID-DEP
 2016-12-16  1712 42.75  33 17.52   35E24.16   7.56  0.32  0.81  1.03                        6.88
                                                                                           SOURCE
 NSTA NPHS  DMIN MODEL GAP ITR NFM NWR NWS NVR REMRKS-AVH  N.XMG-XMMAD-T   N.FMG-FMMAD-T  L F X
   54   54  25.9   Se  247   8  21  48  24  54                                             Z

 XMAG2-N.XMG2-XMMAD-T-S  FMAG2-N.FMG2-FMMAD-T-S  PREF.MAG-N.PMAG-PRMAD-T DEPDAT NS ZT TYP
                                                                             687  5  M CRH
 REGION=

 STA NET COM L CR DIST AZM  AN P/S WT   SEC (TOBS -TCAL -DLY  =RES)  WT   SR  INFO  CAL  DUR-W-FMA(
 GEM              25.9 110  90 IPD    47.18  4.43  4.17 0.00  0.26  1.08  ZB 0.228
                               IS     50.61  7.86  7.30 0.00  0.56* 1.08S EB 0.431
 MMC1             29.0 179  90 IPD    47.36  4.61  4.67 0.00 -0.06  1.08  ZB 0.036
                               IS     51.08  8.33  8.17 0.00  0.16  1.08S ZB 0.058
 MMC2             29.4 178  90 IPD    47.40  4.65  4.74 0.00 -0.09  1.08  ZB 0.036
                               IS     51.08  8.33  8.30 0.00  0.03  1.08S ZB 0.060
 MMB4             30.1 181  90 IPD    47.52  4.77  4.85 0.00 -0.08  1.08  ZB 0.036
                               IS     51.47  8.72  8.49 0.00  0.23  1.08S ZB 0.056
```

Figure 4-20: The output file HYPPRT.OUT from the HYPOINVERSE program.

In figure (4-20), the first line includes the date (yr mo da), the origin time of the earthquake (ORIGIN), the epicenter coordinates in degrees and minutes (LAT-N, LON-E), the depth of focus (DEPTH) in Km, RMS in seconds, the standard of the epicenter position (ERH) and (ERZ) errors in the horizontal and vertical directions (respectively). As well as, the second line includes the non-azimuth coverage (GAP) in degrees. In addition, it includes:

- DMIN: The minimum epicentral distance between the epicenter and the stations.

- ITR: The number of iterations to achieve convergence.

- NWR: The number of phases P used in the calculations for that event.

4-3-5-4. The Calculation of the Vp/Vs Ratios (WADATI method)

The WADATI method is used to estimate the Vp/Vs ratio from the arrival time of the P and S waves of the same event. By linear regression of the line $t_s - t_p = f(t_p)$, assuming a uniform velocity in a homogeneous layer and this ratio can be calculated by using the following equations:

$t_s = t_0 + \frac{d}{v_s}$ --------------- Equation (4-3)

And $t_p = t_0 + \frac{d}{v_p}$ --------------- Equation (4-4)

Hence $t_s - t_p = \left(1 - \frac{v_p}{v_s}\right)\ t_0 + (\frac{v_p}{v_s} - 1)\ t_p$ --------------- Equation (4-5)

The term $(\frac{v_p}{v_s} - 1)$ represents the slope of the straight line that passes through points. These points can be represented by graph, which have t_p axe (the horizontal axe (X)) and $t_s - t_p$ axe (the vertical axe (Y)). On the other hand, the origin time can be determined by the intersection of the straight line and the X axe (Figure 4-21).

The WADATI method is utilized at SEISAN to control the picking, in which all points will be on the straight line in the ideal condition. Mostly, the ideal value of this ratio is ranging from 1.53 to 1.93. In addition, the command “Wadati” in DOS window can calculate this ratio of our study area (Figure 4-22).

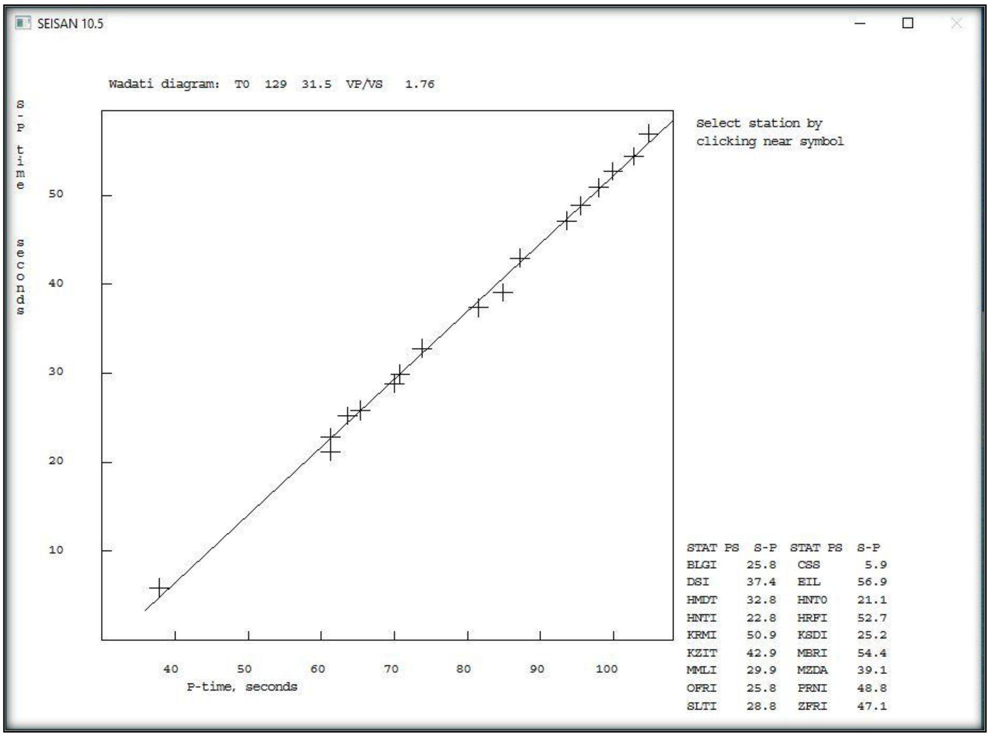

Figure 4-21: The WADATI graph at SEISAN for an earthquake.

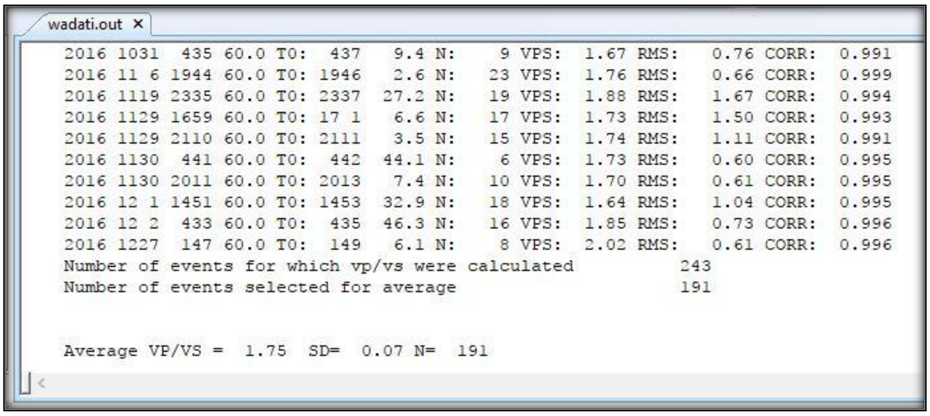

```
wadati.out
2016 1031  435 60.0 T0:  437   9.4 N:   9 VPS:  1.67 RMS:   0.76 CORR:  0.991
2016 11 6 1944 60.0 T0: 1946   2.6 N:  23 VPS:  1.76 RMS:   0.66 CORR:  0.999
2016 1119 2335 60.0 T0: 2337  27.2 N:  19 VPS:  1.88 RMS:   1.67 CORR:  0.994
2016 1129 1659 60.0 T0: 17 1   6.6 N:  17 VPS:  1.73 RMS:   1.50 CORR:  0.993
2016 1129 2110 60.0 T0: 2111   3.5 N:  15 VPS:  1.74 RMS:   1.11 CORR:  0.991
2016 1130  441 60.0 T0:  442  44.1 N:   6 VPS:  1.73 RMS:   0.60 CORR:  0.995
2016 1130 2011 60.0 T0: 2013   7.4 N:  10 VPS:  1.70 RMS:   0.61 CORR:  0.995
2016 12 1 1451 60.0 T0: 1453  32.9 N:  18 VPS:  1.64 RMS:   1.04 CORR:  0.995
2016 12 2  433 60.0 T0:  435  46.3 N:  16 VPS:  1.85 RMS:   0.73 CORR:  0.996
2016 1227  147 60.0 T0:  149   6.1 N:   8 VPS:  2.02 RMS:   0.61 CORR:  0.996
Number of events for which vp/vs were calculated        243
Number of events selected for average                   191


Average VP/VS =  1.75  SD=  0.07 N=  191
```

Figure 4-22: The Output file wadati.out for the study area T0: The original time calculated by Wadati. N: The number of phases used. VPS: The VP / VS ratio. RMS is the root mean square (the time error) in second. SD: The standard deviation in the calculation. Average VP/VS is the ratio for our database.

Chapter Five
Results and Dissections

5-1. Introduction

The main target of this study is determining the Vp/Vs ratio from local seismicity along the DST and the surrounding area, utilizing the recording data during 2010 to 2016. On the other hand, the seismicity distribution is one of the important information considered in the urban planning. In addition to that, it is the first step to understand the seismic hazard and identify the active tectonic structures within a study area.

A number of parameters are used to estimate the earthquake location, such as the V_p/V_s ratio and a velocity model. The recorded events are used to calculate the average of the V_p/V_s ratio. In addition to that, three 1-D velocity models are tested to locate the earthquake locations.

Many criteria are used to optimize the best parameters to estimate the earthquake locations. The root-mean-square (RMS) travel time residual is the most important one. Also are use the horizontal error (ERH) and the depth error (ERZ) to compare these models.

Finally, many factors affect the accuracy of the earthquake location. Two factors are highlighted in this thesis; the picking error and the seismic network(s) geometry.

The SEISAN package software is used during the analysis process.

5-2. The Description Data

All the available earthquake waveforms have been used to study the seismicity of the main geological structures in the Levant region from the beginning of 2010 to the end of 2016 (Figure 5-1). We mainly focus on the study of the seismicity along DST and the surrounding area. Mainly, the DST is limited to the area bound by latitude (28 – 37.5°) N but variable longitudes (34 – 35.3°) E in the south (Aqaba segment) to range (36-37.5°) E in the north (Karasu segment).

Special attention is given to the data within the region bound by latitudes 29° and 30° and longitudes 36° and 36.7° where the Jordan Phosphate Mining company continuous large explosion activates. Therefore, we remove the events that have the following criteria, mentioned by (El-Isa Z. , 2017):

1- The events have magnitude < 4.

2- All the events have been recorded during the working hours of the day (11 am to 2 pm).

3- Mostly, these events have very shallow depths (0-10 km).

Figures (5-1 and 2) represent the temporal distribution of the events. The number of the events was high 2010 to 2013, while the number of the events decreased in 2014 to 2016. In addition, there was high seismic activity during 8 am to 3 pm.

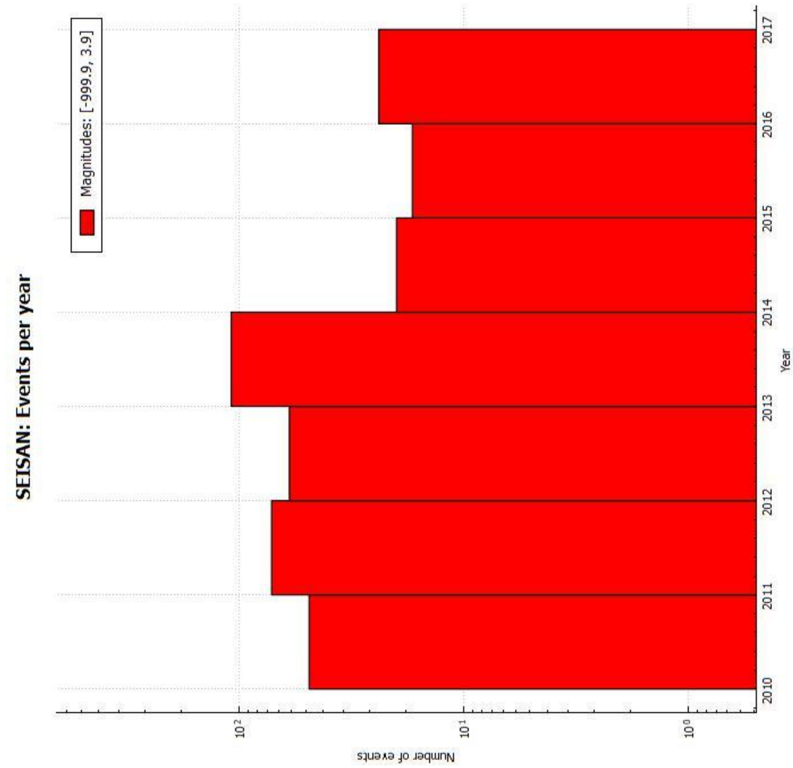

(a)

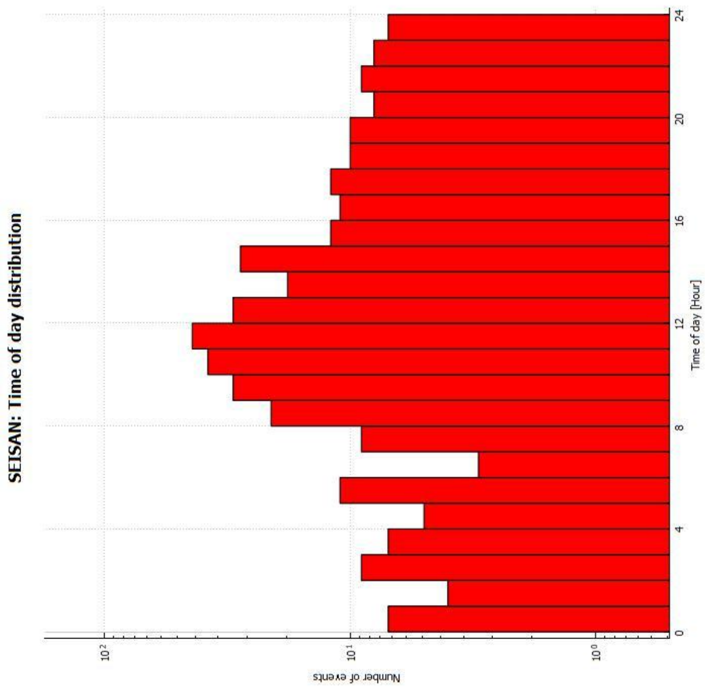

(b)

Figure 5-1: (A) The number of earthquakes each year. (B) The daytime of distribution for all data**.**

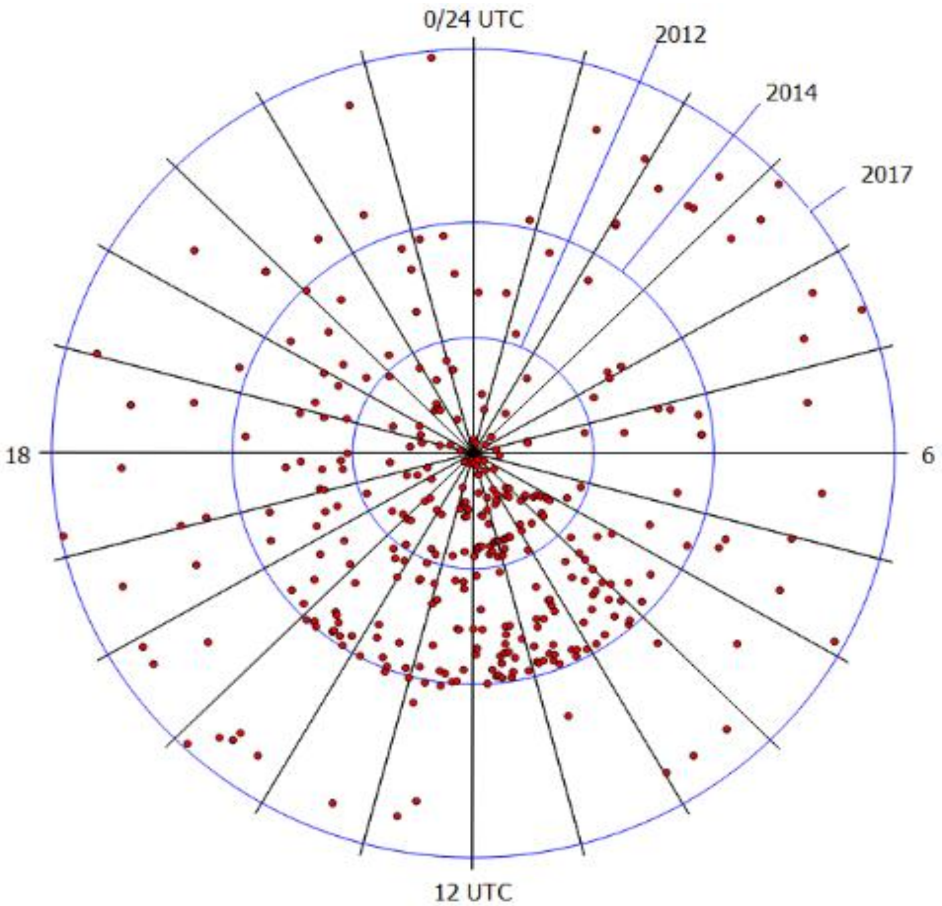

Figure 5-2: The temporal distribution of the earthquakes. The red points represent the earthquakes, organized as time, day, month and year, respectively**.**

5-3. The Determination ($\mathbf{V_p/V_s}$) Ratio

We use SEISAN to analyze the waveforms. SEISAN provides the Wadati tool to calculate the V_p/V_s ratio for each event as well as the study area. In addition to that, the Wadati tool is one important tool to clarify the picking phases. The V_p/V_s ratio is directly related to the geological setting, considering the ideal condition.

Actually, the V_p/V_s ratio is related directly to poison's ratio (γ). It is defined as an elastic constant measure of the compressibility of the perpendicular material to the applied force, or the ratio of latitudinal to longitudinal strain. Simeon Poisson (1781 to 1840) is a French mathematician created the poison ratio formula, which can be presented as:

$$\gamma = \frac{1}{2} \frac{(V_p/V_S)^2 - 2}{(V_p/V_S)^2 - 1} \text{ ------------- (5-1)}$$

The events are used to calculate the ratio within the study area. These events have the following standards:

1- The events recorded by five seismic stations or more. These stations provide both information about the arrival time of the P and S waves.

2- The maximum RMS ≤ 2.8 seconds.

3- The Minimum correlation coefficient ≥ 0.8.

The V_p/V_s ratio ranges from 1.44 to 2.14 for the selected events (Figure 5-3 and 4) and (appendix 3). According to SEISAN results, the ratio average of these events is 1.75 with the standard deviation 0.08.

More than 75% of these earthquakes have the ratio between 1.65 to 1.88 values. While, about 15 % and 9.4% are less and above the 1.65 to 1.88, respectively. However, the ratio values are within the acceptable values according to the geophysical studies that occurred in the study area such as (El-Isa, Mechie, & Prodehl, 1987; Mohsen, 2004).

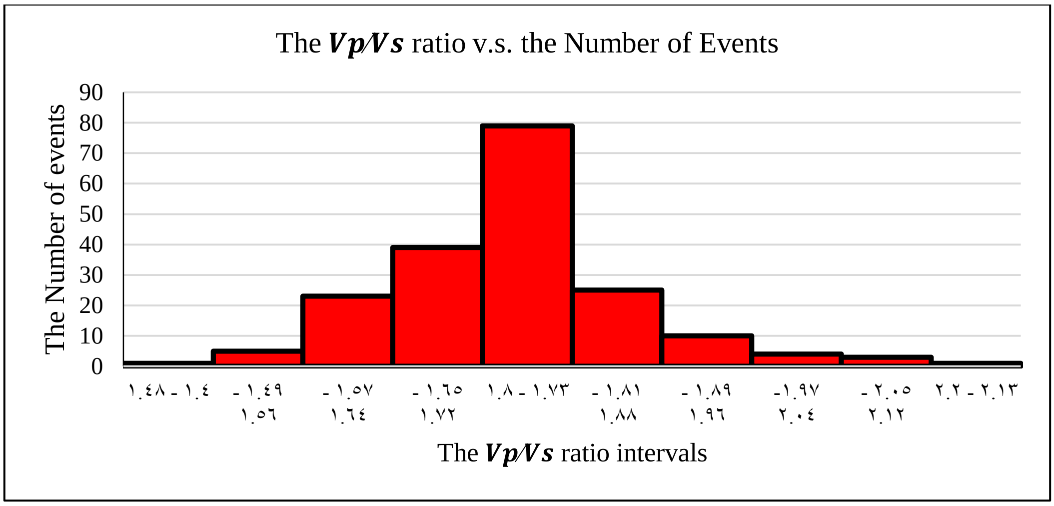

Figure 5-3: The Vp/Vs ratio distribution recorded at least by five stations.

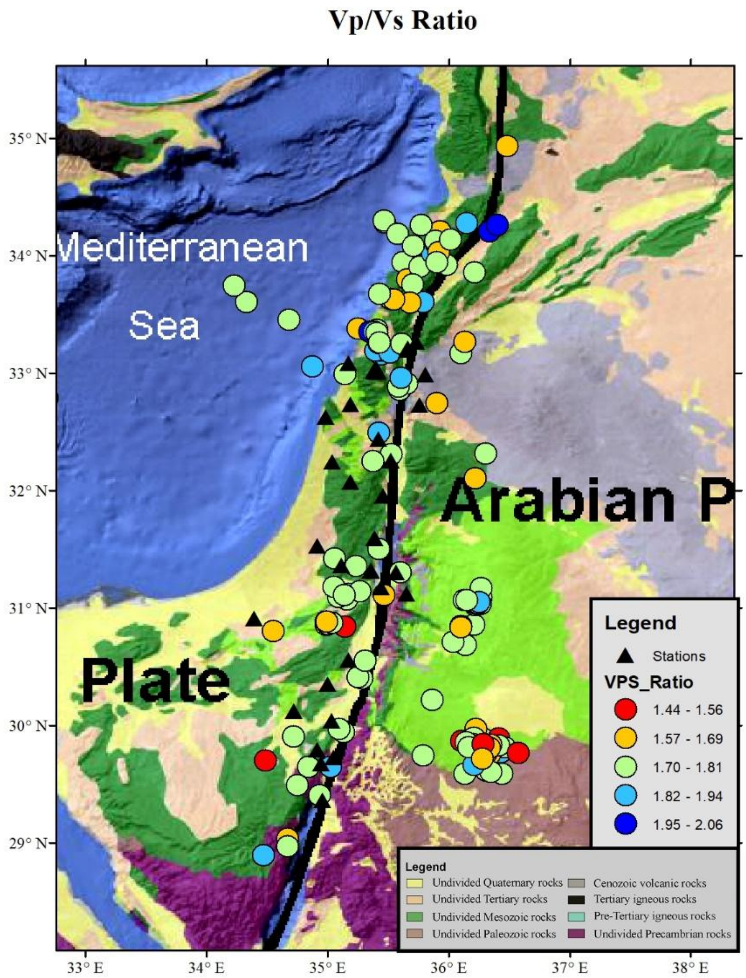

Figure 5-4: The spatial distribution of the (V_p/V_s) ratio, using the Wadati results (after (Radaideh, et al., 2016)).

5-3-1. The Relation between the Correlation Coefficients of the V_p/V_s Ratio and the Number of the Selected Events (Reliability Analysis)

This analysis is an important step to verify the reliability analysis of the (V_p/V_s) ratio value. As well as, the correlation coefficient value improves the linearity of the (V_p/V_s) ratio average (Wang , et al., 2008). The lowest value of the correlation coefficient is 0.83. While, more than 94% of the events has a correlation coefficient above 0.96 (Figure 5-5). Whereas, the standard deviation equals 0.08 the result is taken from the WADATI tool. This means, the error of the (V_p/V_s) ratio value is relatively small. On the other hand, these data demonstrate that the correlation coefficients are linear fitting.

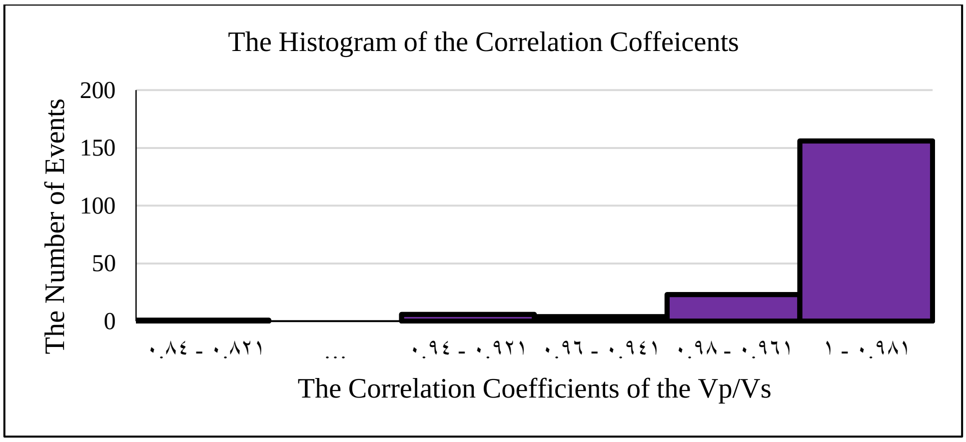

Figure 5-5: The histogram of the correlation coefficient of the selected events, using the Wadati results.

5-3-2. The relation between RMS error and the number of events

The root-mean-square (RMS) travel time residual is presented in seconds. The importance of this parameter is that it measures the fit of the observed and the calculated arrival times from the computed location of the event. The higher RMS value reflects a worse fit of the data. Whereas, the Wadati diagram provides the origin time of the events (calculated time). While, the observed arrival times are considered as the observations times (P- and S-wave arrival times).

Figure (5-6) represents the histogram of the RMS of the selected events. About 70% of the selected events have RMS less than 1 second. While, more than 91% of the selected events have RMS, less than 1.5 seconds.

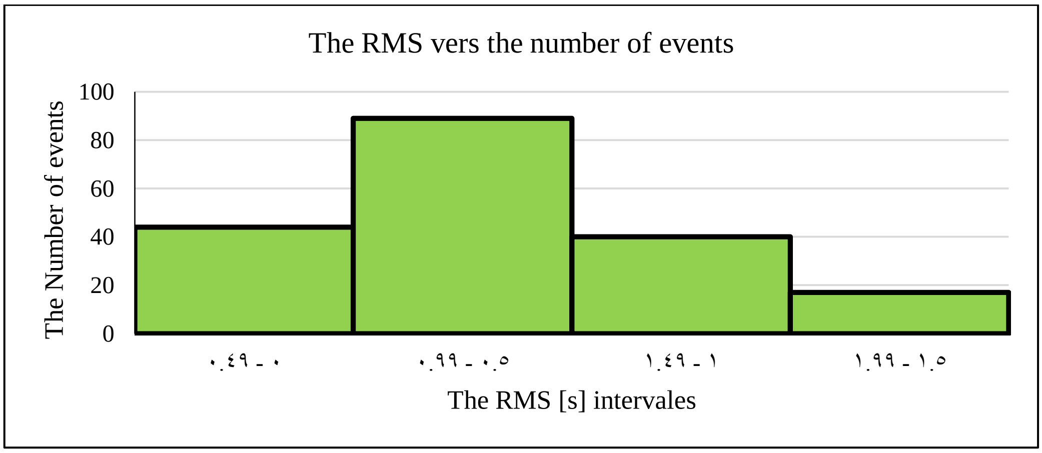

Figure 5-6: The RMS histogram of the selected events, using the Wadati results**.**

The geological structure complexities are one of the most important factors to study this ratio. (Mechie, et al., 2005) provides valuable information about the (V_p/V_s) ratio in the southern part of the our study area. It used the wide-angle reflection/refraction experiment crossing the DST. The average crustal ratio (V_p/V_s = 1.76–1.78) under their profile. In spite of this, the (V_p/V_s) ratio varies between (1.73–1.91) in the first two layers. While, the ratio arrives to (V_p/V_s= 1.78) in the lower crust.

(El-Isa, Mechie, & Prodehl, 1987) used seismic refraction to determine the Poisson's ratio model for the crust of the Jordan-Dead Sea rift and its eastern and western flanks region. It illustrates the Poisson's ratio average 0.25 (V_p/V_s= 1.73) for the upper crust, while this value increases to about 0.32 (V_p/V_s= 1.94) in the north-west Jordan within sediments milieu. While, the Poisson's ratios, ranging from 0.29 (V_p/V_s= 1.84) to 0.32 for the lower crust milieu, which is more than 20 km depth.

(Mohsen, 2004) sheds light on the earth crust and the upper mantle structure in the southern part of the study area using receiver function methods. The (V_p/V_s) ratio ranges 1.73 to 1.83 with an average of 1.77. It is also concluded, if the Moho depth is more than 34 Km, the (V_p/V_s) ratio will be about 1.76.

5-4. The Re-location of the Earthquakes

The velocity model is an important parameter that is used to locate the seismic sources location. The velocity models can be divided into 1-D, gradual and 3-D models. While, the 1-D model is the most common one that is used in the routine earthquake location.

Several authors produced 1-D velocity models for the Levant region from either the local or the region-scales studies of the seismicity. These models include the IS, the JS and the (El-Isa Z., Mechie, et al., 1987) model. The IS, JS and (El-Isa Z., Mechie, et al., 1987) models will be tested and compared later.

The comparing process will use three criteria. The most important one of these criteria is the RMS residual time. In addition to that, the ERH and the ERZ will be used. While, most of the seismological location software programs provide these information.

The HYPOINVERSE software will be used to estimate the earthquake location. This common software is used by the seismologists around the world. It provides important information about the earthquakes location. In addition to that, it shows the location errors (RMS, ERH and ERZ), the number of stations used to estimate the location, gap (as the angle between the epicenter and an area that has not been covered by seismic stations), etc...

5-4-1. Comparing between the velocity models

A 1-D velocity model of specific region is a complicated issue in the seismology, considering the complexity of nature, the geological formation and setting, seismic active zones within mathematical results. Mostly, it is essential to create a 1-D velocity model considering the geophysical(s) information, such as seismic, gravity, etc. However, the three velocity models will be tested to estimate the earthquake locations as mentioned above. These models are used by local agencies (JS and IS). In addition to that, the (El-Isa Z., Mechie, et al., 1987) model was developed by seismic study. Figure (5-7) and (appendix 4) represent the velocity models that will be tested.

The first model is used by JS. This model includes six layers. The top depths of these layers are 0, 1.5, 10, 18, 20, 28.5 and 33.5 km, which have the P velocity 3.5, 6.05, 6.32, 6.5, 6.65, 7.38 and 8.10 km/s, respectively (Al-Tarazi, et al., 2006).

The second model is IS. This model involves the primary wave velocity (P velocity) which is 3 km/s for the surface layer. The P velocity increases to 4.36 km/s in depth 1 km/s. The top depth of the third layer is 3.6 km and has the P velocity 5.51 km/s. The top depth of the fourth layer increases until 10.8 km with the P velocity to 6.23 Km/s. The P velocity is 7.95 km/s for depth 32.44 km or more (Feigin & Shapira, 1994).

The third model is the results of (El-Isa Z., Mechie, et al., 1987). They studied the geological structure of both wings of the DST, which used the seismic refraction method in this study. One important result of this study is creating the 1-D velocity model for their study region. This model contains six layers. The top depths of these layers are 0, 1, 5, 10, 18, 20 and 34 Km that has the P velocity 3, 4.75, 6.20, 6.30, 6.50, 6.65 and 8 km/s, respectively.

Figures (5-8, 9 and 10) represent the earthquake locations by using the JS, IS and (El-Isa Z. , Mechie, et al., 1987) models, respectively.

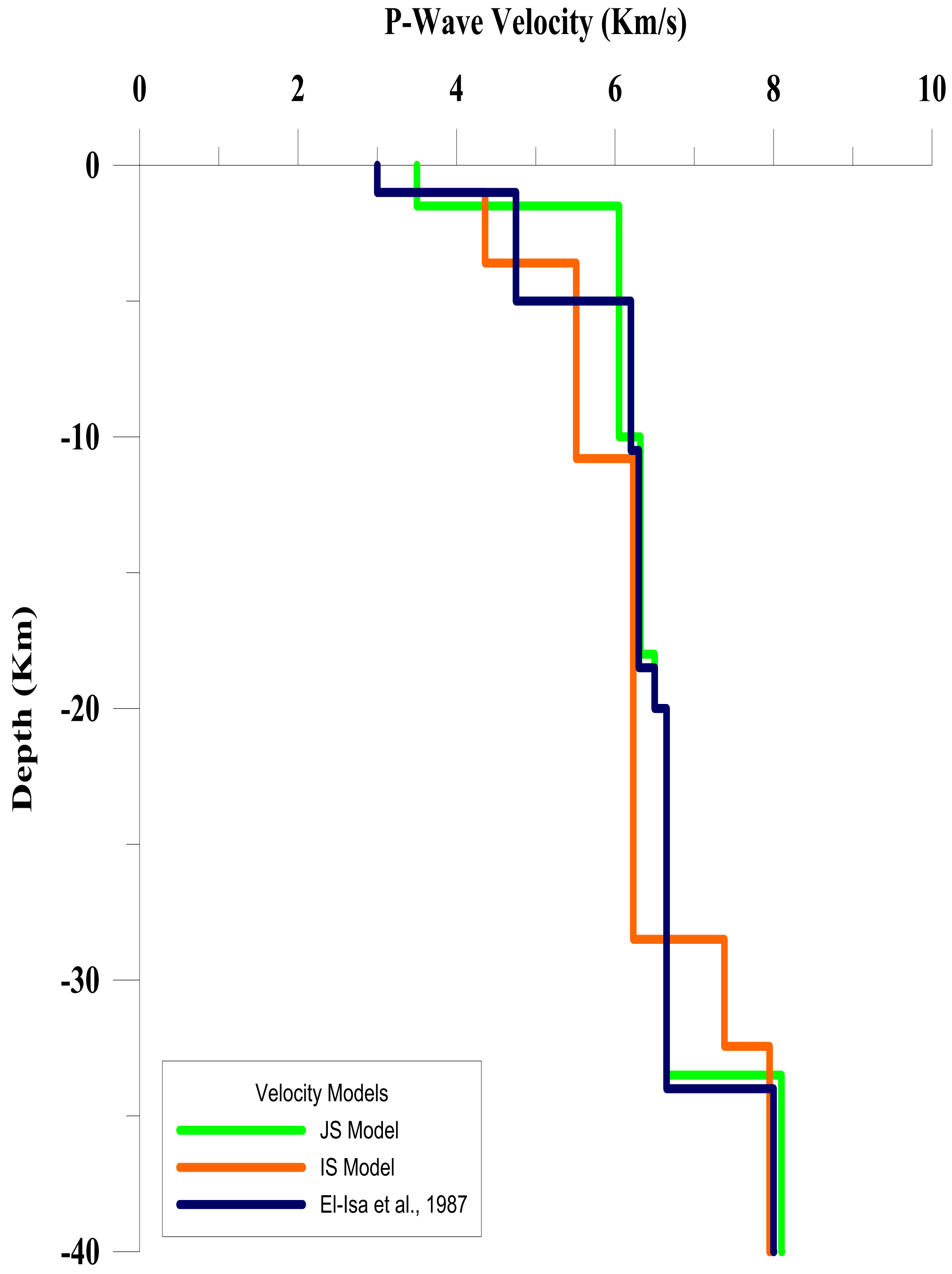

Figure 5-7: The velocity models tested.

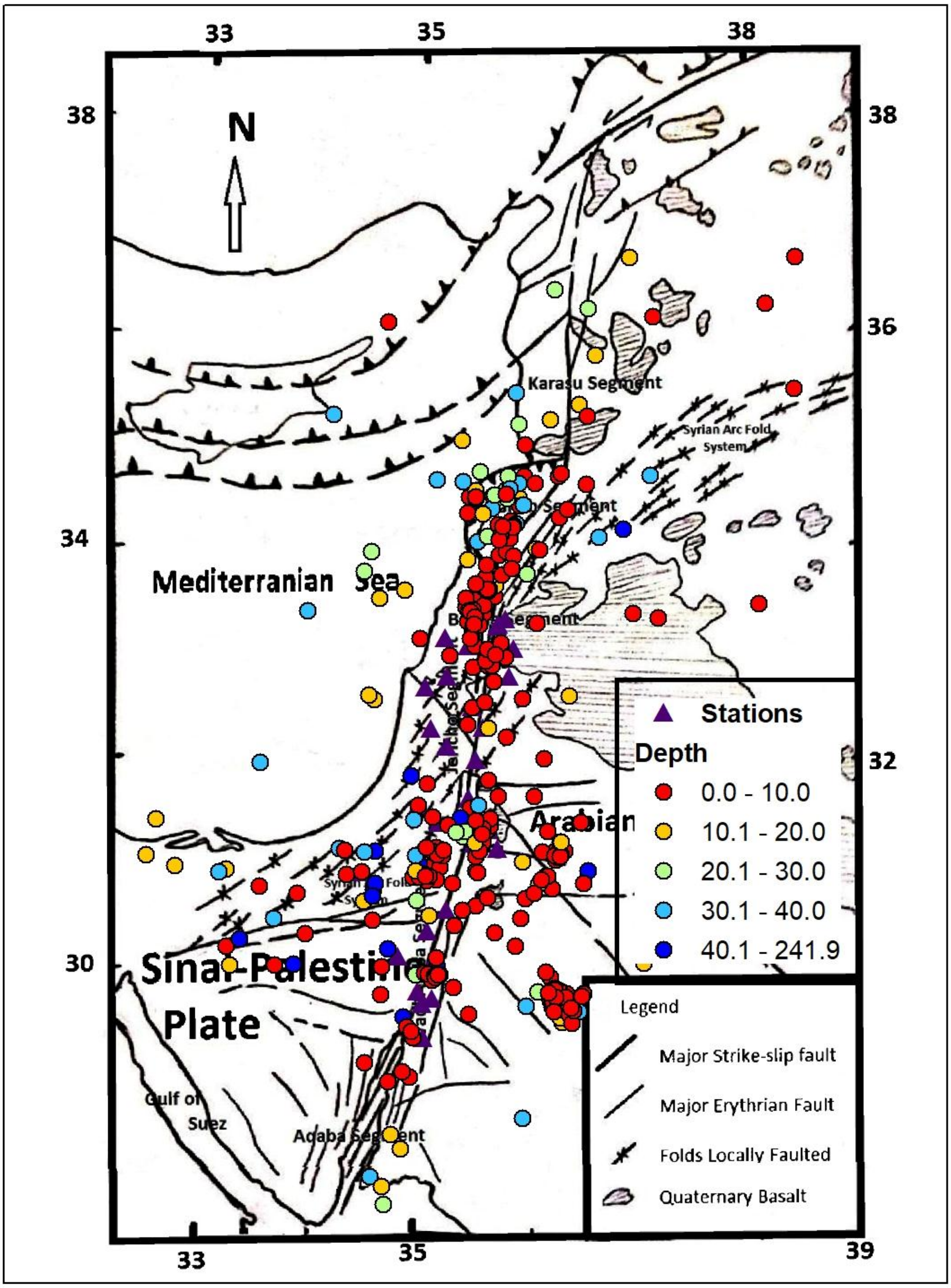

Figure 5-8: The epicenter map represents the earthquake distribution by using JS model.

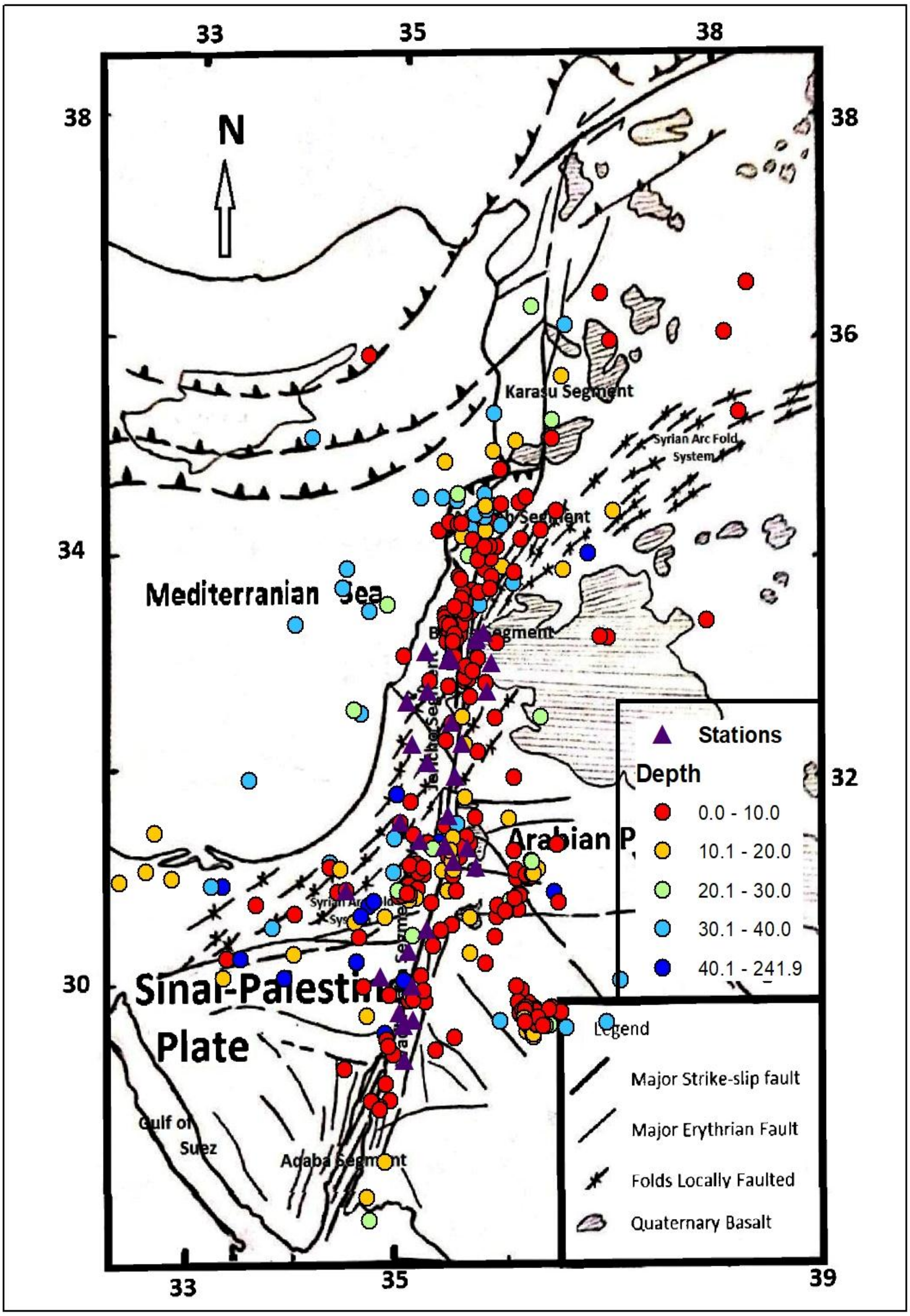

Figure 5-9: The epicenter map represents the earthquake distribution by using IS model**.**

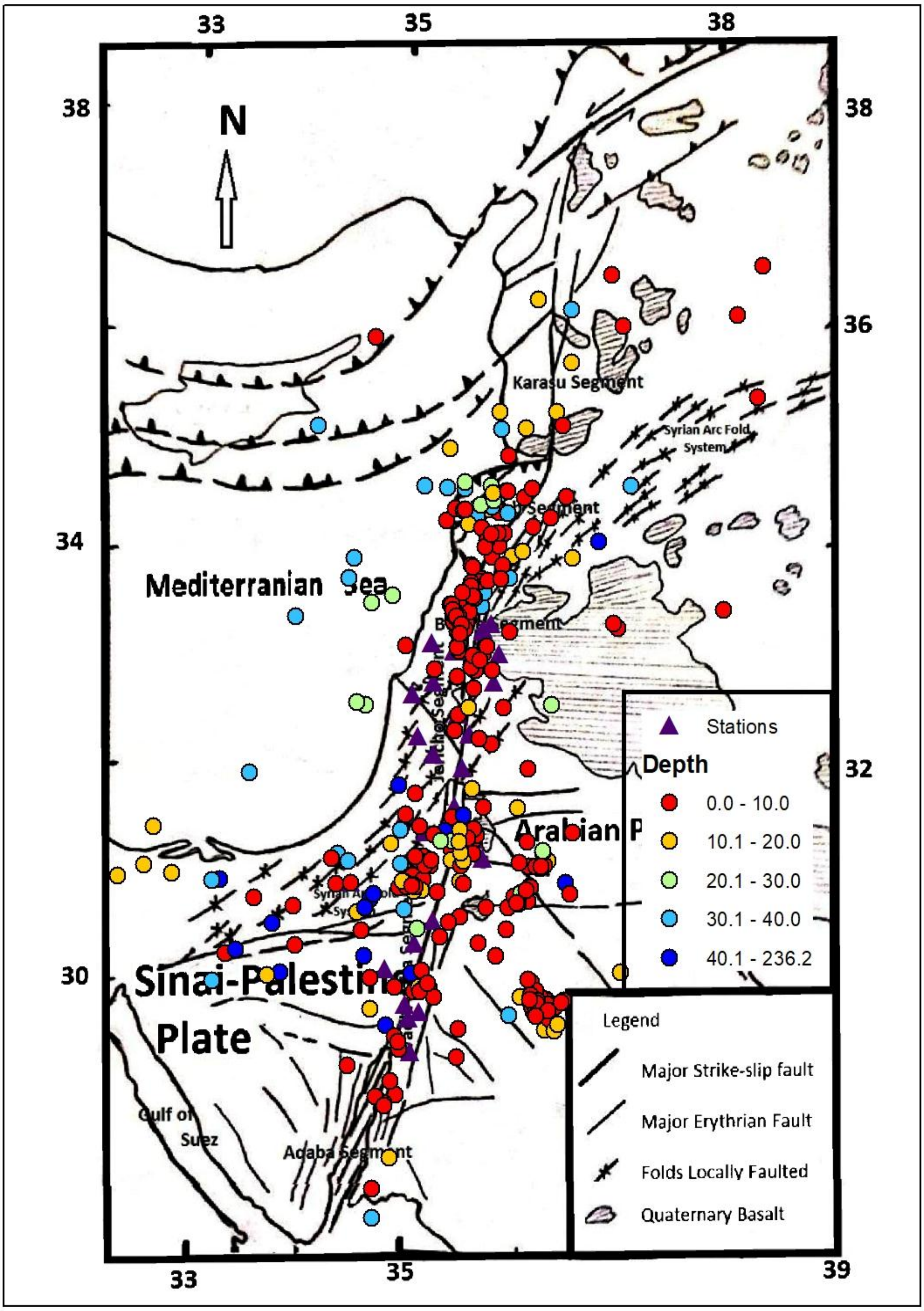

Figure 5-10: The epicenter map represents the earthquake distribution by using (El-Isa Z. , Mechie, et al., 1987) model.

The RMS, ERH and ERZ will be used to compare the results of those models (figure 5-11 and 12). The RMS is mainly affected by the velocity model used to estimate the seismic source location. As well as, it is used to improve the velocity model, which is used in the routine earthquake location. While, the ERH and ERZ considered as secondary criteria, respectively, are used to improve the velocity models.

The average of the RMS for these models ranges 4.29 to 4.45 [s] (figure 5-11). These averages are 4.29, 4.32 and 4.45 [s] for IS, (El-Isa Z. , Mechie, et al., 1987) and JS model, respectively.

The average of the ERH for these models, ranging 49.6 to 52.14 [km] (figure 5-12). The IS, JS and the (El-Isa Z. , Mechie, et al., 1987) model have the average of the ERH 49.6, 50.92 and 52.14 km, respectively.

While, the minimum and maximum average of the ERZ are 40.73 and 43.69 km, respectively. The average of the ERZ are 40.73, 41.84 and 43.69 km for IS, (El-Isa Z. , Mechie, et al., 1987) and JS model, respectively.

The best model is IS. According the criteria are used, which the RMS, ERH and ERZ are 4.29 seconds, 49.6 km and 40.73 km. Whereas, the average of these values represent the lowest values compared with other two models (figure 5-11 and 12).

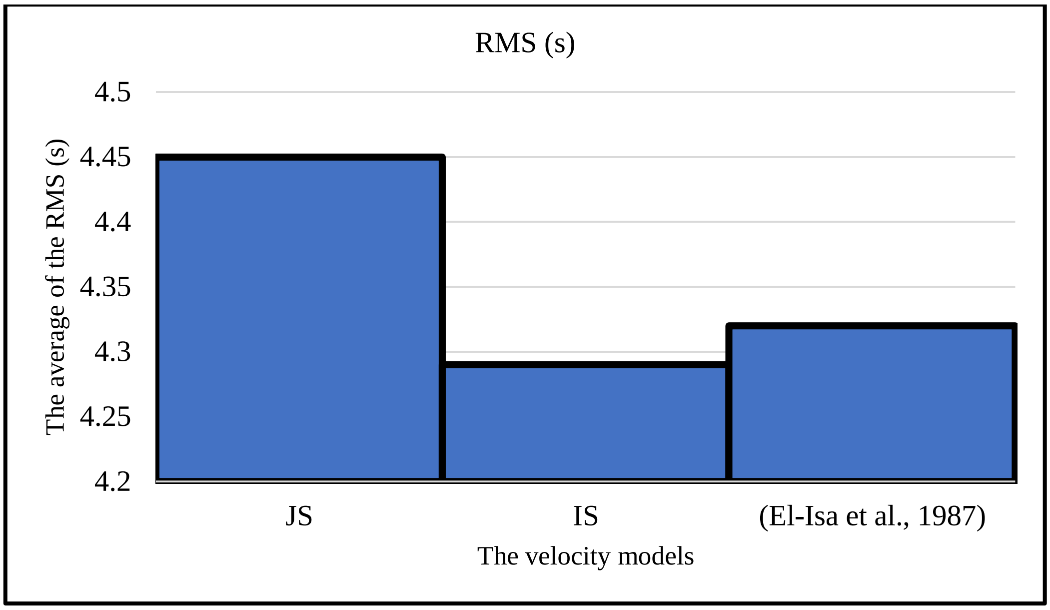

Figure 5-11: The RMS average of the earthquakes tested by the three models.

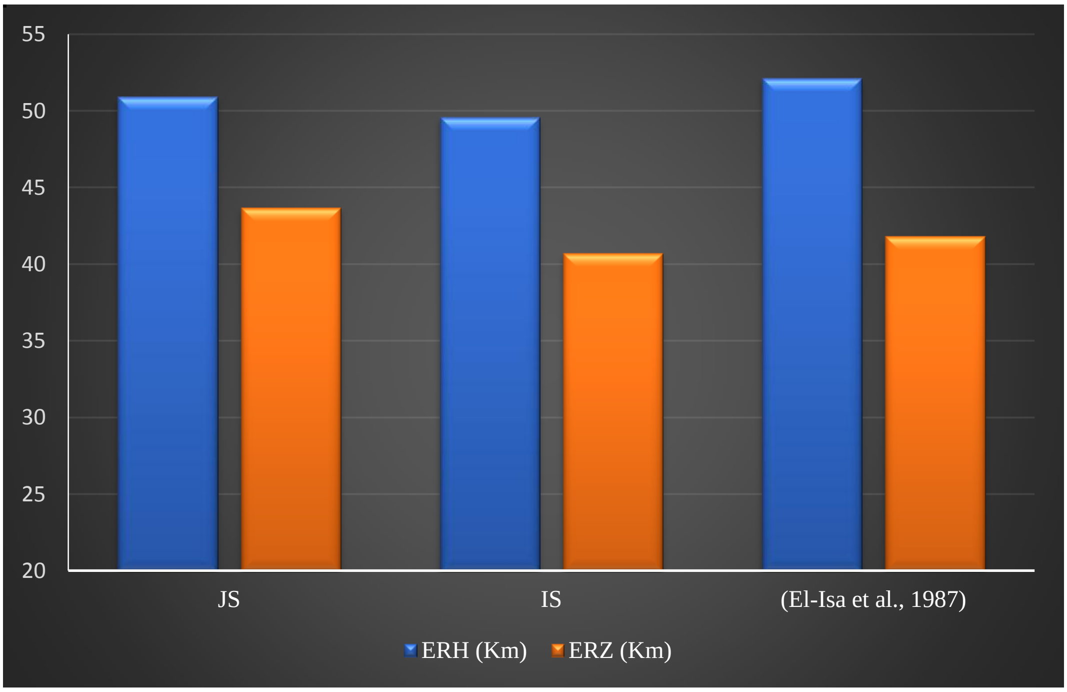

Figure 5-12: The ERH and ERZ average of the earthquakes tested by the three models.

5-4-2. Initiative velocity model and the Epicenter Map

The (El-Isa Z. , Mechie, et al., 1987) model is considered as a reference of the velocity model in this study area. As a general overview, the JS and IS models respect the achieved results.

The (El-Isa Z. , Mechie, et al., 1987) model will be modified to have a stable model. The initiative model keeps the layer thickness of the original model. However, the top depths of these layers are 0, 1, 5, 10, 18, 20 and 34 km, which have modified the P velocity 3, 4.76, 6.25, 6.29, 6.50, 6.58 and 7.65 km/s, respectively. Figure (5-13) and appendix (4) represent (El-Isa Z. , Mechie, et al., 1987) model (red line) and the initiative one (black line).

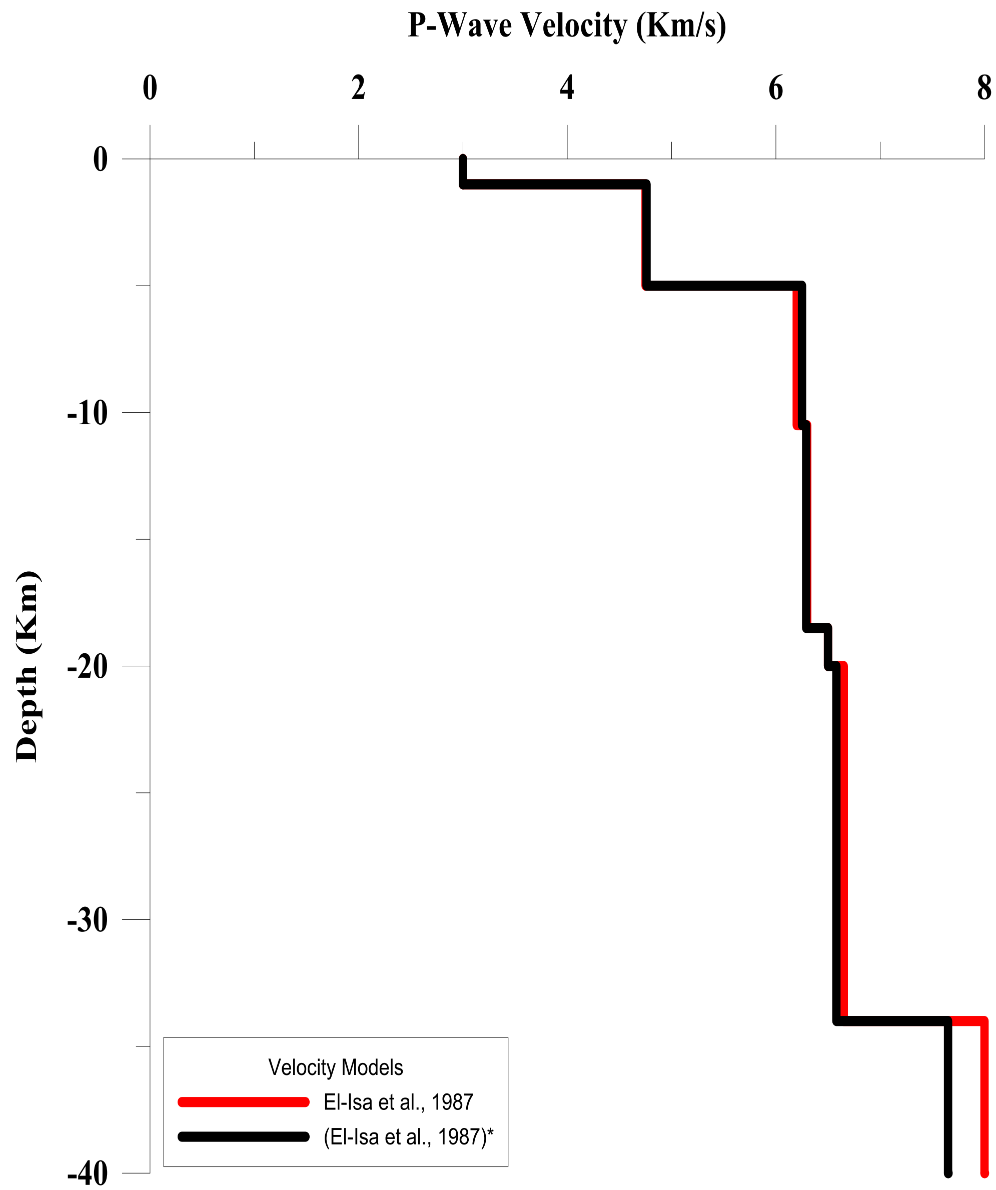

Figure 5-13: The (El-Isa et al., 1987) model is red line. The modification model (El-Isa et al., 1987)* is the black line.

This modification directly affects the earthquake location accuracy. Whereas, the average of the RMS decreases until 4.1 second (figure 5-14). In addition, the average of the ERH decreases until 45.59 Km. While, the average of the ERZ increases to 42.26 Km (figure 5-15). The RMS and ERH represent the lowest values compared with the other velocity. While, the ERZ increases to 42.26 km. However, these results improve the initiative model, which helps to increase the earthquakes location accuracy.

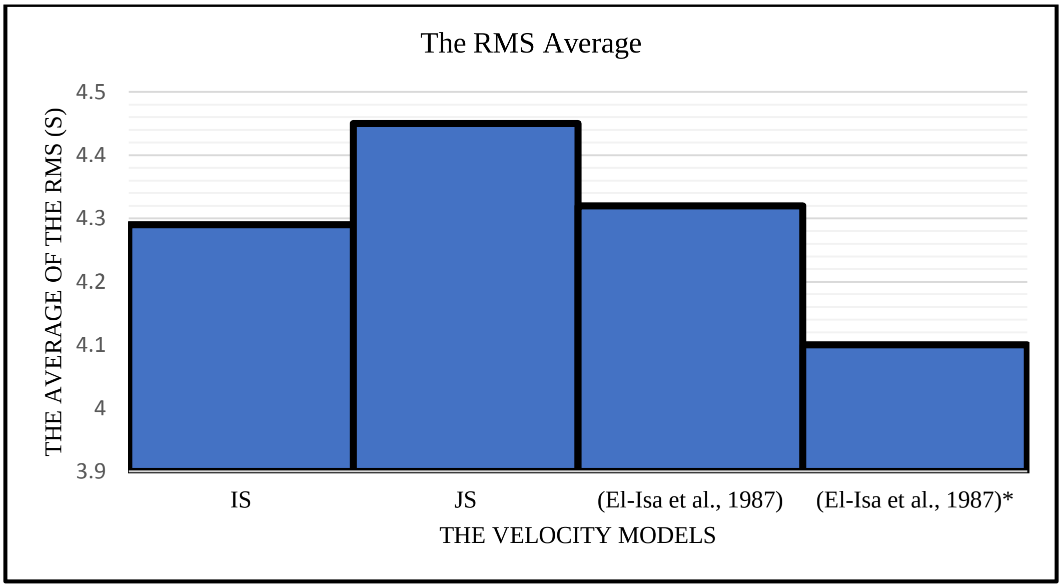

Figure 5-14: The RMS average of the earthquakes including the results of the modification model.

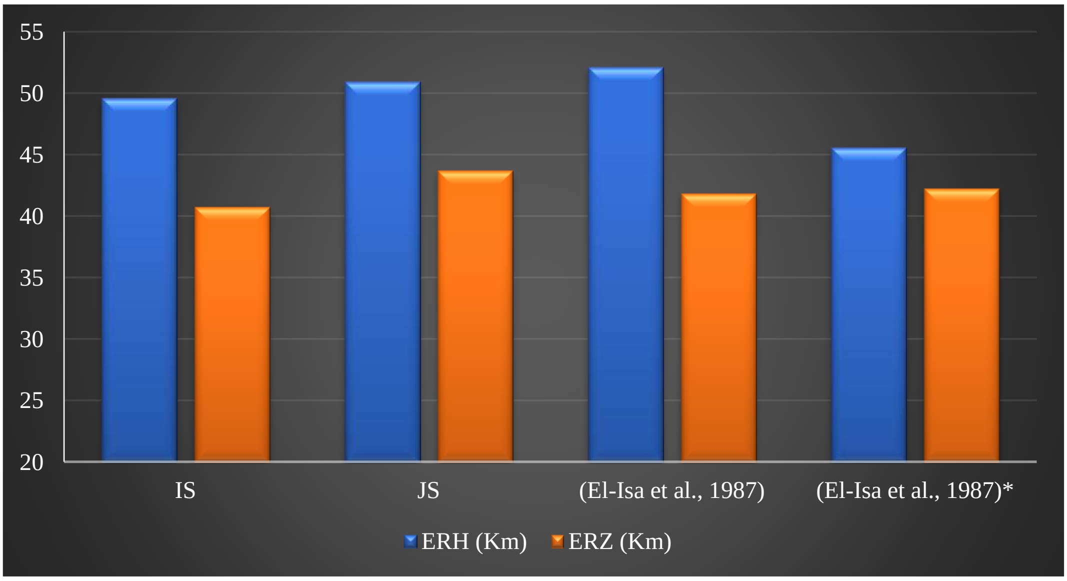

Figure 5-15: The average ERH and ERZ for the earthquakes including the results of the modification model.

Figure (5-16) and appendix (5) represent relocation of the earthquakes, which is prepared by the initiative model. The focal earthquakes have a good correlation with the geological and tectonic structures. Most of the focal earthquakes situated on the tectonic structures.

Most of the focal earthquakes are concentrated in the north of Tiberias (the GHAB basin). Most of the focal earthquakes in this part occurred along DST. The concentration of the focal depth is very shallow (≤ 10 km), except in the most-northern part of the study area (≤ 40 km).

The focal earthquakes dispersed on the south of the Dead Sea. Figure (5-16) shows the Erythrean fault system (the shear belt zone) is more active than the DST in this part. Whereas, the DST has a significant seismic activity. The concentration of the focal depth is more than the northern part of the study area, which is about 40 km.

On the other hand, the focal earthquakes are shallow. Mostly, the depth is less than 40 km. These results are fit with the previous studies such as (Abou Karaki, 1987; Meghraoui, 2015; El-Isa, et al., 2015; El-Isa Z., 2017).

According to the geological and geophysical studies, the focal depth of the most of the earthquakes occurred with the crust (El-Isa Z., Mechie, et al., 1987; Mohsen, 2004; El-Kelani, 2005; Mechie, et al., 2005). Whereas, the crust depth increases in the southern part of the study area, which is roughly 40 km.

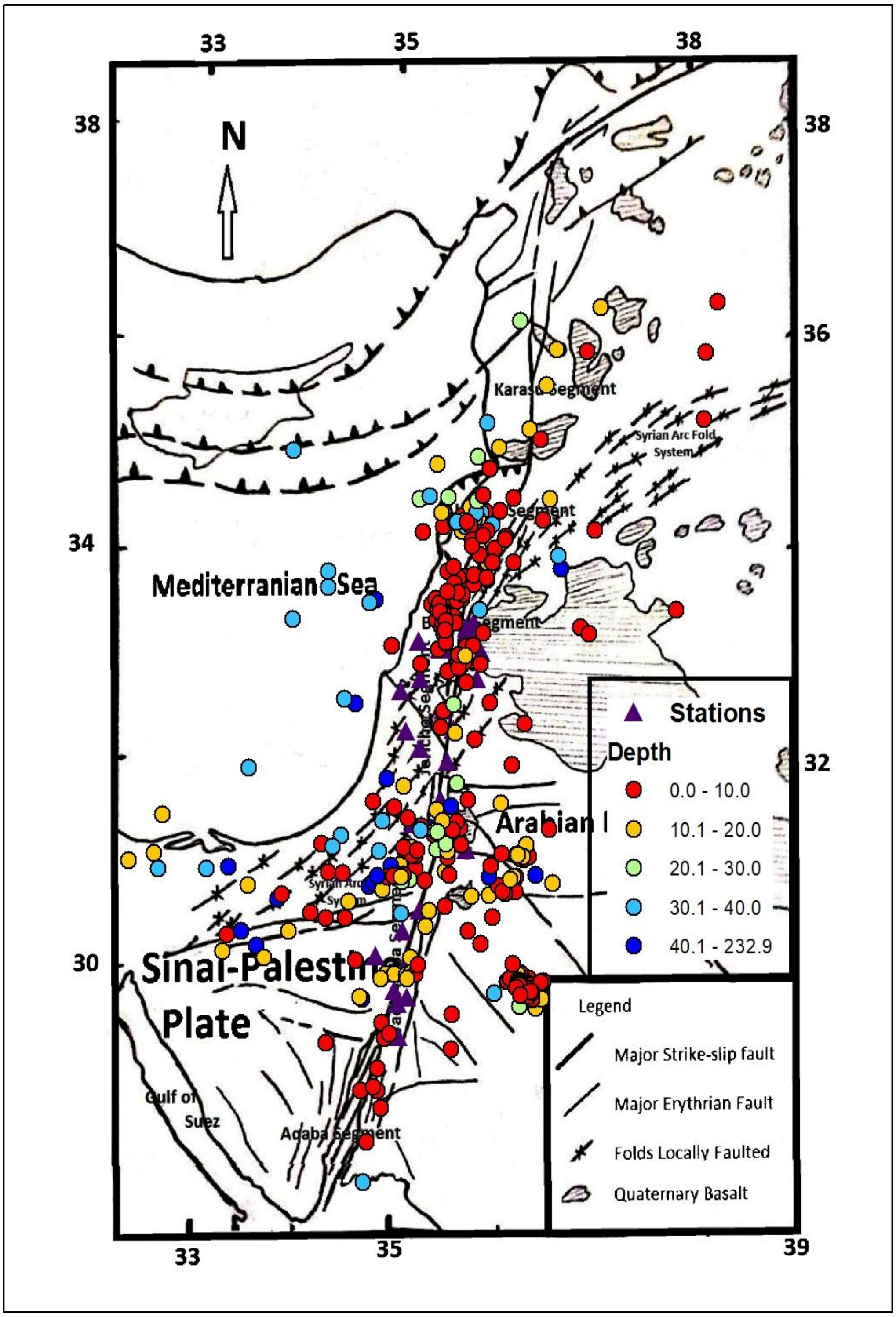

Figure 5-16: The epicenter map, using the modification model.

5-5. Factors affecting the focal location accuracy

The earthquake focal accuracy depends on many factors. The most important of these factors are the seismic network characteristics and the velocity model that used to estimate seismic sources. Whereas, the velocity model effect was discussed on previous section. On the other hand, the quality of the localization is affected on the seismic network geometry, which detect a seismic event.

Two main conditions to have well constrain an earthquake focal, having sufficient number of seismic stations near and around the epicenter recording a seismic event and clear signal to determine the P and S phases (low noise during the recording). Large azimuthal gap or bad seismic distribution (Network(s) geometry) around the epicenter can drive to miss location.

Mostly, high-level noise can lead up to large mistake to determine the principal phases (P and S), which touching the accuracy of the hypocentral parameters. So, the Wadati diagram was used to check and confirm the picking during our analysis.

This section will discuss two important factor can affect the earthquake accuracy; the error picking and the network geometry.

5-5-1. The Error of Arrival Time Picks

The error in picking is one of the important factors influences the estimation of the hypocenter location (Billings, et al., 1994). As well as, it is one of the important information that affect on the RMS arrival time residual. Whereas, the earthquake location is based mainly on identifying the time of the P and S phases.

The significance of this section is highlighted of the errors in picking step and make a comparison the different phase arrival time to verify it. One common way to calculate the error picking using the difference between two readings of phase(s) arrival time. The comparison is done by using the difference of the P-wave arrival time for our data and the European-Mediterranean Seismological Centre (EMSC), which the last one includes the picking time for the local seismic observatories (JS and IS).

Usually, the picking will be different between seismologists, when done manual pick to determine different phases. As well as, the picking will differentiate between seismologist agencies, spatially, when the noise is great.

There are some suggestions for standard setting to measure the noise such as signal-to-noise ratio (SNR) (Zeiler & Velasco, 2009, 2011). Unfortunately, the quality of earthquake waveform is not documented in seismology catalogues such as the International Seismological Centre (ISC) and the EMSC. While, the noise can be shown and estimated by institution or who is making the picks.

In addition to that, the technological development has greatly helped seismologists to determine the different phases of the arrival time. However, this development has not developed enough to give accurate and unquestionable results (Di Stefano, et al., 2006). Whereas, the automatic picking is needed manual checking to conform the automatic results by professional scientists. Therefore, one possibility is causing the picking error that does not check the automatic picking, spatially for small earthquakes. In addition to that, one important factor to note is the analyst's experience has a key role in reducing this error.

Figure (5-17) and appendix (6) represent the error picking of P-wave arrival time. Whereas, about 125 P-wave arrival time are compared between our data and the EMSC catalogue.

However, most of the difference in the figure (5-17) ranges between -0.7 to 1 second. The major of the difference is ranging between -0.2 to 0.2 second. Some of the values are more than previous interval, which represent a small percent of the population of 125 P-wave arrival time.

The error picking is very critical for our data, due to lack of seismic data information. This lack back to a shortfall in seismic stations, especially during the first years within the study period. The second reason is not to share seismic data.

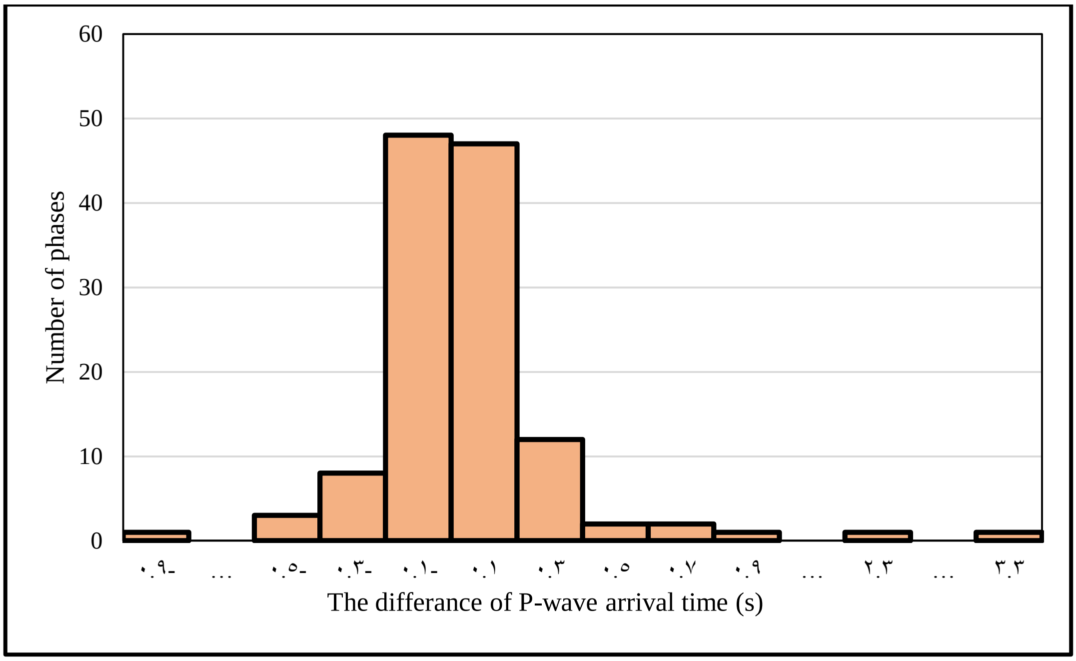

Figure 5-17: Difference in P-wave arrival time between our data and EMSC bulletin, which are more than 120 P-wave arrival time compared.

5-5-2. The Network Geometry

Network geometry (the seismic station distribution) is another important factor that affect the focal location accuracy. Whereas, the software use to estimate the hypocenter location (HYPOINVERSE) provided the gap (azimuthal gap), which it provides the information about seismic station distribution around each event. The azimuthal gap can define as the angle of between seismic stations surrounding the epicenter (the major area that does not provide data to locate the seismic event).

Figure (5-18) represents the spatial distribution of the gap events. Whereas, the low value of gap improves the goodness of seismic station distribution (networks geometry) around the epicenter, while a high value means bad distribution around the epicenter. According figure (5-18), the gap is high, which is it bigger than 75° due to bad seismic station distribution around the epicenters and (or) lack of seismic data sharing among local agencies.

Figure (5-19) provides statically information about the gap of earthquakes that presents in figure (5-18). Whereas, the earthquakes around the Dead Sea have the lowest azimuthal gap values (≤ 180°), which represents about 20%. While, the azimuthal gap increases as we head to the east or west of the Dead Sea. Whereas, the azimuthal gap between (181-240°) represent less than 22%. Whilst, the azimuthal gap (241-300°) represents more than 31%, which it located in the eastern, western and some of it in the northern part of the study area. The highest values of the azimuthal gap (≥ 301°) locate in the most both parts of the north and south of the study area. Lack of data from the neighboring countries is the main reason to increase the azimuthal gap, spatially, in the north and south part of the study area.

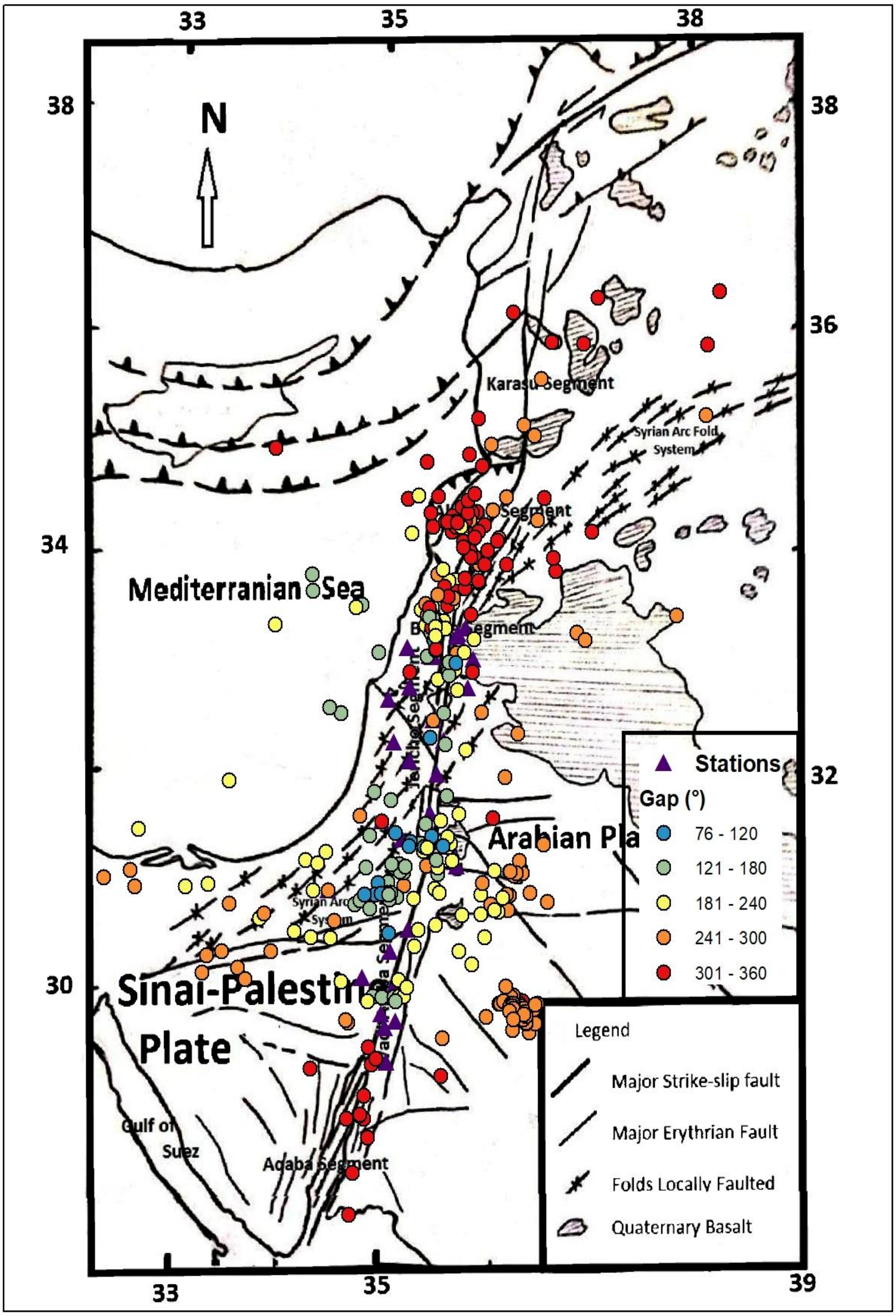

Figure 5-18: The azimuth gap of the spatial distribution of the events.

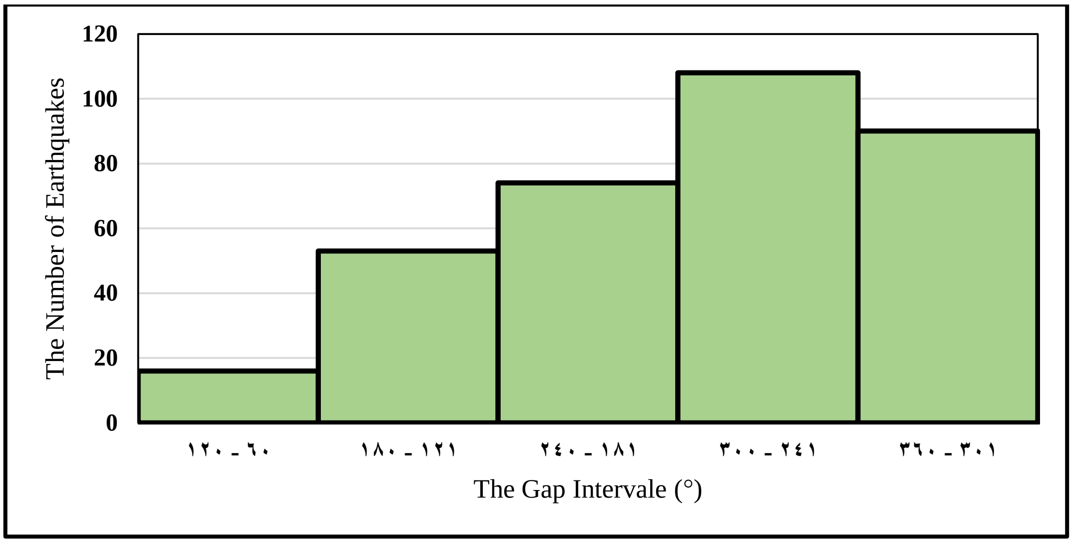

Figure 5-19: Statistical distribution of gap intervals verse the number of earthquakes.

The average of the azimuth gap of our data is about 249° due to lack of the seismic information especially form the neighboring countries that locate in the northern and southern sides of the study area.

As we mention above, there are a strong relation between the azimuth gap and the ERH and the ERZ. Therefore, in the following step are more details of these relationships:

5-5-2-1. The Relation of the azimuth gap and the ERH

More than 31% and about 55% of the earthquakes have ERH less than 20 km and 40 km, respectively, figure (5-20).

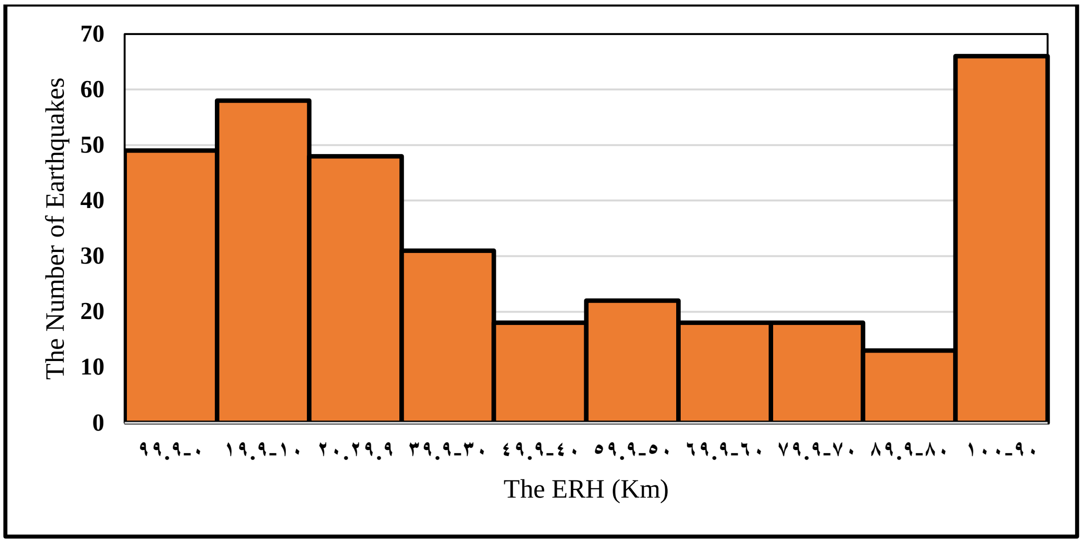

Figure 5-20: The ERH histogram of the Earthquakes.

Figure (5-21) represents the relation between azimuth gap and ERH. The ERH is sharply increasing for the events have azimuth gap more than 180°. Generally, the relationship between the azimuth gap and the ERH is positive. While, some of the events have a high azimuth gap and low ERH.

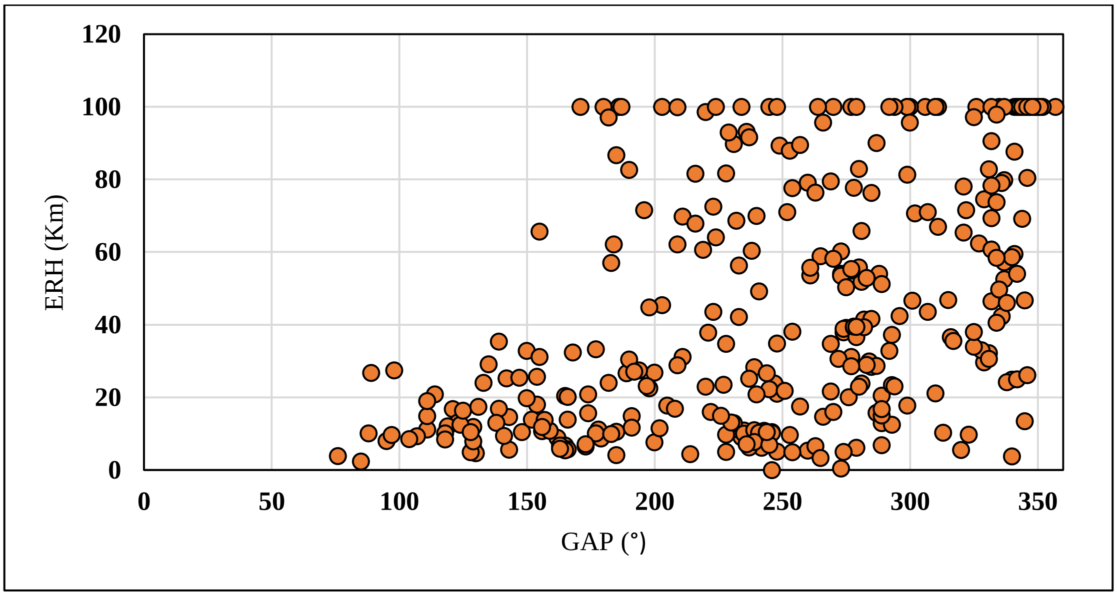

Figure 5-21: The function between ERH and the azimuth gap.

5-5-2-2. The Relation of the azimuth gap and the ERZ

More than 20% and 53% of the earthquakes have ERZ less than 10 and 30 km (figure 5- 22), respectively.

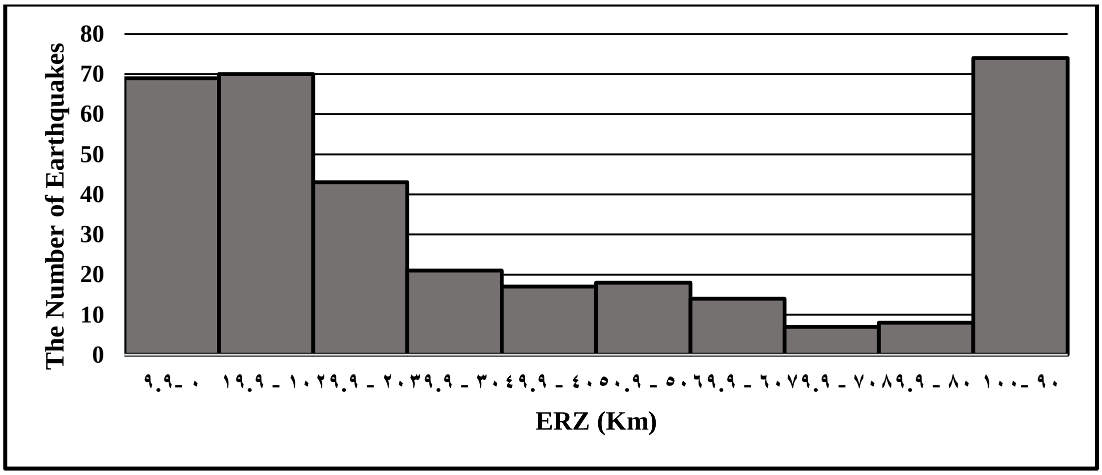

Figure 5-22: The ERZ histogram of the Earthquakes

Figure (5-23) shows the relation between azimuth gap and ERZ. The ERZ is suddenly increasing for the events have the azimuth gap more than 160°. Generally, the relationship between azimuth gap and ERZ is positive. While, some of the events have a high azimuth gap and low ERZ.

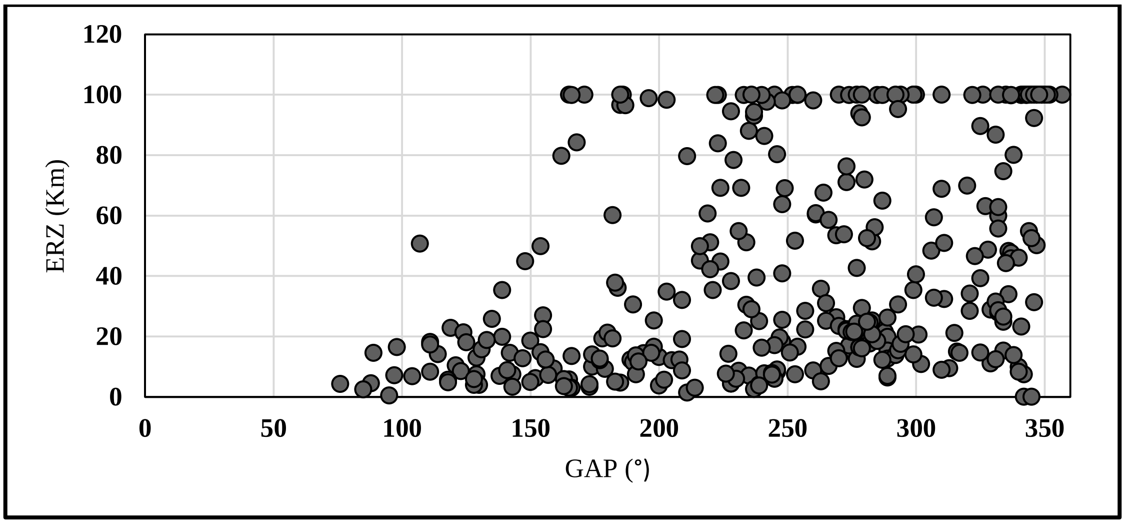

Figure 5-23: The function between ERZ and the azimuth gap.

Chapter Six
Conclusions

6-1. Introduction

Several seismic networks (nationals and global) have recorded the local seismicity that have occurred along the DST and the surrounding area between 2010-2016. These networks have seismic stations on both shoulders of the DST. The global data archive (EIDA) includes the seismic data of both the national and global seismic networks.

6-2. Conclusions

More than 60 seismic stations monitor the local seismicity along the DST and the surrounding area. Mostly, they have different types of sensors (very broadband, broadband and short period). The waveforms recorded by these stations are used to estimate the Vp/Vs ratio and relocate the earthquakes that occurred within the study area. More than 340 earthquakes are analyzed and relocated.

Three criteria (RMS, ERH and ERZ) were used to compare between different velocity models. These models are JS, IS and (El-Isa Z. , Mechie, et al., 1987). According the criteria is mentioned above, IS model considers as the best model.

Finally, many factors have effects on the focal location accuracy. A velocity model used to estimate the earthquake location is one of these factors. In addition to that, the picking error and the network(s) geometry are thoroughly discussed in this study.

6-2-1. The (V_p/V_s) Ratio

About 190 events are used to calculate the average of the (V_p/V_s) ratio. These earthquakes were recorded by five seismic stations at least. While, these earthquakes have a correlation coefficient ≥ 0.8. This ratio ranges between 1.44 -2.14, in which the average is 1.75 (± 0.08). In addition to that, the error of the correlation coefficient is very low, according different statistical analysis. Whereas, most of the earthquakes have a correlation coefficient above 0.96 (figure 5-5).

6-2-2. The Relocation of the earthquakes

The JS, the IS and the (El-Isa Z. , Mechie, et al., 1987) models are tested to locate the earthquakes (figure 5-7). The RMS, ERH and ERZ are criteria used to be compared with the accuracy of the earthquakes locations. The RMS averages are 4.29, 4.32 and 4.45 [s] for IS, (El-Isa Z. , Mechie, et al., 1987) and JS model, respectively (figure 5-11). While, the ERH averages are 49.6, 50.92 and 52.14 km for the IS, JS and the (El-Isa Z. , Mechie, et al., 1987) model, respectively (figure 5-12). In addition to that, the ERZ averages are 40.73, 41.84 and 43.69 km for IS, (El-Isa Z. , Mechie, et al., 1987) and JS model, respectively (figure 5-12).

According to the new epicenter map (figure 5-16), the focal earthquakes have a good correlation with the geological and tectonic structures. While, the map illustrates most of the earthquakes that occurred along the DST in the northern part of the study area. Nevertheless, the seismic activities are distributed in the southern part of the study area with a significant seismic activity along the DST.

The depths of the focal earthquakes are very shallow. Most of them are about 10 km in the northern part of the study area. While, most of them increase to be less than 40 km in the southern part of the study area.

6-2-3. The earthquake location accuracy is affected by

6-2-3-1. The errors in the arrival time picks

More than 120 P-wave arrival times are compared with our picking and the EMSC catalogue (figure 5-17). Most of the P-wave arrival times difference range between -0.7 to 1 second. While, most of them range between -0.2 to 0.2 second.

6-2-3-2. The Network(s) Geometry

The azimuth Gap, ERH and ERZ are used to illustrate the effect of the network(s) geometry. A positive relation between the Gap and ERH is shown in figure (5-21). The ERH is sharply increasing when the gap is more than 180°, where the ERZ is sharply increasing when the gap is more than 160° (figure 5-23).

References

- Al-Tarazi, E., Sandvol, E., & Gomez, F. (2006). **The February 11, 2004 Dead Sea earthquake ML = 5.2 in Jordan and its tectonic implication**. Tectonophysics, *422*(1-4), pp. 149–158. doi:10.1016/j. tecto.2006.05.010

- Helmholtz-Zentrum Potsdam. (2017, July 17). **GEOFON**. Retrieved from GEOFON Program: http://geofon.gfz-potsdam.de/

- Abou Karaki , N. (1987). **Synthese et carte sismotectonique des pays de la bordure orientale de la Mediterranee: Sismicite du systeme de failles du Jourdain**. Mer Marte. PhD thesis, IPGS, Univ. of Strasbourg I, 4l7 (In French).

- Abou Karaki, N. (1994). **Analysis, Relocation , and Focal Mechanism of the Carmel earthquake swarm of 1984**. *Dirasat, Vol.21B*(No.1), 281-291.

- Abou Karaki, N. (1999). **Location of the earthquake of Palestine 11-7-1927 A critical assessment** . Al yarmouk university, Faculty of Graduate Studies, 8(1), pp. 9-34.

- Akbar, A., Ryannugroho, R., Jousset, P., Gassner, A., Jaya, M., Sule, R., . . . Erbas, K. (2015). **Study on Seismicity and Seismic Tomography on a Hydrothermal System in West Java**. Proceedings World Geothermal Congress 2015, pp. 1-5.

- Al-Amri, A., Al-Dail, M., & Al-Haddad, M. (1996). **Recent Swarm Activity in the Gulf of Aqabah Region.** Eleventh World Conference on Earthquake Engineering (p. Paper No. 1945). Elsevier Science Ltd.

- Alavi, M. (1991). **Tectonic Map of the Middle East**, Scale 1:5,000,000. Geological Survey of Iran, Tehran.

- Al-Qaryouti, M. (1990). **Earthquake sequences (swarms): a characteristic of the seismicity of the Jordan rift. Amman**: Thesis (M. Sc. in Geology)-- University of Jordan.

- Al-Qaryouti, M. (2002). **Earthquake Strong Motion Data Analysis of the Gulf of Aqaba Activity for 1993-2001 and Engineering Seismology Implications in Aqaba Area**, Jordan. Jordan: Ph.D thesis, University of Jordan.

- Al-Qaryouti, M., & Al-Tarazi, E. (2007). ***Local Site Effects Estimated from Ambient Vibration Measurements at Aqaba City, Jordan.*** **Journal of Earthquake Engineering**, 11, pp. 1-12. doi:10.1080/13632460601033777.

- Al-Sa'adani, A. (1971). **Kashf al-salsala an wasf al-zalzala. (A.-S. Galal-Aldin, Ed.) Tokyo**: Multilingual Digital Library of Asian Source Materials, The University of Tokyo. Retrieved from http://ricasdb.ioc.u-tokyo.ac.jp.

- Al-Tarazi, E. (2000). **The Major Gulf of the Aqaba Earthquake, 22 November 1995 – Maximum Intensity Distribution**. Natural Hazards, 22, pp. 17–27. doi:10.1023/A:1008109810031

- Al-Tarazi, E. (2005). **Investigation of the Effects of Earthquake Swarms in the Seismic Hazard in the Gulf of Aqaba, Northern Red Sea.** Dirasat, Pure Sciences, 32 (1), pp. 55-68.

- Ambraseys, N. (1978). ***Middle East—A Reappraisal of the Seismicity***. **journal of Engineering Geology and Hydrogeology**, 11, p. 19-32. doi:10.1144/GSL.QJEG.1978.011.01.03.

- Ambraseys, N., & Synolakis, C. (2010). ***Tsunami catalogs for the Eastern Mediterranean, revisited***. **J Earthq Eng**, 14(3), pp. 309–330. doi:10.1080/13632460903277593.

- Ambraseys, N., Melville, R., & Adams, R. (1994). **The seismicity of Egypt, Arabia and the Red Sea. A historical Review**. Cambridge University Press.

- Amireh, B., Schneider, W., & Abed, A. (1994). **Evolving fluvial —transitional—marine deposition through the Cambrian sequence of Jordan**. Sedimentary Geology, Volume 89(Issues 1–2). doi:http://dx.doi.org/10.1016/0037-0738(94)90084-1.

- Beicip. (1981). **Structural Map of Jordan**, Scale 1:5,000,000. Geological Mapping Division, Natural Resources Authority, Amman, Jordan.

- Bender, F. (1975). **Geology of the Arabian Peninsula**: Jordan. U.S. Geological Survey Professional Paper, 560-I. U.S. Government Publishing Office, Washington.

- Bender, F., & Khoury, H. (1981**). Lithostratigraphy of the Triassic in Jordan**. Facies, Volume 4(Issue 1), pp 1–26. doi:10.1007/BF02536584.

- Ben-Menahem, A. (1981). **Variation of slip and creep along the levant rift over the past 4500 years**. Tectonophysics, 80(1-4), pp. 183-197. doi:10.1016/0040-1951(81)90149-9

- Ben-Menahem, A., & Aboodi, E. (1981). **Micro- and macroseismicity of the Dead Sea rift and off-coast eastern Mediterranean**. Tectonophysics, 80(1-4), pp. 199-233. doi:10.1016/0040-1951(81)90150-5.

- Ben-Menahem, A., Nur, A., & Vered, M. (1976). **Tectonics, seismicity and structure of the Afro-Eurasian junction — the breaking of an incoherent plate**. Physics of the Earth and Planetary Interiors, 12, pp. 1-50. doi:10.1016/0031-9201(76)90005-4

- Berger , J., Davis, P., & Ekström, G. (2004). ***Ambient Earth Noise: A Survey of the Global Seismographic Network***,. **JOURNAL OF GEOPHYSICAL RESEARCH,** 109(B11307), pp. 1-10. doi:10.1029/2004JB003408.

- Besnard, M. (1984). **SISMOTECTONIQUE DE L’ARC EGEEN RESULTATS D’UNE CAMPAGNE DE MICROSISMICITE**. THESE DOCTORAT, UNIVERSITE JOSEPH FOURIER DE GRENOBLE (In French).

- Billings, S., Sambridge, M., & Kennett, B. (1994). **Errors in hypocenter location: Picking, model, and magnitude dependence**. Bulletin of the Seismological Society of America, 84(6), pp. 1978-1990.

- Burdon, D. (1959). **Handbook of the Geology of Jordan**; **to accompany and explain the three sheets of 1:250,000 Geological Map, East of the Rift, by A.M. Quennell**. Government of the Hashemite Kingdom of Jordan.

- Clinton, J., & Heaton, T. (2002). **Potential advantages of a strong-motion velocity meter over a strong-motion accelerometer**. Seismological Research Letters, 73(3), pp. 332-342.

- Dewey, J., & Şengör, A. (1979). **Aegean and surrounding regions: Complex multiplate and continuum tectonics in a convergent zone**. Geological Society of America Bulletin, 90(1), p. 84-92. doi:Doi: 10.1130/0016-7606(1979)90<84:AASRCM>2.0.CO;2.

- Di Stefano, R., Aldersons, F., Kissling, E., Baccheschi, P., Chiarabba, C., & Giardini, D. (2006). ***Automatic seismic phase picking and consistent observation error assessment: application to the Italian seismicity.*** **Geophys. J. Int**., *165*(1), pp. 121–134. doi:10.1111/j.1365-246X.2005.02799.x.

- Dilek, Y. (2009). **Eastern Mediterranean geodynamics**. Int. Geol. *Rev, 52 (2–3),* pp. 111–116. doi:http://dx.doi.org/10.1080/00206810902951031.

- Duyverman, H., Harris, N., & Hawkesworth, C. (1982). **Crustal accretion in the Pan African: Nd and Sr isotope evidence from the Arabian Shield**. Earth and Planetary Science Letters, pp. 315-326. doi:http://dx.doi.org/10.1016/0012-821X(82)90134-0.

- El-Isa, Z. (1992). **Seismicity of Wadi Araba-Dead Sea region**. Proc. 1st Arab. Geol. Conf. Ja. Cairo : Cairo University.

- El-Isa, Z. (2012). ***Seismicity and seismotectonics of the Gulf of Aqaba region.*** **Arabian Journal of Geosciences**, *6*(9), pp 3437–3449. doi:10.1007/s12517-012-0604-8.

- El-Isa, Z. (2013). **Continuous-cyclic variations in the b-value of the earthquake frequency-magnitude distribution**. Earthquake Science, 26(5), pp. 301–320. doi:10.1007/s11589-013-0037-9.

- El-Isa, Z. (2017). ***The instrumental seismicity of the Jordan Dead Sea transform***. **Arabian Journal of Geosciences**, 10(203), pp: 1-11. doi:10.1007/s12517-017-3000-6.

- El-Isa, Z., & Al Shanti, A. (1989). ***Seismicity and Tectonics of the Red Sea and Western Arabia***. **Geophy J Int**, 97(3), pp. 449–457. doi:10.1111/j.1365-246X.1989.tb00515.x.

- El-Isa, Z., & Mustafa, H. (1986). ***Earthquake deformations in the Lisan deposits and seismotectonic implications*. Geophys J Roy Astron**, *86*(2), pp. 413–424. doi:10.1111/j.1365-246 X.1986.tb03835.x.

- El-Isa, Z., McKnight, S., & Eaton, D. (2015). ***Historical seismicity of the Jordan Dead Sea Transform region and seismotectonic implications***. **Arabian Journal of Geosciences,** 8(6), pp. 4039–4055. doi:10.1007/s12517-014-1483-y.

- El-Isa, Z., Mechie, J., & Prodehl, C. (1987). ***Shear velocity structure of Jordan from explosion seismic data.*** **Geophys. J. R. astr. SOC**, 90, PP. 265-281.

- El-Isa, Z., Mechie, J., Prodehl, C., Makris, J., & Khim, R. (1987). **A crustal structure study of Jordan derived from seismic refraction data**. Tectonophysics, Volume 138(Issues 2–4), Pages 235–253. doi:10.1016/0040-1951(87)90042-4.

- El-Isa, z., Merghelani, H., & Bazzari , M. (1984). ***The Gulf of Aqaba earthquake swarm of 1983 January -April***. **Geophysical Journal International,** 78 (3), pp. 711-722. doi:10.1111/j.1365-246 X.1984.tb05066.x.

- El-Kelani, R. (2005). ***Three-dimensional Gravity Model of the southern Jordan Dead Sea Transform***. **An-Najah Univ. J. Res**. *(N. Sc.), 19*.

- Eyal, M., Eyal, Y., Bartov, Y., & Steinitz, G. (1981). **The tectonic development of the western margin of the Gulf of Elat (Aqaba) rift**. Tectonophysics, 80(1-4), pp. 39-66. doi:0040-1951(81)90141-4.

- Feigin, G., & Shapira, A. (1994). **A unified crustal model for calculating travel times of seismic waves across the Israel Seismic Network**. IPRG Rep.

- Fox, J., & Ahlbrandt, T. (2002). **Petroleum Geology and Total Petroleum Systems of the Widyan Basin and Interior Platform of Saudi Arabia and Iraq**. U.S. Geological Survey Bulletin 2202–E.

- Freund, R., Garfunkel, Z., Zak, I., Goldberg, M., Weissbrod, T., & Derin, B. (1970). **The Shear along the Dead Sea Rift**. Philos. Trans. R. Soc., Ser.A. 267, 107-130. doi:10.1098/rsta.1970.0027.

- Freund, R., Zak, I., & Garfunkel, Z. (1968). **Age and Rate of the Sinistral Movement along the Dead Sea Rift.** Nature, 220, pp. 253–255. doi:doi:10.1038/220253a0.

- Fritz, H., Abdelsalam, M., Ali, K., Bingen, B., Collins, A., Fowler, A., . . . Viola, G. (2013). ***Orogen styles in the East African Orogen: A review of the Neoproterozoic to Cambrian tectonic evolution***. **Journal of African Earth Sciences**, 86, pp. 65–106. doi:http://dx.doi.org/10.1016/j.jafrearsci.2013.06.004.

- Garfunkel , Z. (1981). **Internal structure of the Dead Sea leaky transform (rift) in relation to plate kinematics**. Tectonophysics, *80*(1-4), pp. 81-101. doi:10.1016/0040-1951(81)90143-8.

- Garfunkel, Z., Ben-Avraham, Z., & Kagan, E. (2014). ***Dead Sea Transform Fault System: Reviews, Modern Approaches in Solid Earth Sciences*** **(Vol. Volume 6).** http://www.springer.com/series/7377. doi:10.1007/978-94-017-8872-4_9.

- Garfunkel, Z., Zak, I., & Freund, R. (1981). **Active faulting in the dead sea rift**. Tectonophysics, 1- 4, pp. 1-26. doi:10.1016/0040-1951(81)90139-6.

- Ginzburg, A., Makris, J., Fuchs, K., & Prodehl, C. (1981). **The structure of the crust and upper mantle in the Dead Sea rift**. Tectonophysics, 80(1-4), Pages 109-119. doi:doi: 10.1016/0040-1951(81)90144-X.

- Ginzburg, A., Makris, J., fuchs, K., Prodehl, C., Kaminski, W., & Amitia, U. (1979). ***A seismic study of the crust and upper mantle of the Jordan-Dead Sea Rift and their transition toward the Mediterranean Sea***. **JOURNAL OF GEOPHYSICAL RESEARCH**, *84*(B4), Pages 1569–1582. doi: 10.1029/JB084iB04p01569.

- Girdler , R. W. (1990). **The Dead Sea transform fault system**. *Tectonophysics*, *180*(1), 1–13. doi:10.1016/0040-1951(90)90367-H.

- Girdler, R. (1985). **Problems concerning the evolution of oceanic lithosphere in the northern Red Sea**. Tectonophysics, 116(1-2), pp. 109-122. doi:10.1016/0040-1951(85)90224-0.

- Hanka, W., & Kind, R. (1994). **The GEOFON Program. Annals of Geophysics.** Annals of Geophysics, 37(5), pp. 1060-1065. doi:10.4401/ag-4196.

- Havskov, J., & Alguacil, G. (2016). **Instrumentation in Earthquake Seismology**. Heidelberg, New York, Dordrecht, London: Springer Dordrecht. doi:10.1007/978-3-319-21314-9.

- Havskov, J., Bormann, P., & Schweitzer, J. (2011). **Seismic source location.** GFZ German Research Centre for Geosciences, pp. 1-36. doi:10.2312/GFZ. NMSOP-2_IS_11.1.

- Hofstetter, R., Klinger, Y., Amrat, A., Rivera, L., & Dorbath, L. (2007). **Stress tensor and focal mechanisms along the Dead Sea fault and related structural elements based on seismological data**. Tectonophysics, 429(3-4), pp. 165-181. doi:10.1016/j.tecto.2006.03.010.

- Hussein, H., Abou Elenean, K., Marzouk, I., Peresan, A., Korrat, I., Abu El-Nader, E., . . . El-Gabry, M. (2008). **Integration and magnitude homogenization of the Egyptian earthquake catalogue**. Nat Hazards, 47, pp. 525–546. doi:10.1007/s11069-008-9237-3.

- Ibrahim, K., & McCourt, W. (1995). ***Neoproterozoic granitic magmatism and tectonic evolution of the northern Arabian Shield: evidence from southwest Jordan.*** **Journal of African Earth Sciences**, *20*(2), pp. 103-118. doi:http://dx.doi.org/10.1016/0899-5362(95) 00037-T.

- Ingate, S., & Berger, J. (2004). ***PROSPECTS FOR LOW-FREQUENCY SEISMOMETRY - A REPORT OF THE IRIS BROADBANDSEISMOMETER WORKSHOP***. Granlibakken, California: IRIS. doi:http://ds.iris.edu/stations/seisWorkshop04/iris_sensor_ws_9.19.05. pdf.

- Jarrar, G., Stern, R., Saffarini, G., & Al-Zubi, H. (2003). **Late- and post-orogenic Neoproterozoic intrusions of Jordan implications for crustal growth in the northernmost segment of the East African Orogen.** Precambrian Research, Volume 123(Issues 2–4), pp. 295–319. doi:http://dx.doi.org/10.1016/S0301-9268(03)00073-1.

- Klein, F. (1978). **Hypocenter location program HYPOINVERSE**. Menlo Park, California: U.S. Geol. Surv. Open- File Report. 78-694.

- Klinger, Y., Avouac, J., Dorbath, L., Abou Karaki, N., & Tisnerat, N. (2000). ***Seismic behaviour of the Dead Sea fault along Araba valley, Jordan***. **Geophys J Int**, 142(3), pp. 769-782. doi:10.1046/j.1365-246x.2000.00166.x.

- Kolodner, K., Avigad, D., McWilliams, M., Wooden , J., Weissbrod, T., & Feinstein, S. (2006). **Provenance of north Gondwana Cambrian–Ordovician sandstone: U–Pb SHRIMP dating of detrital zircons from Israel and Jordan.** Volume 143(Issue 3), pp. 367-391. doi:https://doi.org/10.1017/S0016756805001640.

- Krenkel, F. (1924). **Geologie der Erde. Berlin**: Bd. Gebruder Borntraeger.

- Kröner, A., & Stern, R. (2004). **Pan-African Orogeny North African Phanerozoic Rift Valley**. Encycl. Geol., 1, pp. 1-12. doi:http://dx. doi.org/10.1016/B0-12-369396-9/00431-7.

- Lee, W., & Lahr, J. (1975). *HYPO71 (revised):* **A computer program for determining hypocenter, magnitude and first motion pattern of local earthquakes**. Menlo Park, California: U.S. Geological Survey Open-File Report 75-311.

- Lucente, F. P., Chiarabba, C., & Cimini, G. B. (1999). ***Tomographic constraints on the geodynamic evolution of the Italian region***. **Journal of Geophysical Research**, 104(B9), pp. 20307–20327. doi:10.1029/1999JB900147.

- Maio, R., Ferreira, T. M., & Vicente, R. (2018). ***A critical discussion on the earthquake risk mitigation of urban cultural heritage assets.*** **International Journal of Disaster Risk Reduction**, 27, pp. 239-247. doi:10.1016/j.ijdrr.2017.10.010.

- Mechie, J., Abu-Ayyash, K., Ben-Avraham, Z., El-kelani, R., Mohsen, A., Rümpker, G., . . . Weber, M. (2005). ***Crustal shear velocity structure across the Dead Sea Transform from two-dimensional modelling of DESERT project explosion seismic data***. **Geophys. J. Int.**, 160(3), pp. 910-924. doi:10.1111/j.1365-246X.2005.02526.x.

- Meghraoui, M. (2015). **Paleoseismic History of the Dead Sea Fault Zone**. Encyclopedia of Earthquake Engineering. doi:10.1007/978-3-642-36197-5_40-1.

- Meghraoui, M., Gomez, F., Sbeinati, R., Woerd, J., Mouty, M., Darkal, A., . . . Barazangi, M. (2003). **Evidence for 830 years of seismic quiescence from palaeoseismology, archaeoseismology and historical seismicity along the Dead Sea fault in Syria**. Earth and Planetary Science Letters, pp. 35 - 52.

- Mohsen, A. (2004). **A receiver function study of the crust and upper mantle across the Dead Sea Transform**. Berlin: Ph.D. Thesis. Freien Universität Berlin.

- Ottem¨oller, L., Voss, P., & Havskov, J. (2016). **SEISAN EARTHQUAKE ANALYSIS SOFTWARE FOR WINDOWS, SOLARIS, LINUX and MACOSX** (Version 10.5).

- Powell, J. (1989). **Stratigraphy and Sedimentation of the Phanerozoic Rocks in Central and South Jordan**, Part A: Ram and Khreim Groups. Geology Directorate, Geological Mapping Division, Bulletin 11. Natural Resources Authority, Amman, Jordan.

- Powell, J., & Moh'd, B. (2011). **Evolution of Cretaceous to Eocene alluvial and carbonate platform sequences in central and south Jordan.** GeoArabia, v. 16(no. 4), pp. 29-82.

- Powell, J., Abed, A., & Le Nindre, Y. (2014). **Cambrian stratigraphy of Jordan**. GeoArabia, v. 19(no. 3), pp. 81-134.

- Quennell, A. (1958). ***The Structural and Geomorphic Evolution of the Dead Sea Rift***. **Quarterly Journal of the Geological Society of London,** *V. 114*, 2-24. doi:10.1144/gsjgs.114.1.0001.

- Quennell, A. (1959). **Tectonics of the Dead Sea rift**. *20th* International Geological Congress (pp. PP. 385-403). Mexico, 1956: Associacion de Servicos Geologicos.

- Quennell, A. M. (1984). **The Western Arabia rift system. Geological Society London, Special Publications** *17*(1), 775-788. doi:10.1144/GSL.SP.1984.017.01.62.

- Radaideh, O., & Melichar, R. (2015). **Tectonic paleostress fields in the southwestern part of Jordan: New insights from the fault slip data in the southeastern flank of the Dead Sea Fault Zone**. Tectonics, Volume 34(Issue 9), pp. 1863–1891. doi:10.1002/2015TC003919.

- Radaideh, O., Grasemann, B., Melichar, R., & Mosar, J. (2016). **Detection and analysis of morphotectonic features utilizing satellite remote sensing and GIS: An example in SW Jordan**. Geomorphology, Volume 275, pp. 58–79. doi:10.1016/j.geomorph.2016.09.033.

- Rashdan, M. (1988). **The Regional Geology of Aqaba-Wadi Araba Area**, . Geology Directorate, Geological Mapping Division, Bulletin 7. Natural Resources Authority, Amman, Jordan, Map Sheet 3049 III, 2949 II. page: 87.

- Sadeh, M., Ziv, A., & Wust-Bloch, H. (2014). ***Real-time magnitude proxies for earthquake early warning in Israel***. **Geophys J. Int,** 196, PP. 939–950. doi:10.1093/gji/ggt407.

- Salamon, A. (2010). ***Patterns of seismic sequences in the Levant interpretation*. J Seismology,** 14, pp. 339–367.

- Salamon, A., Rockwell, T., Ward, S., Guidoboni, E., & Comastri, A. (2007). **Tsunami hazard evaluation of the eastern Mediterranean: historical analysis and selected modeling**. Bulletin of the Seismological Society of America, 97(3), pp.705–724. doi:10.1785/0120060147.

- Sawires, R., Peláez, J., Fat-Helbary, R., & Ibrahim, H. (2016). **An Earthquake Catalogue (2200 B.C. to 2013) for Seismotectonic and Seismic Hazard Assessment Studies in Egypt.** In S. D'Amico, Earthquakes and Their Impact on Society (pp. pp 97-136). Springer Natural Hazards. doi:10.1007/978-3-319-21753-6_4.

- Sbeinati, M., Darawcheh, R., & Mouty, M. (2005). **The historical earthquakes of Syria: an analysis of large and moderate earthquakes** from 1365 B.C. to 1900 A.D. ANNALS OF GEOPHYSICS, 48(3).

- SEED, S. (2012). **Standard for the exchange of earthquake data, SEED format version 2.4**. International Federation of Digital Seismograph Networks Incorporated Research Institutions for Seismology (IRIS), USGS. Retrieved from http://www.fdsn.org/seed_manual/SEEDManual_V2.4.pdf.

- Şengör, A. (1979). T***he North Anatolian transform fault: its age, offset and tectonic significance***. **Journal of the Geological Society, Volume** 174(Number 1), pp. 269-282. doi:DOI: 10.1144/gsjgs.136.3.0269.

- Stern, R. (1994). **Arc-assembly and continental collision in the Neoproterozoic east African Orogen: implications for the consolidation of Gondwanaland**. Annu. Rev. Earth Planet. Sci., 22, pp. 319-51. doi:10.1146/annurev.ea.22.050194.001535.

- Stern, R., Ali, K., Liégeois, J., Johnson, P., Kozdroj, W., & Kattan, F. (2010). °***Distribution and significance of pre-Neoproterozoic zircons in juvenile Neoproterozoic igneous rocks of the Arabian-Nubian Shield***. **Am. J. Sci.**, 310(9), pp. 791–811. doi:10.2475/09.2010.02.

- Stoeser, D., & Frost, C. (2006). **Nd, Pb, Sr, and O isotopic characterization of Saudi Arabian Shield terranes.** Chemical Geology, V. 226 (Issues 3–4), pp. 163–188. doi:http://dx.doi.org/10.1016/j.chemgeo.2005.09.019.

- Taymaz, T., Jackson, J., & McKenzie, D. (1991). ***Active tectonics of the north and central Aegean Sea***. **Geophys. J. Int**., V. 106 (Issue 2), pp. 433-490. doi:https://doi.org/10.1111/j.1365-246X.1991.tb03906.x.

- Walley , C. D. (1988). **A braided strike - slip model for the northern continuation of the Dead Sea Fault and its implications for Levantine tectonics**. Tectonophysics, 145(1-2), Pages 63-72. doi:10.1016/0040-1951(88)90316-2.

- Wang , L., Guo, Y., Liu , F., & Jiang , C. (2008). T**emporal vP/vS variation characteristics in different zones of China's Capital Circle area before and after Wen'an earthquake.** ACTA SEISMOLOGICA SINICA, 21(3), PP. 243-257. doi:10.1007/s11589-008-0243-z.

- Willis , B. (1928). **Earthquakes in the Holy Land**. Bull Seism Soc Amer, 18(2).

- Zain-Eldeen, U., Delvaux, D., & Jacobs, P. (2002). **Tectonic evolution in the Wadi Araba Segment of the Dead Sea Rift, South-West Jordan**. European Geosciences Union, Special Publication Series, Vol. 2, pp. 63–81.

- Zeiler, C., & Velasco, A. (2009). **Seismogram Picking Error from Analyst Review (SPEAR): Single-Analyst and Institution Analysis**. Bulletin of the Seismological Society of America, 99(5), pp. 2759–2770. doi:10.1785/0120080131.

- Zeiler, C., & Velasco, A. (2011). **Seismogram Picking Error from Analyst Review (SPEAR) (Information Sheet).** GFZ, pp- 1-8. doi:10.2312/GFZ.NMSOP-2_IS_11.5.

- Zhou, Y.-Q., Peng, T.-M., Zhou, T.-F., Zhang, Z.-K., Tian, H., Liang, W.-D., . . . Sun, L.-F. (2017). S***oft-sediment deformation structures related to volcanic earthquakes of the Lower Cretaceous Qingshan Group in Lingshan Island, Shandong Province, East China***. **Journal of Palaeogeography,** 6(2), pp. 162-181. doi:10.1016/j.jop.2017.02.002.

- Zohar, M., & Marco, S. (2012). ***Re-estimating the epicenter of the 1927 Jericho earthquake using spatial distribution of intensity data***. **Journal of Applied Geophysics,** 82, pp. 19–29. doi:10.1016/j.jappgeo.2012.03.004.

- Zohar, M., Rubin, R., & Salamon, A. (2014). **Earthquake Damage and Repair: New Evidence from Jerusalem on the 1927 Jericho Earthquake**. Seismological Research Letters, 85(4), pp. 912 - 922. doi:10.1785/0220140009.

APPENDIX 1

THE SEISMIC STATIONS

Number	Station code	Latitude	Longitude	Altitude	Network code	SOURCE
1	EIL	29.67	34.95	210	GE and IS	GEOFON
2	GHAJ	31.3	35.57	-58	GE	GEOFON
3	JER	31.77	35.2	770	GE and IS	GEOFON
4	KSDI	33.19	35.66	123	GE and IS	GEOFON
5	MRNI	33.01	35.39	918	GE	GEOFON
6	MSBI	31.31	35.36	-314	GE	GEOFON
7	SALP	32.07	35.19	475	GE	GEOFON
8	UJAP	31.95	35.46	-200	GE	GEOFON
9	AMAZ	31.53	34.92	400	IS	GEOFON
10	AMZI	31.55	34.91	396	IS	GEOFON
11	BGIO	31.72	35.09	752	IS	GEOFON
12	BLGI	32.73	35.19	190	IS	GEOFON
13	DSI	31.59	35.39	12	IS	GEOFON
14	DSI0	31.59	35.39	12	IS	GII*
15	DAM2	31.17	35.44	-374	IS	GII*
16	GLH0	32.71	35.65	330	IS	GII*
17	GEM	33.21	35.66	195	IS	GEOFON
18	HMDT	32.25	35.53	151	IS	GEOFON
19	HNTI	33.08	35.17	301	IS	GEOFON
20	HNT0	33.08	35.17	301	IS	GII*
21	HRFI	30.04	35.03	438	IS	GEOFON
22	KMTI	30.1	34.73	473	IS	(Sadeh, Ziv, & Wust-Bloch, 2014)
23	KRMI	30.12	34.73	502	IS	GEOFON
24	krm0	30.12	34.73	502	IS	GII*
25	KSH0	32.98	35.81	719	IS	GII*
26	KZIT	30.91	34.4	248	IS	GEOFON
27	MBRI	29.79	34.92	874	IS	GEOFON
28	MBH0	29.79	34.92	842	IS	GII*
29	MDBI	31.31	35.36	-314	IS	GEOFON
30	MMA0	33.02	35.4	810	IS	GEOFON
31	MMA0B	33.02	35.4	810	IS	GEOFON
32	MMA1	33.02	35.4	810	IS	GEOFON
33	MMA2	33.01	35.41	810	IS	GEOFON
34	MMA3	33.01	35.41	810	IS	GEOFON

Number	Station code	Latitude	Longitude	Altitude	Network code	SOURCE
35	MMA4	33.01	35.4	810	IS	GEOFON
36	MMB1	33.02	35.41	810	IS	GEOFON
37	MMB2	33.01	35.4	810	IS	GEOFON
38	MMB3	33.02	35.39	810	IS	GEOFON
39	MMB4	33.02	35.4	810	IS	GEOFON
40	MMC1	33.03	35.4	810	IS	GEOFON
41	MMC2	33.03	35.41	810	IS	GEOFON
42	MMC3	33.02	35.41	810	IS	GEOFON
43	MMC4	33.01	35.42	810	IS	GEOFON
44	MMC5	33.01	35.41	810	IS	GEOFON
45	MMC6	33.01	35.39	810	IS	GEOFON
46	MMC7	33.02	35.39	810	IS	GEOFON
47	MMLI	32.44	35.42	511	IS	GEOFON
48	MML	32.44	35.42	510	IS	(Sadeh, Ziv, & Wust-Bloch, 2014)
49	MRNI	33.12	35.39	918	IS	GEOFON
50	MZDA	31.31	35.36	-275	IS	GEOFON
51	MZD0	31.31	35.36	-275	IS	FDSN**
52	MSBI	31.31	35.36	-314	IS	GII*
53	RMN0	30.6	34.76	853	IS	GII*
54	NATI	33.26	35.74	975	IS	GEOFON
55	OFRI	32.62	34.99	161	IS	GEOFON
56	PRNI	30.35	35.01	411	IS	GEOFON
57	PRN0	30.35	35.01	411	IS	GII*
58	RTMI	31.05	34.69	261	IS	(Sadeh, Ziv, & Wust-Bloch, 2014)
59	REVI	31.04	34.72	273	IS	(Sadeh, Ziv, & Wust-Bloch, 2014)
60	SLTI	32.24	35.04	250	IS	GEOFON
61	SLT0	32.24	35.04	250	IS	GII*
62	YTIR	31.36	35.12	902	IS	GEOFON
63	ZFRI	30.57	35.18	-37	IS	GEOFON
64	ZFR0	30.57	35.18	-37	IS	GII*
65	AJLJ	32.33	35.73	1175	JS	GEOFON
66	AQBJ	29.73	35.05	170	JS	GEOFON
67	ASF	32.17	36.85	929	JS	GEOFON
68	AZQJ	31.75	36.76	400	JS	GEOFON
69	BYRJ	30.85	36.5	1008	JS	GEOFON
70	DRHJ	29.36	34.96	10	JS	GEOFON

Number	Station code	Latitude	Longitude	Altitude	Network code	SOURCE
71	HITJ	29.74	35.84	1660	JS	GEOFON
72	HSNJ	30.26	35.69	1176	JS	GEOFON
73	JDRJ	30.73	35.77	1219	JS	GEOFON
74	JSOJ	31.96	35.85	930	JS	GEOFON
75	JUFJ	32.09	35.6	-0.25	JS	GEOFON
76	JUSJ	32.47	35.97	550	JS	GEOFON
77	KARJ	32	35.58	-124	JS	GEOFON
78	LISJ	31.24	35.48	-327	JS	GEOFON
79	QRNJ	32.35	35.58	95	JS	GEOFON
80	SHMJ	32.73	35.75	363	JS	GEOFON
81	SWQJ	31.24	36.06	876	JS	GEOFON
82	WALJ	31.56	35.81	53	JS	GEOFON

*GII: http://seis.gii.co.il/en/network/seismicNetwork.php

** FDSN: http://www.fdsn.org/networks/detail/IS/

APPENDIX 2

WAVEFORMS

AMAZ

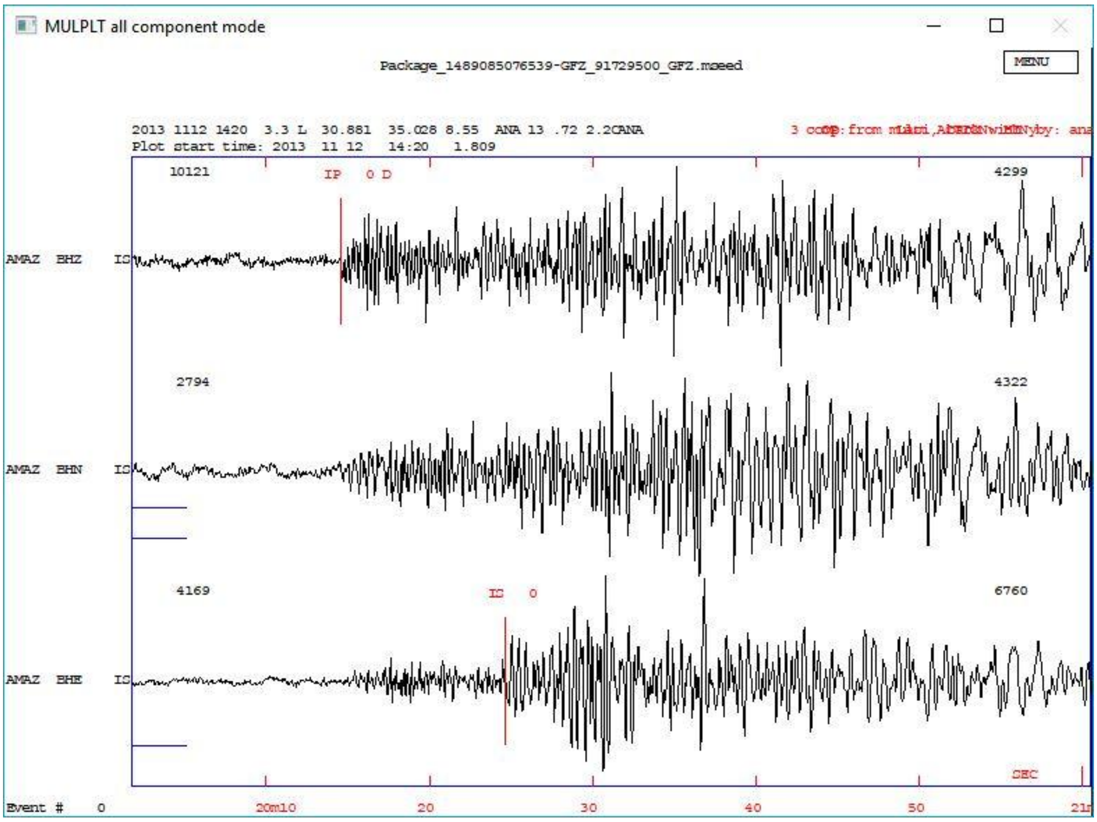

DAM2

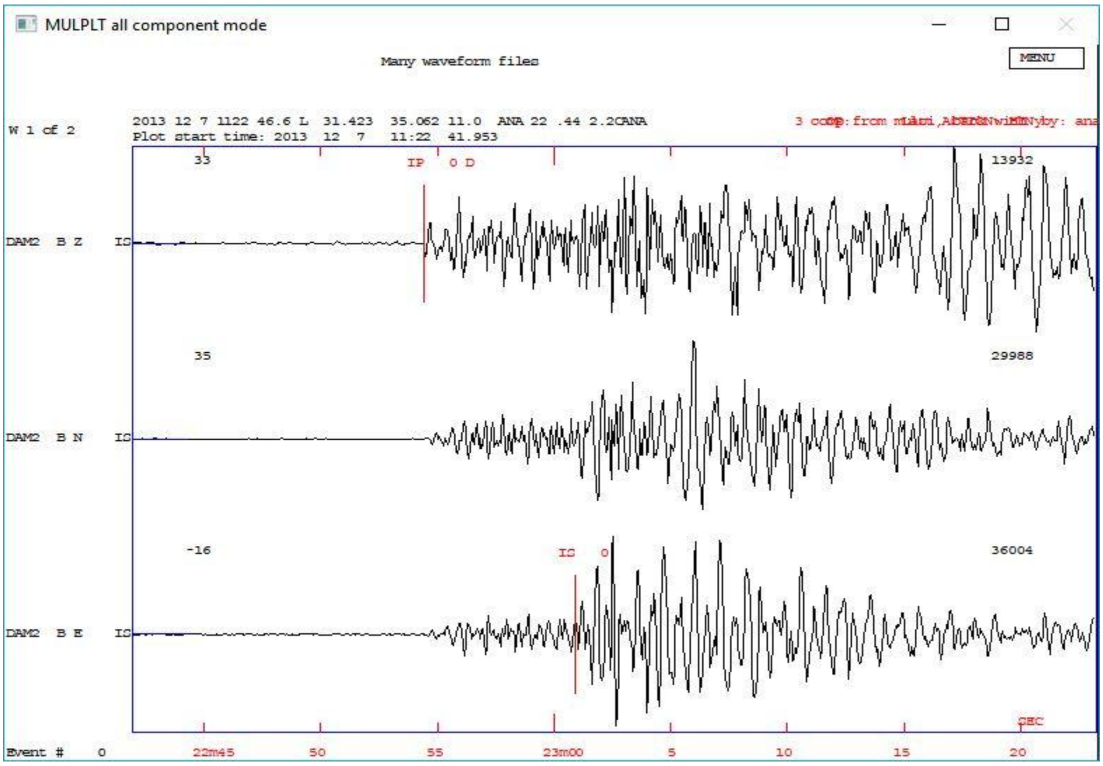

DSI

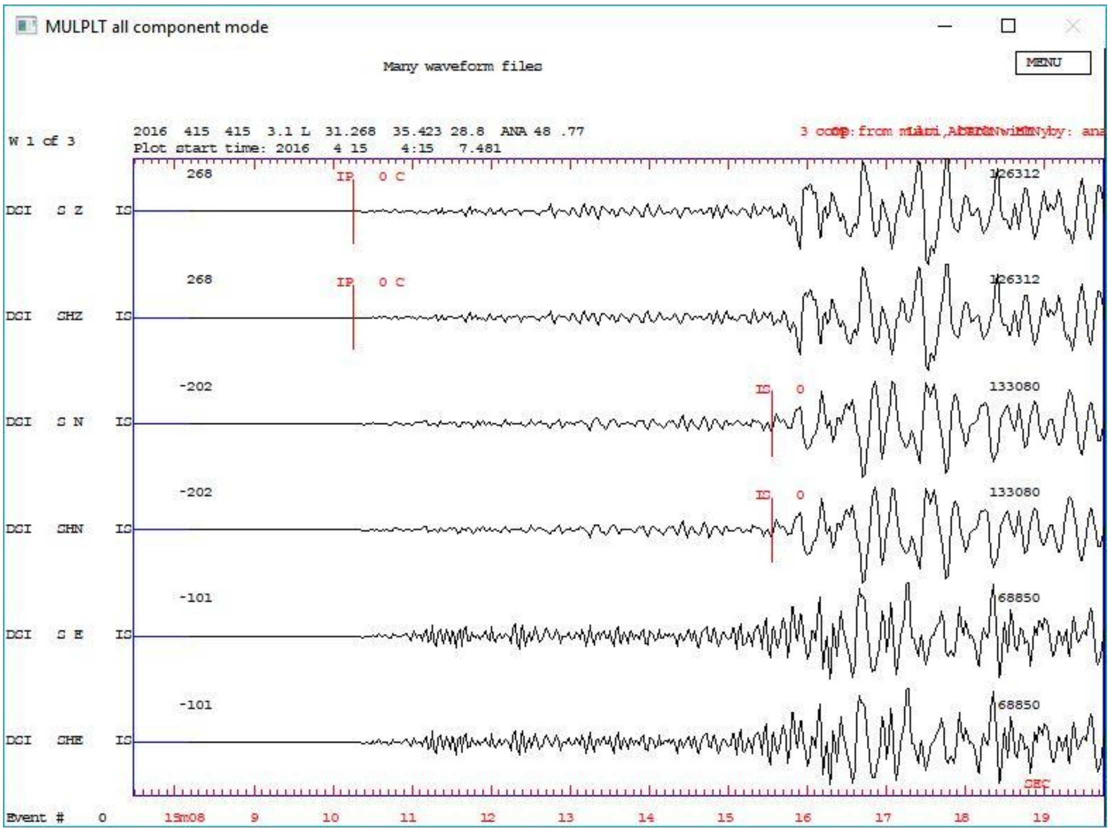
MULPLT all component mode
Many waveform files
MENU
W 1 of 3
2016 415 415 3.1 L 31.268 35.423 28.8 ANA 48 .77
Plot start time: 2016 4 15 4:15 7.481
DSI S Z IS
DSI SHZ IS
DSI S N IS
DSI SHN IS
DSI S E IS
DSI SHE IS
Event # 0

EIL

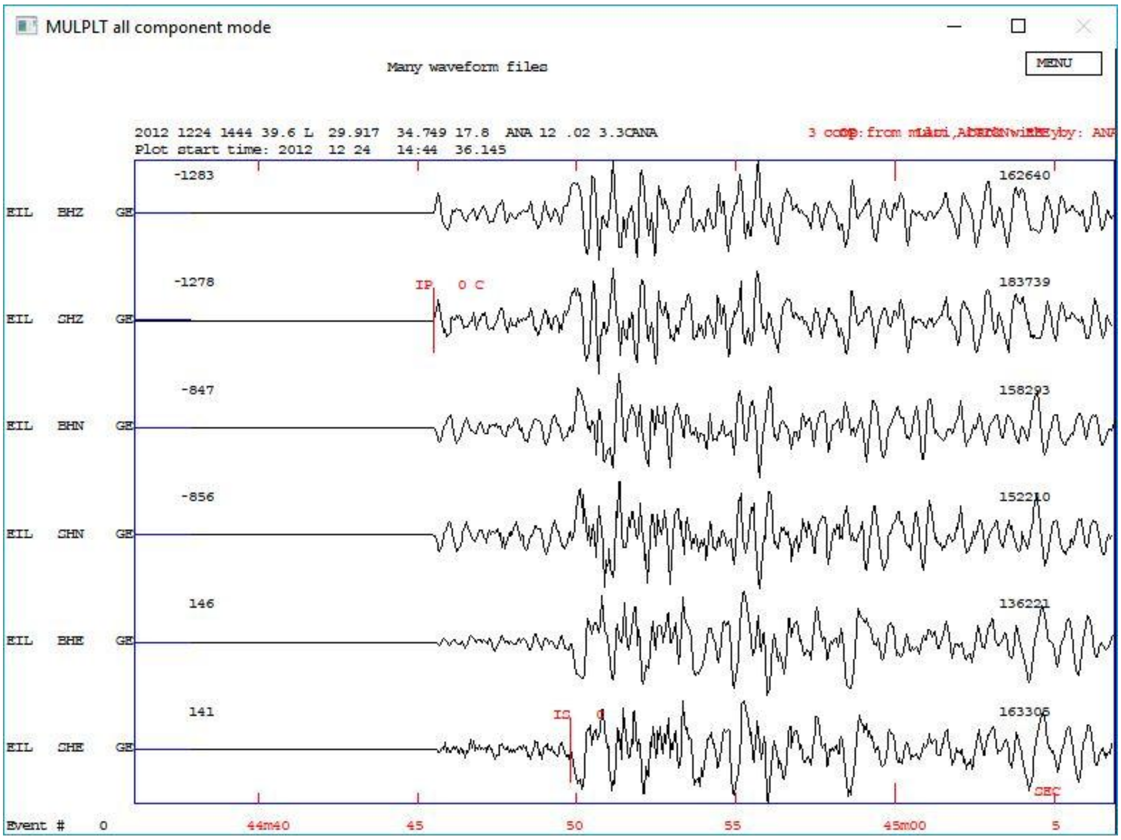
MULPLT all component mode
Many waveform files
MENU
2012 1224 1444 39.6 L 29.917 34.749 17.8 ANA 12 .02 3.3CANA
Plot start time: 2012 12 24 14:44 36.145
EIL BHZ GE
EIL SHZ GE
EIL BHN GE
EIL SHN GE
EIL BHE GE
EIL SHE GE
Event # 0

GHAJ

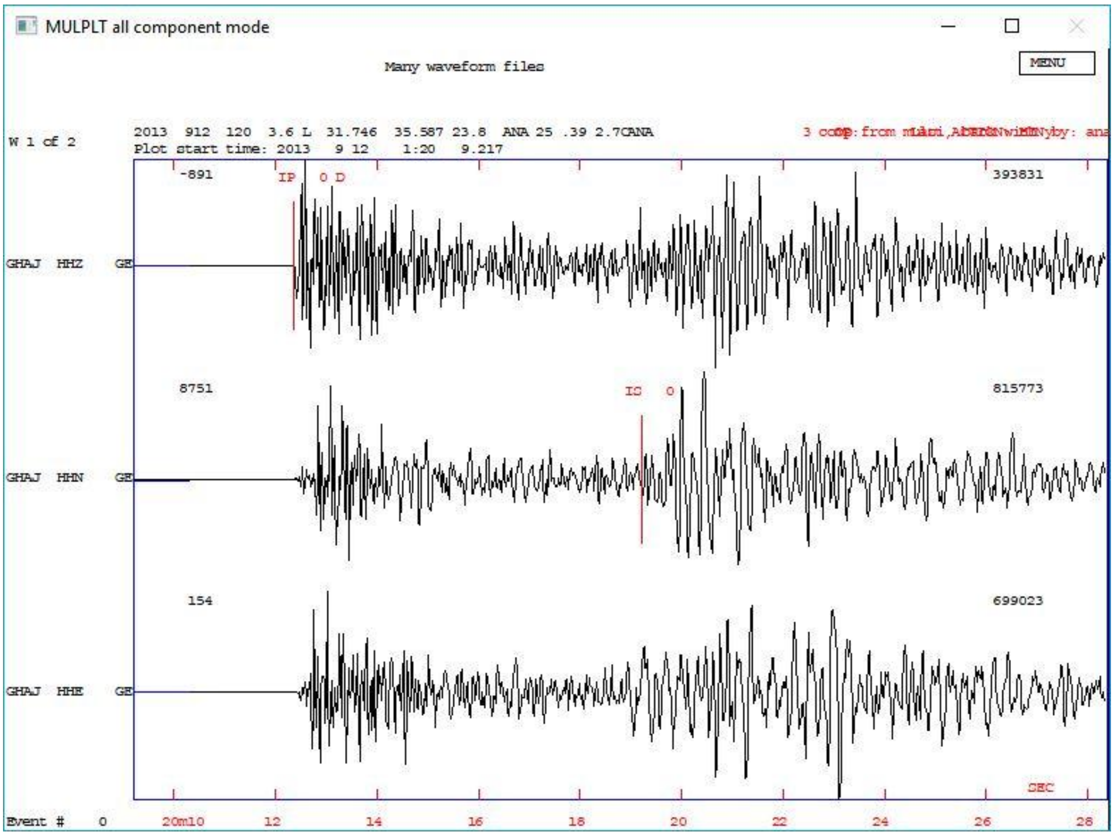
MULPLT all component mode
Many waveform files
MENU
W 1 of 2
2013 912 120 3.6 L 31.746 35.587 23.8 ANA 25 .39 2.7CANA
Plot start time: 2013 9 12 1:20 9.217
GHAJ HHZ GE
GHAJ HHN GE
GHAJ HHE GE
-891
393831
8751
815773
154
699023
IP
D
IS
SEC
Event # 0
20m10
12
14
16
18
20
22
24
26
28

HMDT

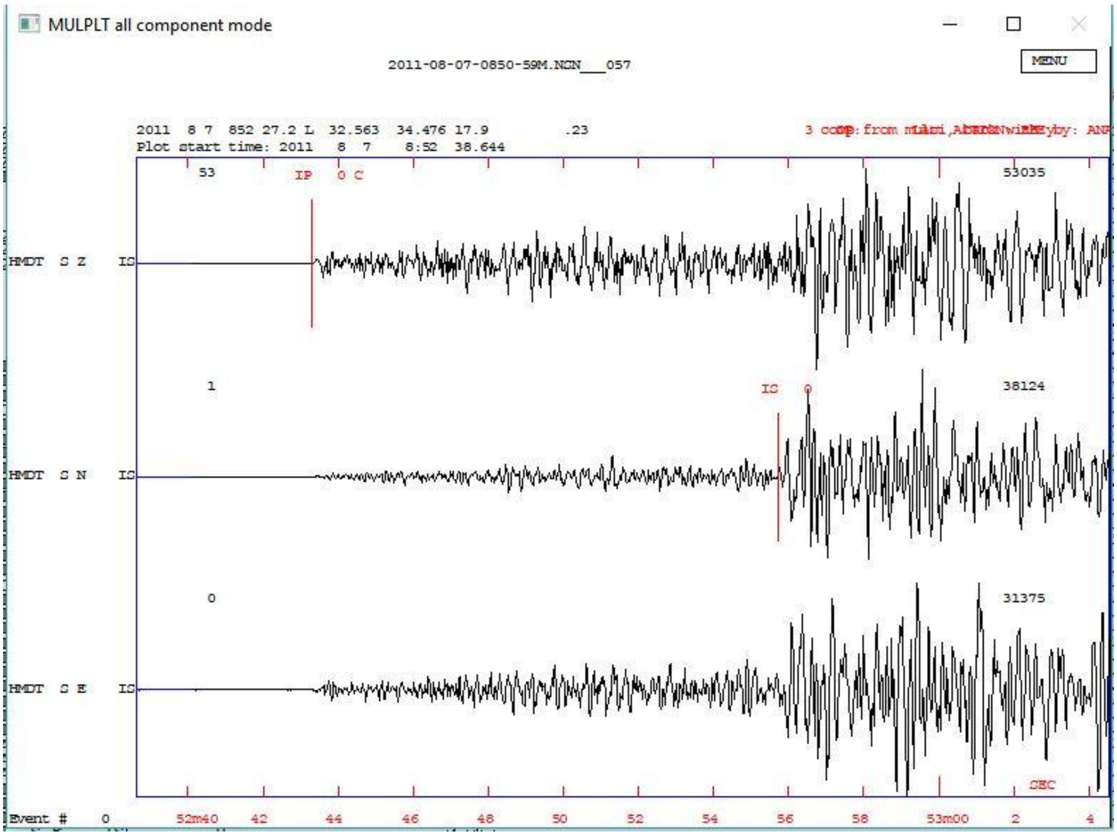
MULPLT all component mode
2011-08-07-0850-59M.NCN___057
MENU
2011 8 7 852 27.2 L 32.563 34.476 17.9 .23
Plot start time: 2011 8 7 8:52 38.644
HMDT S Z IS
HMDT S N IS
HMDT S E IS
53
53035
1
38124
0
31375
IP
C
IS
SEC
Event # 0
52m40
42
44
46
48
50
52
54
56
58
53m00
2
4

HNTI

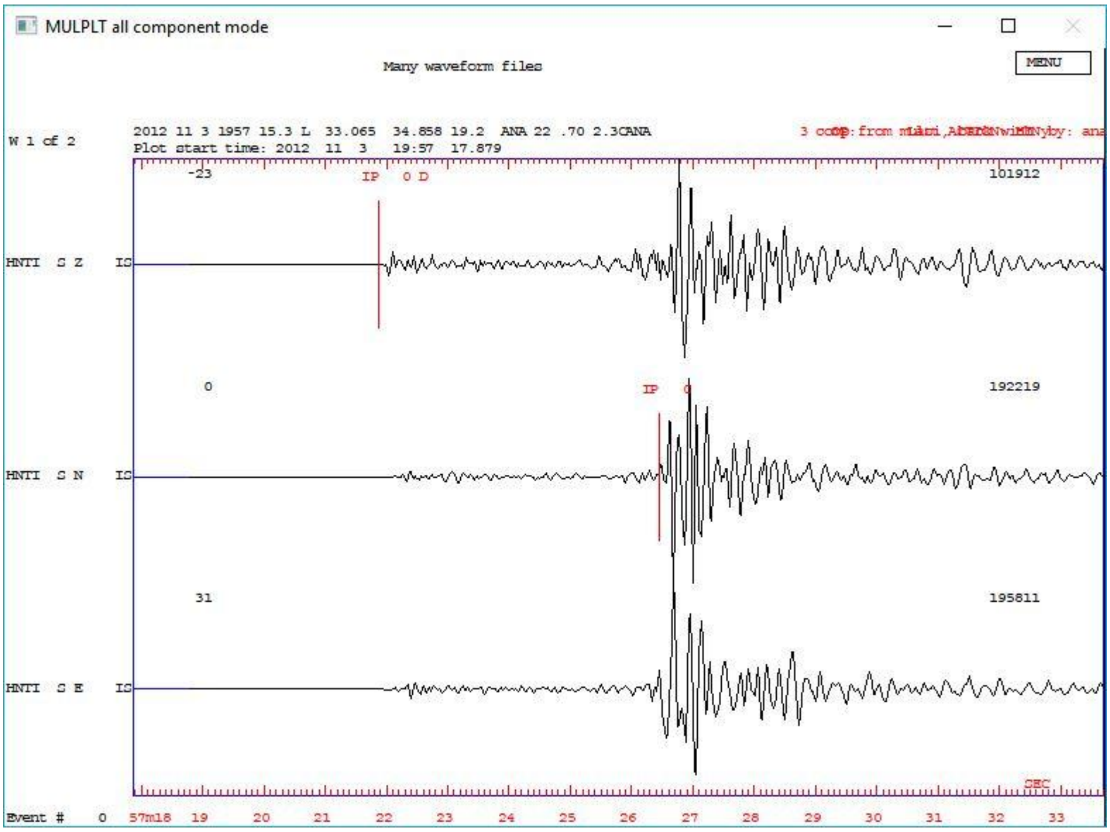
MULPLT all component mode
Many waveform files
MENU
W 1 of 2
2012 11 3 1957 15.3 L 33.065 34.858 19.2 ANA 22 .70 2.3CANA
Plot start time: 2012 11 3 19:57 17.879
HNTI S Z
HNTI S N
HNTI S E
Event # 0

HRFI

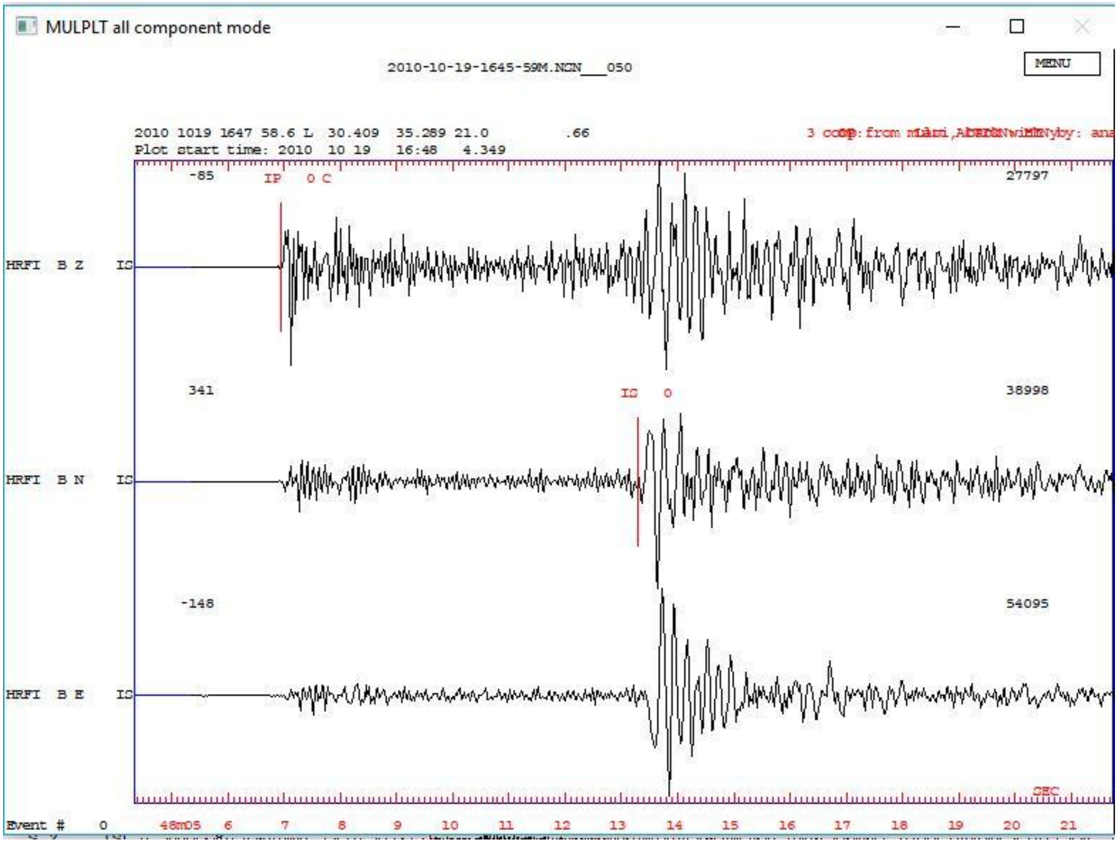
MULPLT all component mode
2010-10-19-1645-59M.NCN___050
MENU
2010 1019 1647 58.6 L 30.409 35.289 21.0 .66
Plot start time: 2010 10 19 16:48 4.349
HRFI B Z
HRFI B N
HRFI B E
Event # 0

KARJ

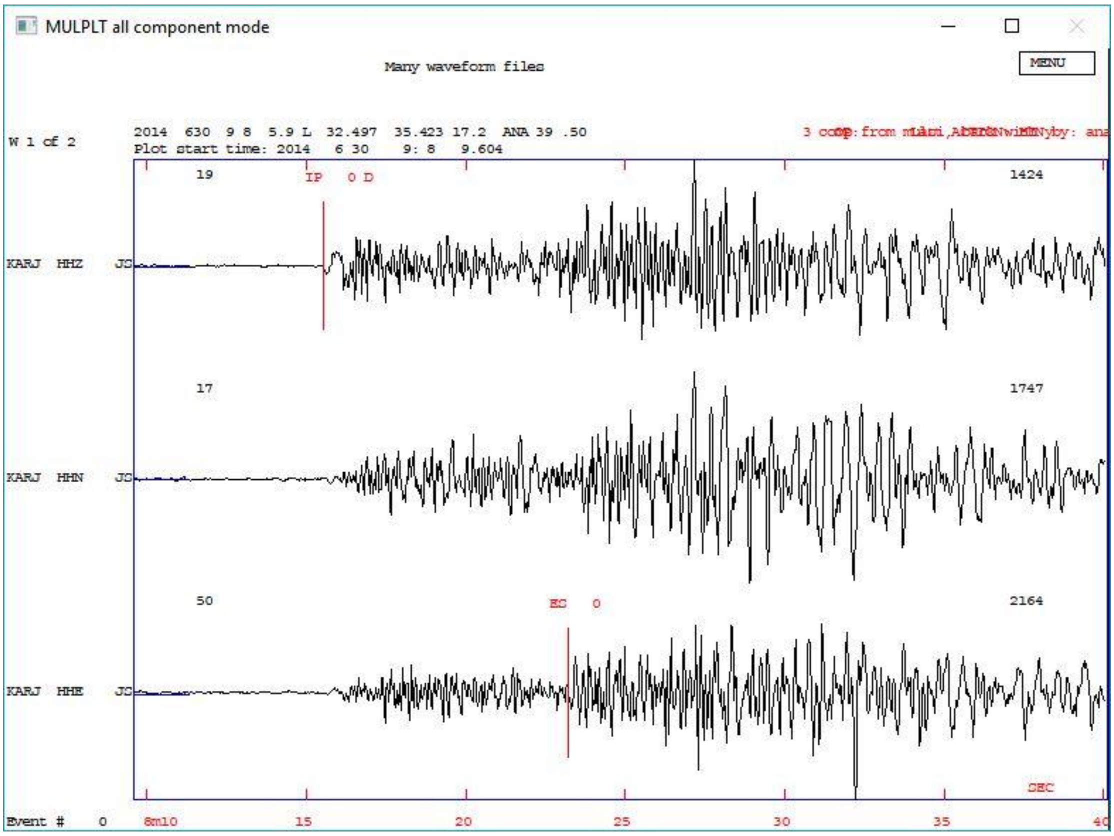
MULPLT all component mode
Many waveform files
MENU
W 1 of 2
2014 630 9 8 5.9 L 32.497 35.423 17.2 ANA 39 .50
Plot start time: 2014 6 30 9: 8 9.604
KARJ HHZ
KARJ HHN
KARJ HHE
Event # 0 8m10 15 20 25 30 35 40
SEC

KRMI

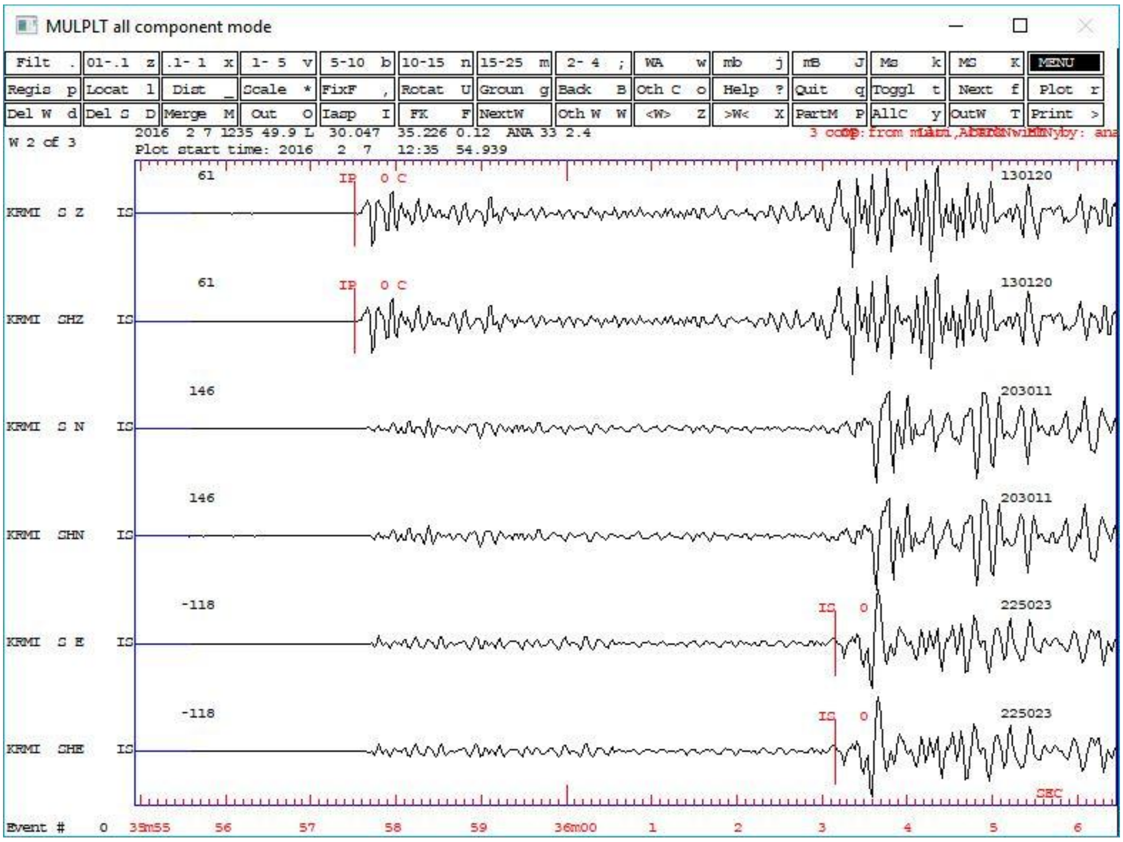
MULPLT all component mode
W 2 of 3
2016 2 7 1235 49.9 L 30.047 35.226 0.12 ANA 33 2.4
Plot start time: 2016 2 7 12:35 54.939
KRMI S Z
KRMI SHZ
KRMI S N
KRMI SHN
KRMI S E
KRMI SHE
Event # 0 35m55 56 57 58 59 36m00 1 2 3 4 5 6
SEC

KSDI

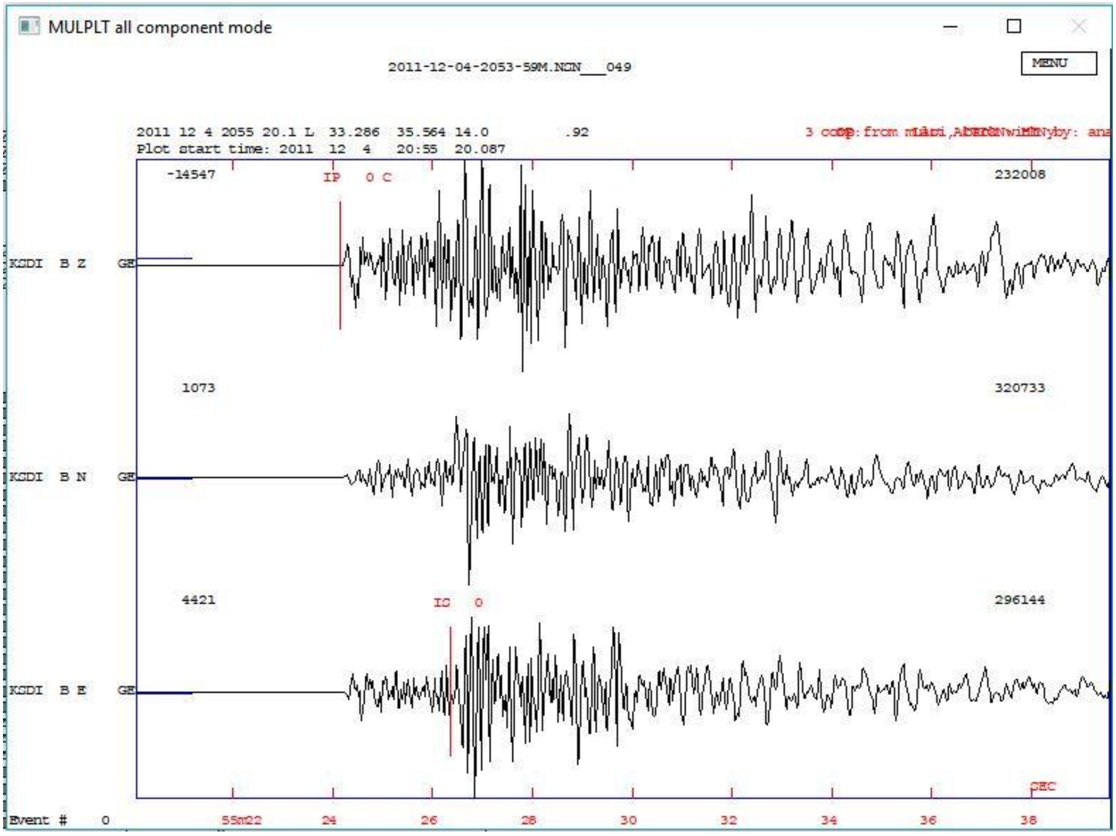
MULPLT all component mode
2011-12-04-2053-59M.NSN___049
MENU
2011 12 4 2055 20.1 L 33.286 35.564 14.0 .92
Plot start time: 2011 12 4 20:55 20.087
KSDI B Z
KSDI B N
KSDI B E
SEC
Event # 0

KZIT

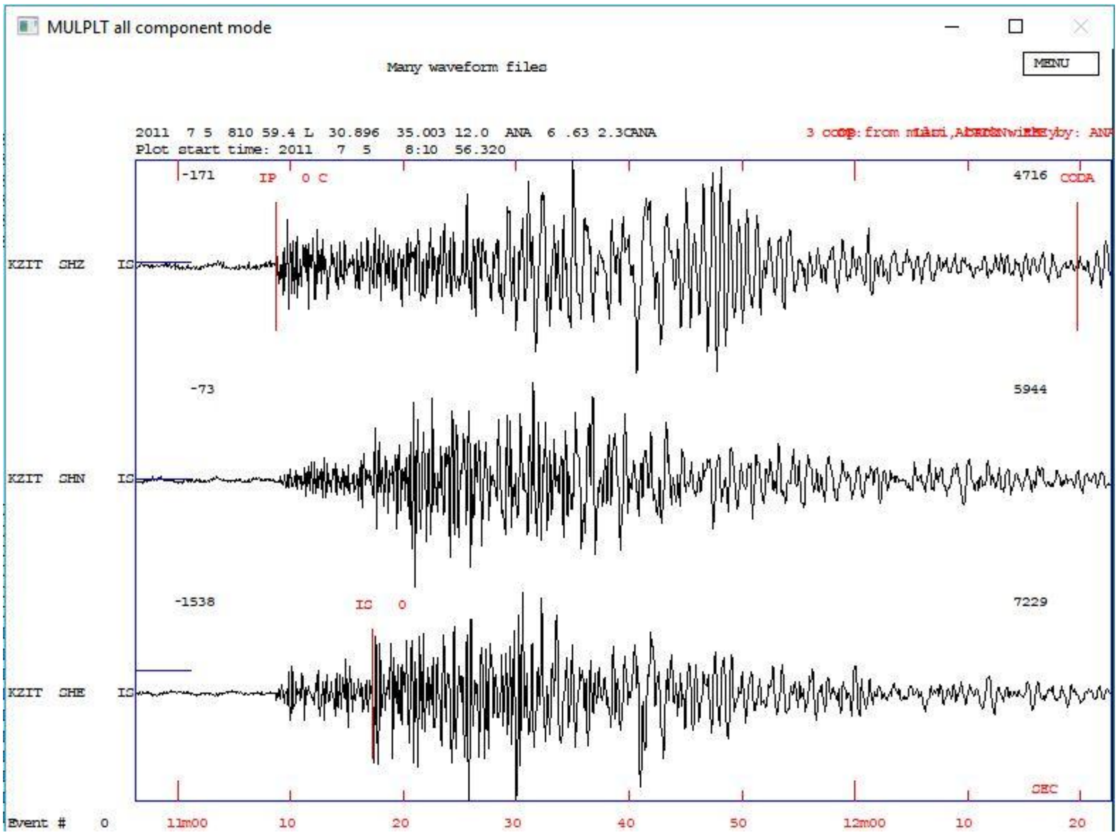
MULPLT all component mode
Many waveform files
MENU
2011 7 5 810 59.4 L 30.896 35.003 12.0 ANA 6 .63 2.3CANA
Plot start time: 2011 7 5 8:10 56.320
KZIT SHZ
KZIT SHN
KZIT SHE
CODA
SEC
Event # 0

MDBI

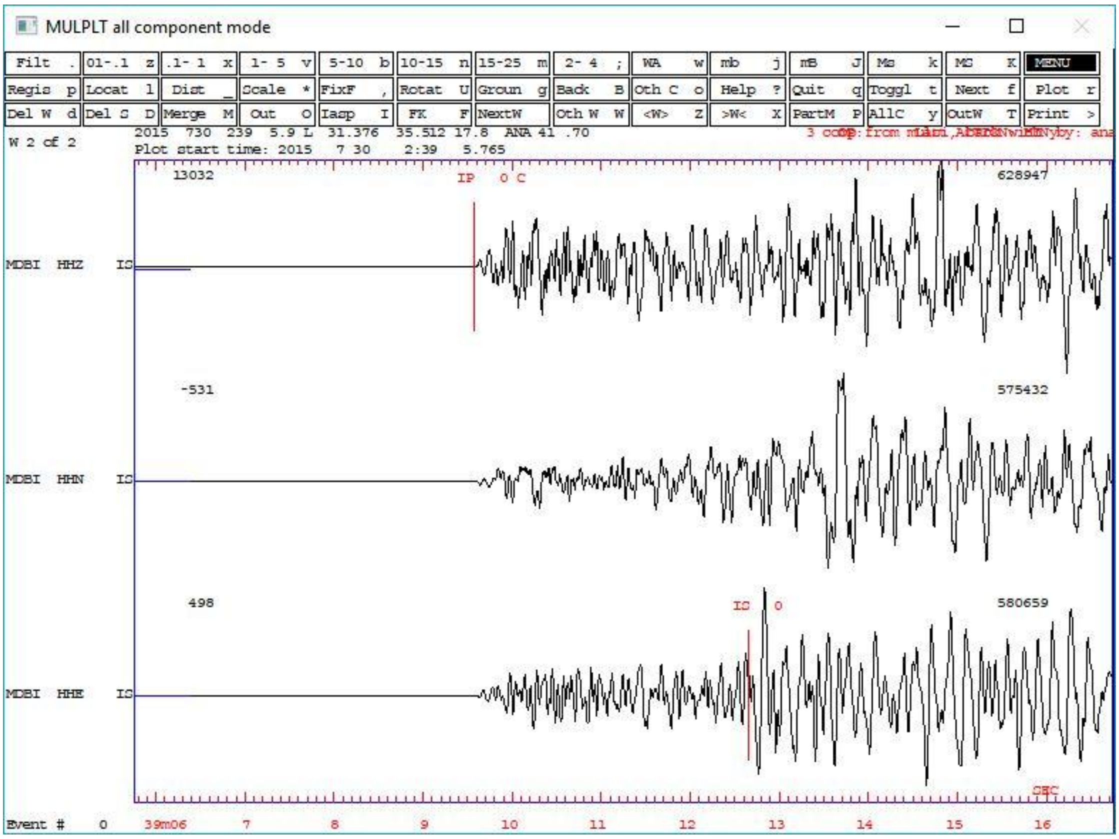
MULPLT all component mode
2015 730 239 5.9 L 31.376 35.512 17.8 ANA 41 .70
Plot start time: 2015 7 30 2:39 5.765
MDBI HHZ
MDBI HHN
MDBI HHE
Event # 0
SEC

MMLI

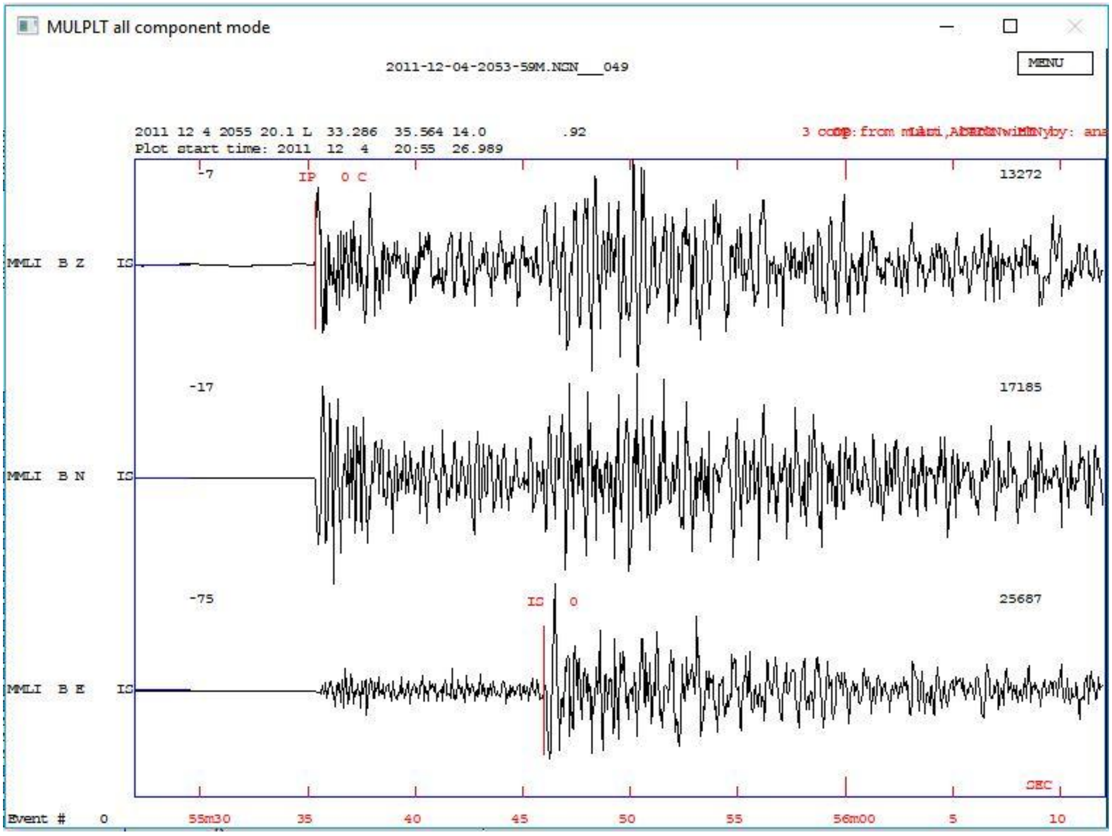
MULPLT all component mode
2011-12-04-2053-59M.NCN___049
2011 12 4 2055 20.1 L 33.286 35.564 14.0 .92
Plot start time: 2011 12 4 20:55 26.989
MMLI B Z
MMLI B N
MMLI B E
Event # 0
SEC

MSBI

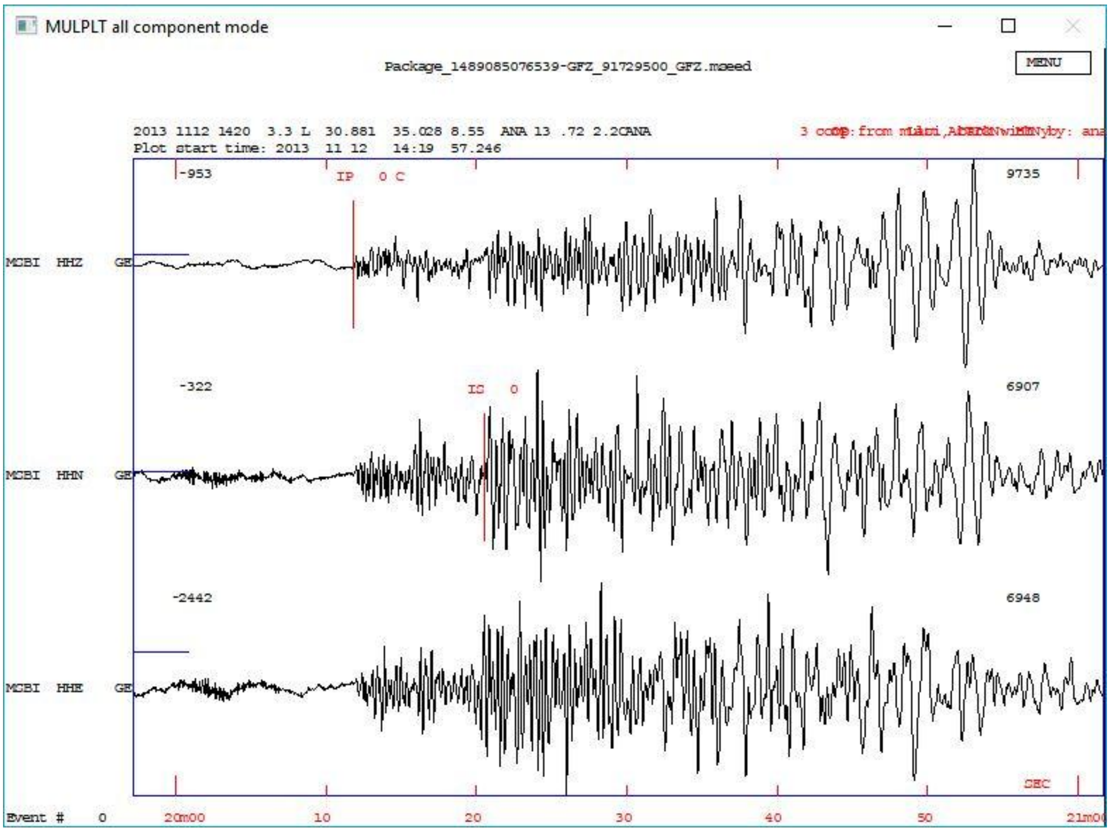
MULPLT all component mode
Package_1489085076539-GFZ_91729500_GFZ.mseed
MENU
2013 1112 1420 3.3 L 30.881 35.028 8.55 ANA 13 .72 2.2CANA
Plot start time: 2013 11 12 14:19 57.246
MSBI HHZ
MSBI HHN
MSBI HHE
IP
IS
SEC
Event # 0
20m00
10
20
30
40
50

MZDA

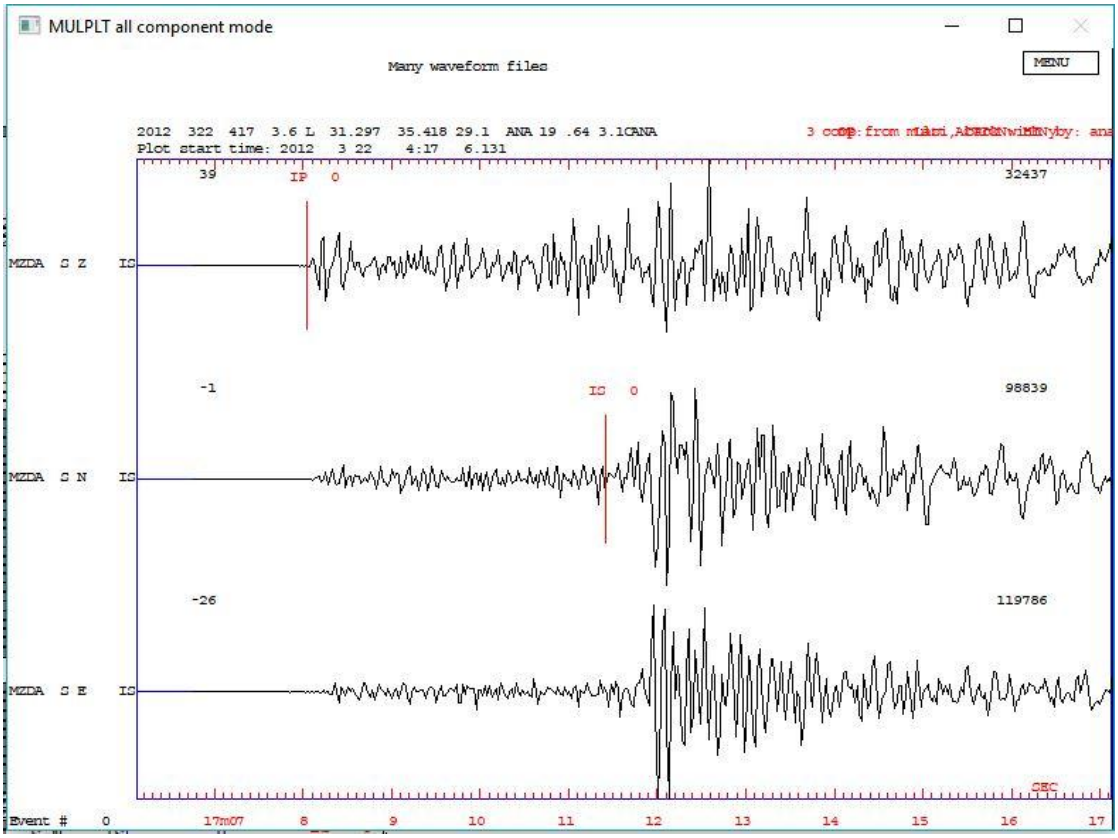
MULPLT all component mode
Many waveform files
MENU
2012 322 417 3.6 L 31.297 35.418 29.1 ANA 19 .64 3.1CANA
Plot start time: 2012 3 22 4:17 6.131
MZDA S Z
MZDA S N
MZDA S E
IP
IS
SEC
Event # 0
17m07
8
9
10
11
12
13
14
15
16
17

PRNI

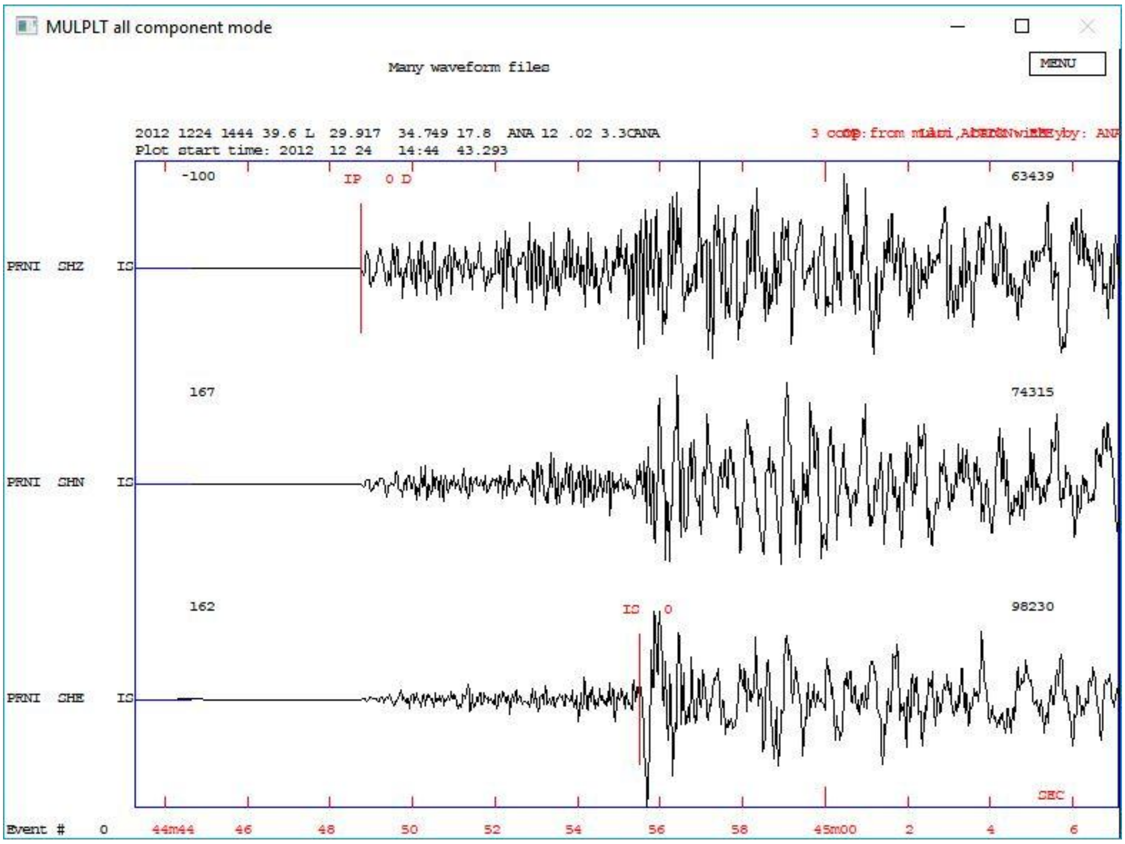
MULPLT all component mode
Many waveform files
MENU
2012 1224 1444 39.6 L 29.917 34.749 17.8 ANA 12 .02 3.3CANA
Plot start time: 2012 12 24 14:44 43.293
PRNI SHZ
PRNI SHN
PRNI SHE
Event # 0

SLTI

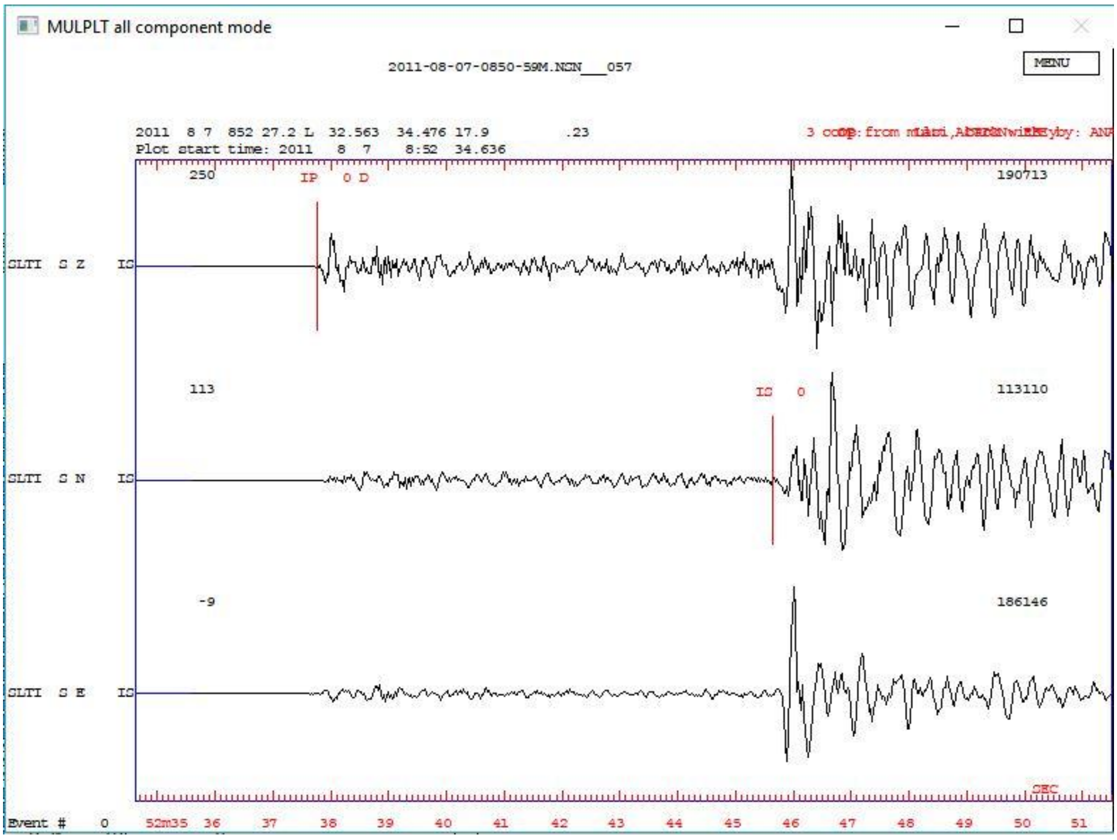
MULPLT all component mode
2011-08-07-0850-59M.NSN___057
MENU
2011 8 7 852 27.2 L 32.563 34.476 17.9 .23
Plot start time: 2011 8 7 8:52 34.636
SLTI S Z
SLTI S N
SLTI S E
Event # 0

UJAP

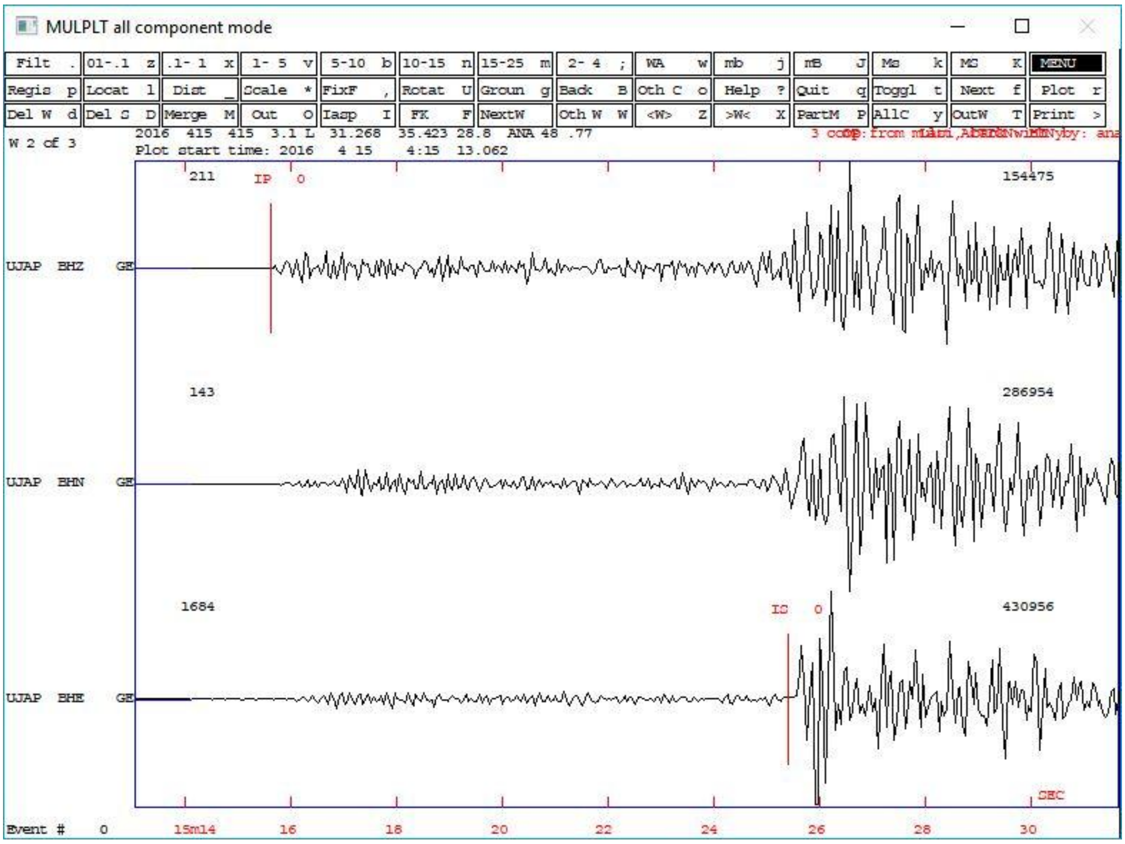

YTIR

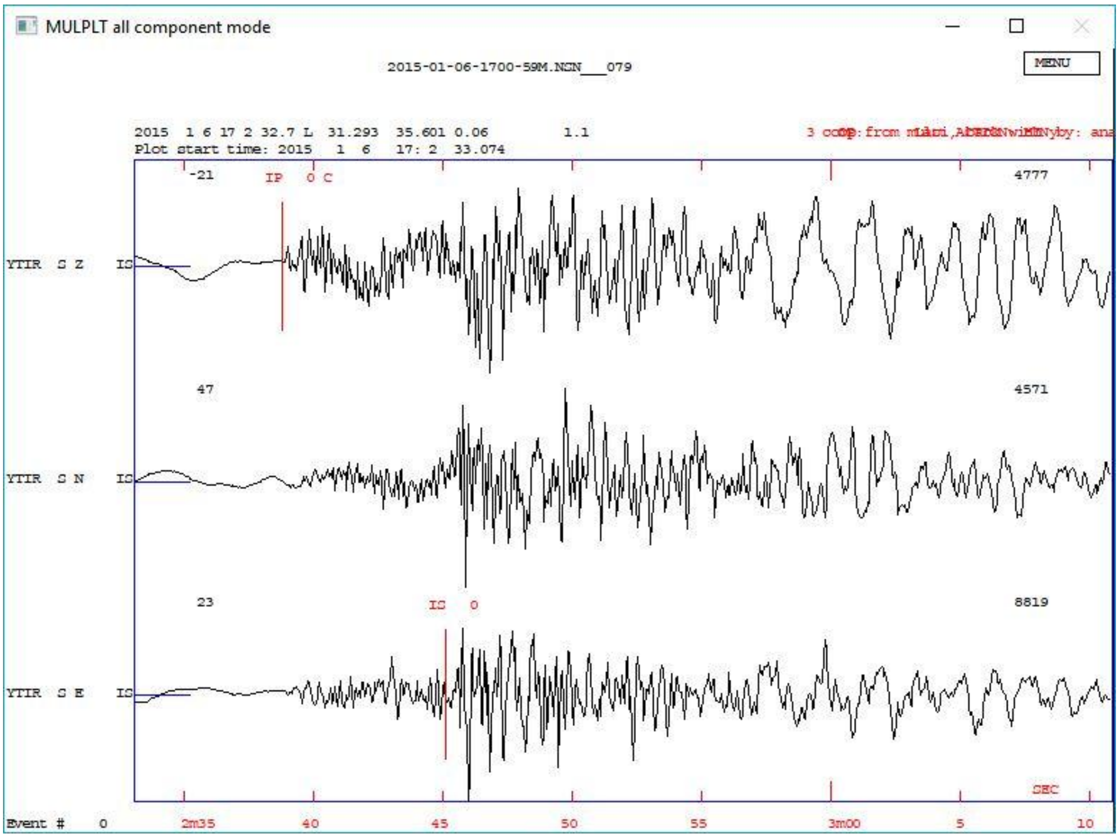

ZFRI

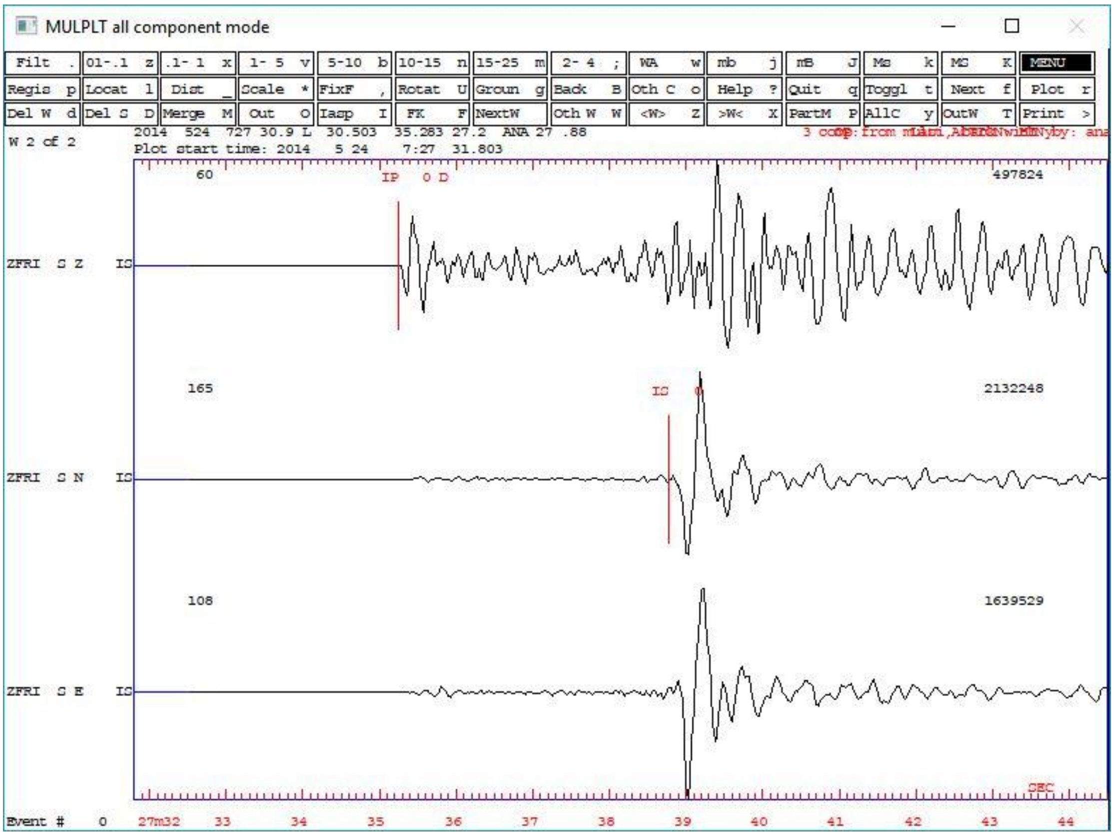
MULPLT all component mode
W 2 of 2
2014 524 727 30.9 L 30.503 35.283 27.2 ANA 27 .88
Plot start time: 2014 5 24 7:27 31.803
ZFRI S Z IS
60
IP 0 D
497824
ZFRI S N IS
165
IS
2132248
ZFRI S E IS
108
1639529
SEC
Event # 0 27m32 33 34 35 36 37 38 39 40 41 42 43 44

APPENDIX 3

LIST OF WADATI RESULT

Num. of Events	Wadati calculated origin time						Num. of Stations	VPS Ratio	RMS	CORR.
	Year	M.	D.	H.	Min.	Sec.				
1	2010	3	9	0	50	52.2	5	1.8	0.57	0.998
2	2010	3	12	14	48	42.8	5	1.57	0.52	0.997
3	2010	5	28	19	21	10.4	5	1.85	1.64	0.99
4	2010	10	19	16	47	58.6	13	1.76	0.42	0.999
5	2010	11	14	18	48	14	11	1.85	0.79	0.998
6	2010	11	16	2	2	2.8	15	1.88	1.43	0.995
7	2010	11	25	10	17	38	11	1.84	0.86	0.998
8	2010	12	1	5	8	49.2	16	1.73	0.88	0.993
9	2010	12	4	19	19	37.9	5	1.68	1.98	0.965
10	2011	1	1	16	31	1.2	5	1.65	0.47	0.987
11	2011	1	20	21	38	50.3	15	1.82	1.83	0.988
12	2011	5	29	19	17	30.8	6	1.74	1.55	0.966
13	2011	7	5	8	1	1.5	6	2.04	0.68	0.981
14	2011	7	15	8	8	58	5	1.78	0.77	0.963
15	2011	7	26	10	59	43.8	5	1.89	1.88	0.944
16	2011	8	7	8	2	26.4	16	1.72	0.64	0.995
17	2012	1	19	13	28	5.9	6	1.81	1	0.985
18	2012	2	4	18	0	17.2	6	1.72	0.26	0.999
19	2012	2	9	11	11	56.8	18	1.76	0.78	0.998
20	2012	2	13	14	34	58.7	6	1.83	0.48	0.995
21	2012	2	15	11	53	57	6	1.54	0.28	0.995
22	2012	3	7	8	7	56.2	18	1.9	1.61	0.992
23	2012	3	7	14	6	11.9	17	1.75	0.78	0.998
24	2012	3	7	17	31	18.7	6	1.71	0.7	0.996
25	2012	3	7	19	3	33.7	6	1.64	0.89	0.99
26	2012	3	8	1	5	52.1	16	1.72	1.03	0.995
27	2012	3	22	4	7	2.8	32	1.77	0.86	0.997
28	2012	3	24	12	16	14.5	5	1.44	0.88	0.976
29	2012	5	9	12	14	45.3	5	1.81	0.46	0.987
30	2012	6	20	8	7	53.8	5	1.75	0.7	0.975
31	2012	6	28	14	2	2.1	6	1.63	0.53	0.993
32	2012	7	8	8	9	43.7	9	1.66	1	0.966
33	2012	7	10	17	35	4.6	46	1.97	1.8	0.991
34	2012	7	14	5	7	34.5	12	1.73	1.54	0.99
35	2012	8	11	4	0	47	31	1.74	1.06	0.995
36	2012	8	13	8	8	46.8	7	1.72	0.57	0.993
37	2012	8	14	17	50	48.7	8	1.77	0.66	0.995
38	2012	8	15	15	39	19.1	45	1.75	1.4	0.99
39	2012	8	16	22	36	2.5	11	1.71	0.49	0.998

Num. of Events	Wadati calculated origin time						Num. of Stations	VPS Ratio	RMS	CORR.
	Year	M.	D.	H.	Min.	Sec.				
40	2012	8	21	3	1	13.8	6	2.03	0.78	0.997
41	2012	8	25	20	22	6.4	13	1.73	1.22	0.993
42	2012	8	28	16	30	42.1	11	1.83	0.94	0.996
43	2012	9	10	8	4	37.3	9	1.74	0.88	0.984
44	2012	9	12	12	58	46.9	8	1.72	0.72	0.998
45	2012	9	15	9	0	39.3	5	1.79	0.49	0.997
46	2012	10	8	19	14	38.2	5	1.72	0.31	1
47	2012	10	15	0	7	23.3	10	1.93	1.96	0.983
48	2012	10	27	9	1	15.8	9	1.55	1.41	0.966
49	2012	10	30	0	44	52.9	6	1.68	0.28	0.999
50	2012	11	2	10	13	35	5	1.91	0.61	0.999
51	2012	11	2	10	15	47.4	5	1.64	0.13	0.998
52	2012	11	3	19	57	18.6	44	1.92	1.28	0.993
53	2012	11	18	3	4	5.3	18	1.79	1.05	0.996
54	2012	11	18	9	9	51	14	1.72	0.72	0.989
55	2012	12	9	10	15	5.3	8	1.77	0.66	0.987
56	2012	12	17	18	54	21.3	9	1.79	0.56	0.996
57	2012	12	24	14	44	40.7	9	1.81	1.03	0.997
58	2013	1	17	11	59	42.4	5	1.73	0.15	0.999
59	2013	1	18	11	19	37.5	8	1.85	0.17	1
60	2013	1	19	11	14	2.2	7	1.69	0.18	0.999
61	2013	1	20	10	14	47.3	7	1.75	0.19	0.999
62	2013	1	20	12	20	0.2	6	1.74	0.78	0.979
63	2013	1	22	11	48	38.8	5	1.73	0.3	0.996
64	2013	1	24	12	17	38.6	7	1.71	0.18	0.998
65	2013	2	6	10	30	54.7	8	1.63	0.4	0.996
66	2013	2	7	9	5	7.4	7	1.72	0.28	0.996
67	2013	2	15	17	42	20.3	7	1.77	0.38	0.999
68	2013	2	16	23	37	46.3	7	1.69	0.7	0.996
69	2013	2	19	9	7	45	5	1.68	0.2	0.997
70	2013	2	28	9	3	43.9	6	1.78	0.5	0.994
71	2013	3	8	11	20	28.5	9	1.71	0.54	0.993
72	2013	3	11	10	41	33.3	5	1.69	0.22	0.998
73	2013	3	19	8	9	14	5	2.06	0.84	0.995
74	2013	5	12	5	7	44.7	5	1.62	0.57	0.996
75	2013	5	17	11	55	51.9	7	1.91	0.87	0.978
76	2013	5	22	12	45	49.2	6	1.77	0.21	0.998
77	2013	6	1	8	3	45.7	11	1.75	0.59	0.991
78	2013	6	5	15	21	29.3	6	1.7	0.52	0.968
79	2013	6	11	21	22	15.5	47	1.79	0.45	0.998
80	2013	6	15	9	1	46.8	6	1.74	0.81	0.995
81	2013	6	26	11	57	1	5	1.62	0.76	0.997
82	2013	6	29	10	52	43.9	5	1.71	0.21	0.999

Num. of Events	Wadati calculated origin time						Num. of Stations	VPS Ratio	RMS	CORR.
	Year	M.	D.	H.	Min.	Sec.				
83	2013	6	29	11	21	23.7	5	1.84	0.11	0.999
84	2013	7	2	13	22	9.8	6	1.59	0.68	0.981
85	2013	7	12	16	53	4.4	8	1.84	1.1	0.979
86	2013	7	16	11	30	59.2	7	1.74	0.57	0.994
87	2013	7	18	9	4	33.5	10	1.77	0.7	0.995
88	2013	7	19	2	0	9.2	8	1.79	0.79	0.996
89	2013	7	26	13	46	35.9	10	1.83	0.39	0.999
90	2013	7	27	10	32	43	8	1.74	0.74	0.981
91	2013	7	28	14	39	9.9	9	1.64	0.38	0.996
92	2013	8	6	20	10	45.3	8	1.74	0.68	0.997
93	2013	8	10	14	36	17.3	6	1.91	1.4	0.986
94	2013	8	11	11	15	41.6	5	1.74	0.57	0.998
95	2013	8	15	8	1	46.7	10	1.6	0.74	0.984
96	2013	9	1	11	30	32.7	6	1.78	0.99	0.984
97	2013	9	4	9	1	4.4	6	1.69	0.14	0.998
98	2013	9	8	16	23	26.8	8	1.74	0.46	0.993
99	2013	9	9	14	29	19.6	6	1.64	0.18	0.999
100	2013	9	11	10	39	46.7	6	1.74	0.36	0.997
101	2013	9	12	1	0	5.4	63	1.9	1.01	0.991
102	2013	9	25	22	46	14.8	6	1.72	0.41	0.997
103	2013	9	27	10	35	3.5	5	1.64	0.14	0.998
104	2013	10	2	14	10	10.8	11	1.74	0.74	0.99
105	2013	10	5	11	40	40.9	9	1.77	0.86	0.988
106	2013	10	6	10	54	52.6	9	1.73	0.41	0.992
107	2013	10	10	10	17	5	6	1.64	0.66	0.969
108	2013	10	17	10	53	13.1	7	1.75	0.14	0.998
109	2013	10	17	18	17	52.5	58	1.75	1.07	0.995
110	2013	10	18	23	30	30.6	12	1.79	0.62	0.998
111	2013	10	20	5	9	39.8	5	1.78	0.37	0.999
112	2013	10	20	8	0	3	11	1.73	0.52	0.999
113	2013	10	20	12	54	5.3	59	1.75	0.87	0.997
114	2013	10	22	5	0	49.8	10	1.75	1.06	0.994
115	2013	10	22	5	0	50.5	21	1.77	1.02	0.996
116	2013	10	23	12	33	53.8	31	1.81	1.88	0.976
117	2013	10	30	9	0	42.3	5	1.7	1.46	0.83
118	2013	11	1	10	38	34.6	8	1.73	0.66	0.995
119	2013	11	1	15	27	20.3	10	1.64	1.47	0.986
120	2013	11	4	11	20	13.5	10	1.73	0.5	0.985
121	2013	11	4	12	27	51.2	5	1.49	0.14	0.997
122	2013	11	5	14	28	5	7	1.75	0.63	0.994
123	2013	11	12	11	35	2.8	9	1.71	0.44	0.985
124	2013	11	12	14	20	1.7	13	1.8	0.53	0.996
125	2013	11	16	14	28	53.3	6	1.76	0.19	0.999

Num. of Events	Wadati calculated origin time						Num. of Stations	VPS Ratio	RMS	CORR.
	Year	M.	D.	H.	Min.	Sec.				
126	2013	11	18	11	5	1.4	9	1.73	0.88	0.956
127	2013	11	19	9	52	53.6	8	1.68	0.57	0.993
128	2013	11	19	10	3	35.5	5	1.85	0.81	0.935
129	2013	11	20	11	37	14.2	8	1.79	0.3	0.996
130	2013	11	25	7	6	53.9	8	1.69	0.44	0.996
131	2013	11	30	10	16	7.8	9	1.72	0.57	0.963
132	2013	12	2	10	34	4.1	6	1.74	0.85	0.956
133	2013	12	3	11	31	55.5	7	1.77	0.96	0.921
134	2013	12	4	14	48	55.5	7	1.7	0.77	0.976
135	2013	12	6	9	5	38.7	7	1.64	0.39	0.992
136	2013	12	7	11	22	45.2	60	1.75	0.85	0.991
137	2013	12	12	21	2	23.8	55	1.78	0.74	0.993
138	2013	12	15	12	15	57.9	9	1.86	1.06	0.949
139	2013	12	21	14	12	44.5	7	1.84	1.19	0.962
140	2013	12	22	12	20	17	5	1.71	0.74	0.968
141	2013	12	24	13	52	45	10	1.58	0.98	0.93
142	2013	12	24	14	44	13.6	8	1.72	0.72	0.978
143	2013	12	30	11	46	29.2	8	1.56	0.67	0.982
144	2013	12	31	14	55	32.8	11	1.62	0.86	0.987
145	2014	1	13	13	1	47.1	23	1.9	1.76	0.991
146	2014	1	20	12	45	48.4	8	1.76	0.7	0.982
147	2014	1	24	12	30	43.2	13	1.56	0.94	0.98
148	2014	2	24	0		14.6	24	1.79	1.61	0.99
149	2014	2	28	19	24	1	93	1.75	0.6	0.998
150	2014	5	24	7	7	30.4	41	1.78	1.1	0.996
151	2014	6	7	12	52	4.3	26	1.7	1.42	0.989
152	2014	6	14	7	8	20.6	16	1.74	0.53	0.998
153	2014	6	30	9	8	6.7	92	1.84	1.25	0.993
154	2014	7	5	22	25	11.6	29	1.62	0.8	0.997
155	2014	7	27	17	3	46.1	24	1.58	0.7	0.991
156	2014	8	7	2	3	42.7	29	1.81	1.57	0.991
157	2014	9	1	20	50	16.1	33	2.06	1.67	0.993
158	2014	9	1	20	50	16	15	2.03	1.69	0.981
159	2014	9	20	18	43	10.1	21	1.77	1.07	0.927
160	2014	10	25	10	43	23.1	15	1.59	1.07	0.991
161	2014	12	28	16	28	57.1	34	1.67	1.45	0.99
162	2015	1	6	17	2	30.5	20	1.79	0.98	0.986
163	2015	6	29	7	2	29.8	8	1.59	0.64	0.995
164	2015	7	8	2	5	39.3	7	2.14	0.8	0.998
165	2015	7	30	2	9	5.7	83	1.79	0.95	0.993
166	2015	8	8	2	3	13	19	1.87	1.1	0.993
167	2015	8	15	7	9	50.7	36	1.83	1.01	0.989
168	2015	8	16	5	4	11	14	1.76	1.29	0.984

Num. of Events	Wadati calculated origin time						Num. of Stations	VPS Ratio	RMS	CORR.
	Year	M.	D.	H.	Min.	Sec.				
169	2015	9	3	3	6	28.2	14	2.08	1.16	0.996
170	2015	10	1	18	33	48.4	8	1.72	0.69	0.994
171	2015	10	23	20	29	6.3	19	1.71	1.43	0.992
172	2015	11	2	6	7	23.9	24	1.82	0.57	0.977
173	2015	11	4	4	0	29.6	26	1.7	1	0.995
174	2015	11	6	17	50	28.6	22	1.92	1.94	0.99
175	2016	3	13	14	34	39.1	7	1.73	0.85	0.994
176	2016	4	5	3	8	54.4	6	1.69	0.66	0.987
177	2016	4	5	16	33	55.2	22	1.73	1.47	0.926
178	2016	4	15	4	5	3.5	95	1.78	0.87	0.995
179	2016	5	4	14	17	31.9	26	1.64	1.11	0.987
180	2016	5	12	22	44	48.1	30	1.76	1	0.996
181	2016	5	24	9	9	24.9	21	1.63	1	0.928
182	2016	5	29	12	45	37.2	25	1.77	1.03	0.979
183	2016	6	6	15	54	31.2	26	1.74	1.91	0.971
184	2016	6	25	14	42	29	30	1.71	1.13	0.993
185	2016	10	31	7	4	4	7	1.73	0.76	0.977
186	2016	11	19	23	37	26.5	13	1.83	1.2	0.992
187	2016	11	22	3	9	45.9	6	1.79	0.07	1
188	2016	12	1	14	53	35.6	46	1.73	0.55	0.998
189	2016	12	2	4	5	46.3	16	1.85	0.71	0.996
190	2016	12	16	17	12	42.3	27	1.74	0.64	0.999

APPENDIX 4

THE VELOCITY MODELS

Number	P velocity [km/s]	S velocity [km/s]	Depth [km]	Agency or source
1	3	1.7	0	IS
	4.36	2.41	1	
	5.51	3.1	3.6	
	6.23	3.6	10.8	
	7.95	4.45	32.44	
	8.15	4.58	132.44	
	****	****	****	****
2	3.5		0	JS
	6.05		1.5	
	6.32		10	
	6.50		18	
	6.65		20	
	7.38		28.5	
	8.10		33.5	
	****	****	****	****
3	3		0	Derived from (El-Isa Z. , Mechie, Prodehl, Makris, & Khim, 1987)
	4.75		1	
	6.20		5	
	6.30		10	
	6.50		18	
	6.65		20	
	8.00		34	
	****	****	****	****
	3		0	Initiative model
	4.76		1	
	6.25		5	
	6.29		10	
	6.50		18	
	6.58		20	
	7.65		34	

APPENDIX 5

RELOCATION OF EARTHQUAKES

Num.	Date			Time			Latitude (° N)	Longitude (° E)	Depth (Km)	GAP (°)	Dmin (Km)	Rms (sec)	ERH (Km)	ERZ (Km)
	Y.	M.	D.	H.	M.	S.								
1	10	2	16	12	27	34.17	30.0858	34.5243	5.1	211	49.7	8.601	69.72	1.41
2	10	2	21	9	43	53.23	30.8385	35.2285	4.6	186	90.8	0.979	99.99	99.99
3	10	3	2	11	42	1.95	31.2568	34.3740	35.3	185	149.5	5.196	4.11	96.55
4	10	3	9	0	50	49.31	33.4798	34.7248	42.2	148	60.7	0.51	10.4	44.9
5	10	3	12	12	52	29.92	29.9577	34.8332	15	178	21.5	0.6	11.1	19.3
6	10	3	12	14	49	0.88	34.0767	36.0623	0	260	191.3	4.043	79.1	98.03
7	10	3	15	23	36	40.15	33.4907	35.6120	0	224	33.4	3.331	64	44.71
8	10	3	20	18	45	27.78	33.0122	35.3653	0	121	33.9	1.51	16.8	10.4
9	10	3	23	8	25	13.94	32.5030	34.5222	50.8	154	84.9	0.55	18	49.8
10	10	3	24	10	58	40.37	34.1240	35.8257	7.1	349	190.8	3.709	99.99	99.99
11	10	3	27	0	5	16.16	33.8392	35.8698	15	252	160.9	2.12	70.99	99.9
12	10	4	3	3	33	0.34	31.2665	35.3282	0	216	139.2	1.813	67.8	45.13
13	10	5	10	9	42	59.28	31.1023	35.1287	0	174	73.2	0.91	20.8	10
14	10	5	15	11	9	46.51	35.0950	36.3052	15	285	219.3	5.211	76.29	99.91
15	10	5	20	11	2	45.24	31.0775	36.1643	9.3	313	158.2	0.29	10.3	9.5
16	10	5	28	19	21	5.81	33.6978	35.6380	0	234	56.1	3.482	9	51.11
17	10	5	30	3	6	2.68	29.9730	35.1202	13.3	200	10.7	0.31	7.6	3.7
18	10	6	10	6	19	51.97	34.1313	35.6095	16.7	347	188.6	14.369	99.99	99.99
19	10	6	10	8	34	20.96	30.7830	34.6577	64.4	135	28.4	0.93	29.1	25.8
20	10	8	22	22	25	4.71	33.3152	35.3985	34.5	232	264.1	1.555	68.63	69.15
21	10	9	16	10	8	3.67	34.8312	35.7775	21.7	350	267.5	6.359	99.99	99.99
22	10	10	19	16	47	50.67	30.3590	35.6747	0	223	305.8	14.581	72.5	83.91
23	10	10	21	10	53	5.28	29.6510	36.1987	24.3	285	120.1	1.19	28.4	22.4
24	10	10	22	9	10	53.95	30.9652	33.2253	91.6	231	112.2	5.421	89.74	54.81
25	10	10	25	10	3	8.55	30.8235	34.7055	59.9	139	30.9	1.1	35.3	35.3
26	10	10	27	15	48	59.86	33.0388	35.6512	0.6	245	70	5.679	99.99	99.99
27	10	11	8	9	2	38.04	33.4285	35.4162	5	228	109.9	11.198	81.63	94.48
28	10	11	10	12	34	52.53	29.7685	35.9395	33.9	273	96.2	4.922	60.12	71.01
29	10	11	14	12	45	18.29	30.3247	33.2053	0	248	183.4	4.482	34.8	98.12
30	10	11	14	18	48	10.97	33.1567	35.4323	0	123	21.5	1.41	13.1	8.5
31	10	11	16	2	31	59.45	33.2195	35.4287	0.1	142	21.7	2.29	25.2	14.6
32	10	11	25	10	17	34.86	33.1772	35.4270	0	129	21.7	1.18	11.8	7.4
33	10	11	29	9	35	18.43	30.6963	35.8870	11.6	231	109.7	0.24	11.2	7.4
34	10	12	1	5	8	50.49	31.5063	35.3475	10.6	152	10.5	0.92	13.9	6.2
35	10	12	4	5	15	17.42	33.1782	35.4222	0	200	22.1	2.15	26.8	13.2
36	10	12	4	19	19	40.54	33.2933	35.3480	1	220	95.1	3.521	98.5	42.21
37	10	12	4	21	36	37.01	28.8563	34.7440	0	337	92.4	3.753	79.8	99.72
38	10	12	15	10	29	43.26	30.1723	33.1607	15	254	181.5	5.711	77.59	99.91
39	10	12	17	9	27	50.42	30.9108	34.2480	9.4	239	123	0.73	28.3	25

Num.	Date			Time			Latitude (° N)	Longitude (° E)	Depth (Km)	GAP (°)	Dmin (Km)	Rms (sec)	ERH (Km)	ERZ (Km)
	Y.	M.	D.	H.	M.	S.								
40	10	12	20	21	31	14.45	36.2953	38.2228	0	311	499.4	6.919	99.94	32.39
41	10	12	22	12	19	39.14	29.9170	36.2553	0	316	118.3	0.52	36.6	15
42	10	12	25	12	51	25.83	29.7365	36.3203	12.9	283	128.3	0.99	40.9	51.4
43	10	12	25	21	15	34.95	34.1203	35.2132	4.6	235	187.6	3.412	10.9	88.01
44	10	12	31	12	21	31.73	29.6320	36.3600	19	288	135.5	0.97	54	21.4
45	11	1	1	16	31	7.12	32.7072	35.6547	8.4	231	37	0.56	12.9	8.6
46	11	1	3	11	6	44.16	30.9848	34.9765	11.1	162	56	6.411	8.81	79.7
47	11	1	3	19	52	4.33	34.2453	35.7012	32.2	349	202.1	4.629	99.99	99.99
48	11	1	13	0	31	6.73	35.8255	36.8892	0	302	342.6	3.129	70.63	10.87
49	11	1	20	18	25	24.35	33.3870	35.7943	32.8	345	305	1.919	99.99	99.99
50	11	1	20	21	38	46.73	33.2270	35.4022	0	143	24.3	1.53	14.6	7.4
51	11	1	21	14	49	53.17	28.8483	31.1795	0	306	385.6	10.559	99.95	48.39
52	11	1	31	11	31	1.92	33.4573	34.6727	34.2	211	207.8	1.601	31.1	79.61
53	11	2	8	11	26	32.72	30.3365	38.3768	15	300	323.3	38.109	99.99	99.99
54	11	2	10	12	23	58.08	30.7500	34.8010	15	180	82.3	17.389	99.99	21.19
55	11	2	11	12	28	55.82	30.6610	33.7253	44.5	223	143.9	1.062	43.49	99.92
56	11	2	16	8	38	40.45	33.3018	33.8808	35.5	187	221.3	12.149	99.93	96.49
57	11	2	22	9	4	48.4	31.1308	35.3552	21.7	299	94.8	0.66	17.7	14
58	11	2	23	8	45	48.63	31.5383	35.4982	46.6	222	126.2	2.813	15.99	99.93
59	11	2	25	14	6	21.63	30.1883	37.0675	35.2	287	196.4	4.323	89.99	99.93
60	11	2	27	14	55	58.96	29.9097	36.2913	0	317	121.9	0.5	35.5	14.5
61	11	3	1	16	43	28.57	31.1828	34.1722	1	203	37.4	11.489	99.94	34.79
62	11	3	6	13	45	24.8	29.9507	34.9217	17.2	171	14.6	10.399	99.99	99.99
63	11	4	1	11	12	24.56	31.5318	34.9205	0	320	0.2	27.368	5.5	69.85
64	11	4	4	8	28	32.81	30.9522	35.1347	0.3	279	70.7	0.566	6.15	29.44
65	11	4	11	8	17	3.9	30.9263	35.4385	17.6	235	83.2	0.19	10	7
66	11	5	5	8	15	37.53	30.7818	35.9808	0	269	122.7	1.13	79.4	26.3
67	11	5	22	17	34	17.46	30.9083	34.3957	0	248	0.3	38.279	99.91	40.89
68	11	5	28	22	17	53.89	33.7512	35.4640	0	242	251.5	3.894	6.1	97.63
69	11	5	29	19	17	31.77	33.1697	35.8233	0	238	200.7	3.331	60.3	39.41
70	11	6	9	8	10	43.91	31.7975	34.8427	145.7	150	30.5	3.091	32.81	4.91
71	11	6	15	9	50	33.69	33.3853	37.7960	0	280	339.7	4.733	82.91	21.83
72	11	6	24	23	6	26.55	35.1860	38.0872	0	299	501.2	21.749	99.99	99.99
73	11	6	26	23	8	19.23	34.9193	30.6435	84.8	299	547.7	18.709	99.99	99.99
74	11	7	5	8	10	58.05	30.8867	35.0040	0.1	129	58.1	0.67	6	5
75	11	7	15	8	48	57.21	30.8578	35.0047	0.1	130	58.3	0.5	4.6	3.9
76	11	7	21	9	25	15.62	31.3305	35.2960	68	156	26.3	0.53	10.7	12.2
77	11	7	21	10	30	21.66	29.8885	36.2615	0	282	119.3	0.63	41.4	17.6
78	11	7	21	14	47	25.01	30.9765	34.8833	71.1	111	47.1	0.55	11.1	18.2
79	11	7	24	10	31	42.56	30.6393	34.4520	18.9	260	87.4	0.03	5.3	8.7
80	11	7	25	9	55	51.5	29.8885	36.4412	0	289	136.5	0.78	51.2	19.8
81	11	7	26	10	59	41.19	31.1190	35.1217	2.9	119	47.2	1.38	12	22.8
82	11	7	26	11	6	18.41	30.8865	36.3640	55.2	284	88.6	1.03	29.9	56.1

Num.	Date			Time			Latitude (° N)	Longitude (° E)	Depth (Km)	GAP (°)	Dmin (Km)	Rms (sec)	ERH (Km)	ERZ (Km)
	Y.	M.	D.	H.	M.	S.								
83	11	7	27	15	11	47.96	30.8613	34.9680	27.7	179	54.8	0.57	8.7	9.3
84	11	7	28	2	18	5.95	33.7792	36.6205	182.7	346	296	0.77	80.4	92.2
85	11	7	28	10	40	22.99	31.5618	36.0047	17.3	321	50.5	2.35	65.4	28.4
86	11	7	28	10	44	29.72	31.3000	35.5698	0	221	0	35.337	37.83	35.33
87	11	7	29	10	28	11.34	29.8403	36.4033	4.8	289	133.7	0.35	20.5	15.3
88	11	7	29	10	55	2.05	29.9030	37.2713	0	310	288.5	14.669	99.99	68.79
89	11	7	31	11	9	41.43	30.7330	36.1547	8.4	266	84.1	0.41	14.7	10.2
90	11	7	31	14	55	38.81	31.1172	34.7653	34.7	165	79.3	7.735	20.39	99.95
91	11	8	7	8	52	25.08	32.5525	34.4120	31.3	159	54.4	1.24	10.8	9.4
92	11	8	13	11	39	16.54	31.0948	32.4605	15	248	286.8	7.333	5.04	63.72
93	11	8	18	11	19	8.87	29.7963	36.6763	0	294	167.5	19.989	99.99	99.99
94	11	8	20	11	46	39.82	30.4855	34.2225	0	205	114.5	0.78	17.7	12.1
95	11	8	30	22	58	41.16	34.9180	35.9910	15	270	243.1	5.509	99.99	99.99
96	11	9	2	11	50	50.28	29.2423	35.4977	1	310	71.1	60.099	99.99	99.99
97	11	9	17	12	19	7.92	31.1533	34.2898	38	185	123.1	17.687	86.69	99.97
98	11	9	21	21	56	6.42	33.5523	35.5797	34.6	233	249.7	0.51	56.29	99.9
99	11	9	23	11	17	42.21	30.9468	32.5035	34.6	249	274.7	5.351	89.32	69.01
100	11	9	25	10	49	46.93	29.8872	36.0655	15	274	110.4	3.773	4.99	99.92
101	11	9	28	7	45	11.02	31.9003	33.4317	34.8	203	213.6	5.271	45.42	98.31
102	11	10	8	11	24	44.76	30.9467	33.0023	35.4	237	234.9	4.371	25.11	93.01
103	11	10	13	11	57	50.55	30.5365	34.0610	0	214	128.8	0.14	4.4	3
104	11	10	17	13	30	26.75	35.5083	36.4747	15	292	292.5	6.679	99.99	99.99
105	11	10	21	12	43	44.36	30.6573	31.1537	15	277	381.8	17.249	99.99	99.99
106	11	11	1	10	58	6.09	31.4010	34.7997	36.7	166	74.1	0.821	13.89	99.91
107	11	11	3	11	8	20.41	31.0285	32.2053	15	254	303.9	13.976	4.89	99.94
108	11	11	10	13	18	15.06	31.4593	32.5458	15	240	304.3	7.613	69.89	99.93
109	11	11	19	7	12	7.59	27.2590	33.2478	15	326	315	8.429	99.99	99.99
110	11	11	20	5	15	48.67	26.4812	33.5333	26.6	335	379.9	6.599	99.99	99.99
111	11	11	24	16	33	39.48	33.2233	36.8250	0	264	243.8	5.099	99.93	67.59
112	11	12	4	20	55	18.25	33.3308	35.5252	0	189	19.8	2.34	26.6	12.3
113	11	12	8	14	21	15.8	29.5772	35.5093	5.1	279	55	39.889	99.99	99.99
114	12	1	19	13	28	4.31	29.8827	36.2113	0	274	114.6	0.96	37.9	15.3
115	12	2	4	18	0	16.07	33.6013	34.2455	37	168	169.5	1.13	32.37	84.2
116	12	2	9	11	11	56.03	32.8663	35.5835	0.1	173	36.8	0.74	6.5	3.3
117	12	2	13	14	34	58.09	30.8817	35.0002	0.1	128	57.7	0.55	4.9	3.9
118	12	2	15	11	54	10.83	30.8478	35.0712	23.6	139	64.8	1.69	16.9	19.8
119	12	3	7	8	47	49.94	33.4533	35.4165	0	190	36.7	2.28	30.4	11.5
120	12	3	7	14	6	11.97	33.3317	35.4220	0	265	27	2.57	58.8	25.2
121	12	3	7	17	31	21.41	33.2767	35.4693	0	336	93.1	2.421	42.3	48.31
122	12	3	7	19	3	38.21	33.4365	35.3017	5	220	111.3	2.761	22.9	51.11
123	12	3	8	1	15	51.69	33.4085	35.3958	4.1	182	34.3	2.17	24	19.3
124	12	3	14	17	46	43.34	34.3110	35.8497	0	349	211.5	4.969	99.99	99.99
125	12	3	14	20	25	51.76	34.3037	35.8087	30.5	344	210	4.359	99.99	99.99

Num.	Date			Time			Latitude (° N)	Longitude (° E)	Depth (Km)	GAP (°)	Dmin (Km)	Rms (sec)	ERH (Km)	ERZ (Km)
	Y.	M.	D.	H.	M.	S.								
126	12	3	14	21	22	30.5	34.2370	35.7843	10.2	253	202.4	4.002	87.92	51.62
127	12	3	21	12	30	35.66	34.4357	36.5100	15	347	243.6	7.639	99.99	99.99
128	12	3	22	4	17	3.21	31.3033	35.3365	28.9	88	2.6	1.01	10.1	4.5
129	12	3	24	12	16	35.58	29.9475	36.1763	0	270	110.4	1.52	58.1	23.5
130	12	3	26	14	22	0.8	30.8572	34.9937	12.3	129	57.3	0.78	7.9	13
131	12	5	5	13	4	3.49	32.8757	35.8037	4.8	331	60.3	2.081	32.2	86.7
132	12	5	9	12	14	43.96	31.0615	36.2520	6.8	253	70.2	0.53	9.6	7.5
133	12	5	15	13	28	31.07	34.0073	35.7760	0	347	177.2	1.179	99.99	50.14
134	12	6	3	9	23	1.32	31.1452	35.0922	14.5	124	48.7	1.21	12.5	21.3
135	12	6	20	8	57	54.51	30.8715	35.8890	95.7	229	56.4	4.11	92.9	78.4
136	12	6	28	14	2	13.21	29.8867	36.0760	0	269	101.7	3.771	34.7	53.41
137	12	7	8	8	19	51.96	30.8862	34.9707	12	125	54.9	1.82	16.3	18.1
138	12	7	10	17	34	58.58	33.3848	35.3635	0	280	37.8	2.15	55.8	24.1
139	12	7	10	19	50	33.47	34.1763	35.4188	0	344	161.8	1.681	69.1	54.8
140	12	7	14	5	27	35.96	33.2678	35.4098	0	325	63.1	3.26	97.1	39.3
141	12	7	15	10	23	40.61	32.1693	35.7383	5.1	234	22.1	27.019	99.97	30.49
142	12	7	21	17	2	56.59	33.4872	35.3460	0	299	47.6	3.27	81.3	35.3
143	12	7	21	18	56	46.08	33.3682	35.4207	0	329	74	2.43	74.5	28.9
144	12	8	10	12	53	14.15	32.8085	35.4673	0	216	74.7	10.972	81.51	49.82
145	12	8	11	4	0	47.35	29.9498	35.0388	16.4	177	9.6	2.21	33.2	12.1
146	12	8	13	8	58	51.26	31.1092	35.0532	0.1	114	48.3	2.26	20.8	14.1
147	12	8	14	17	5	48.49	29.9590	35.0885	13.8	185	9.9	0.57	10.5	4.7
148	12	8	15	15	39	18.52	29.9557	35.1335	0.9	194	12.9	3.09	27.4	14.4
149	12	8	16	22	36	3.06	33.7528	34.2437	34.6	174	143.3	0.72	15.6	14
150	12	8	21	3	51	37.46	32.2815	35.3918	1	95	17.6	15.431	8.01	0.5
151	12	8	25	20	22	8.33	32.8747	35.1903	0	301	16	2.66	46.6	20.6
152	12	8	28	16	30	41.45	33.0753	35.4452	0	315	45.1	1.64	46.8	21.1
153	12	9	10	8	4	39.69	31.0702	35.1327	0	128	34.4	1	10.4	5.9
154	12	9	12	12	58	49.11	34.2417	35.7407	34.6	341	175.3	5.732	59.49	99.92
155	12	9	15	9	30	34.63	34.2722	35.6140	0	343	175.5	4.249	99.99	99.98
156	12	9	17	11	49	40.91	30.8897	35.4785	4.8	190	46.3	11.811	82.62	30.61
157	12	10	8	19	14	41.1	29.3468	34.8170	0	327	38.1	2.801	62.4	63.1
158	12	10	15	0	7	18.36	28.6898	34.7828	0	337	109.8	3.311	57.2	47.61
159	12	10	21	15	7	26.13	34.7595	35.3610	14.8	357	257.5	2.969	99.99	99.99
160	12	10	27	9	1	29.07	29.7738	36.2260	12	278	118.5	2.24	77.7	93.8
161	12	10	30	0	44	51.03	34.1787	35.6435	33.3	342	287.7	6.229	99.99	99.99
162	12	11	2	10	13	26.76	30.2185	33.5093	96.5	241	148.6	5.531	49.12	86.31
163	12	11	2	10	15	51.06	29.9648	36.2035	5	289	112.8	0.23	6.8	6.4
164	12	11	3	19	57	14.39	33.0507	34.8895	0	147	26.8	2.34	25.4	12.8
165	12	11	13	17	49	4.32	33.9012	36.5948	34.1	332	195.7	6.429	99.99	99.99
166	12	11	18	3	54	3.63	33.1582	35.4297	0	111	21.7	1.76	14.8	8.3
167	12	11	18	9	19	49.87	31.1727	35.6045	0	198	50.8	5.57	44.8	25.3
168	12	11	21	16	16	51.27	34.4317	35.1757	28.6	349	201.5	8.359	99.99	99.99

Num.	Date			Time			Latitude (° N)	Longitude (° E)	Depth (Km)	GAP (°)	Dmin (Km)	Rms (sec)	ERH (Km)	ERZ (Km)
	Y.	M.	D.	H.	M.	S.								
169	12	12	9	10	15	5.16	31.0817	35.0990	0	138	52.5	1.09	13	6.9
170	12	12	17	18	54	20.09	30.4075	35.2362	14.4	191	23.1	1.11	14.8	13.7
171	12	12	24	14	44	38.69	29.9123	34.7800	10.8	198	31.6	1.22	22.5	16.6
172	13	1	17	11	59	42.85	29.7167	36.4218	15.2	293	138.4	0.59	23.4	30.6
173	13	1	18	11	19	27.97	29.7238	34.5877	187.1	246	55.5	4.632	0	80.31
174	13	1	19	11	14	4.2	31.0412	36.2237	7.8	263	68.6	0.39	6.6	5.1
175	13	1	20	10	14	47.27	30.7160	36.0532	0.7	239	79.5	0.5	11	4.1
176	13	1	20	12	19	59.26	30.1093	33.5867	17.9	287	140.1	4.331	28.61	64.9
177	13	1	21	10	39	43.38	29.9510	36.1797	13.7	289	121.6	3.481	12.91	12.6
178	13	1	22	11	48	40.43	30.8675	36.1642	7.1	243	74.3	0.64	10.8	6.8
179	13	1	24	12	17	40.63	30.8695	36.1365	13.8	241	72.1	0.67	10.3	7.8
180	13	2	2	15	42	1.81	34.2218	35.5395	0	347	218.3	2.169	99.99	99.99
181	13	2	6	10	31	1.46	29.8692	36.2752	0	275	121	1.04	39.1	15.7
182	13	2	7	9	5	8.54	30.7337	36.0223	0	237	76.2	0.32	6.2	2.6
183	13	2	15	17	42	18.52	34.3578	35.6988	17.1	345	186.6	3.179	99.99	99.99
184	13	2	16	23	37	51.05	34.3022	35.4013	15	343	175.5	3.029	99.99	99.93
185	13	2	19	9	17	48.09	29.7110	36.3300	12.4	283	130	1.25	28.9	25.3
186	13	2	28	9	23	43.05	29.8485	36.1900	0	274	113.2	1.18	38.9	17
187	13	3	2	5	3	56.87	34.1905	35.9203	34.2	343	194.5	1.199	99.99	99.94
188	13	3	7	7	31	35.51	33.9072	35.8302	0	340	162.8	0.35	24.9	9.9
189	13	3	8	11	20	30.85	29.8467	36.3082	0	277	124.5	0.88	31.1	12.5
190	13	3	9	20	45	10.66	33.3080	35.4418	0	336	68.3	1.46	79	34
191	13	3	11	10	41	41.23	31.1460	35.0135	0.1	166	37.9	1.76	20.1	13.5
192	13	3	19	8	59	10.37	32.5112	35.8948	0	281	45	1.46	51.8	23.5
193	13	4	24	11	3	29.74	29.9133	36.1080	0	272	115.1	1.251	30.6	53.81
194	13	5	4	22	48	54.06	33.6753	35.8745	35.4	236	195.2	8.497	93.09	99.97
195	13	5	5	11	23	20.24	31.5978	35.6718	0	224	34.4	5.169	99.91	69.19
196	13	5	7	9	35	37.8	31.3328	35.5950	0	209	4.3	3.34	99.9	32
197	13	5	9	13	51	35.99	31.3857	35.5617	5.1	184	9.5	1.11	62.1	36.1
198	13	5	12	5	7	50.07	31.9245	36.1225	0	261	67.1	5.101	53.6	60.31
199	13	5	17	11	55	47.11	29.8922	36.1797	0	292	111.5	0.83	32.8	13.8
200	13	5	22	12	46	11.12	30.5983	35.4412	0	196	73.4	12.651	71.5	98.81
201	13	5	23	9	13	48.55	30.6885	35.7055	15	219	96.7	15.283	60.63	60.63
202	13	6	1	8	43	47.41	31.0567	35.4637	6.6	177	28.8	0.87	10.1	12.6
203	13	6	5	15	21	30.12	32.3192	36.2500	0	285	68.6	1.33	41.6	18.5
204	13	6	11	21	22	14.73	30.5533	35.2775	18	191	9.6	1.17	11.7	7.4
205	13	6	15	9	51	45.69	29.3047	34.2153	1.6	311	82	1.9	66.9	50.9
206	13	6	17	6	45	32.13	34.4553	35.4715	29.1	346	248.9	4.579	99.99	99.99
207	13	6	26	11	57	8.01	34.2253	35.6362	22.4	344	199.2	3.659	99.99	99.99
208	13	6	29	10	52	51.74	30.0473	36.1342	0	263	105.8	2.52	76.4	35.8
209	13	6	29	11	21	23.61	31.0867	36.0173	0	233	67.4	2.38	42.1	22
210	13	7	2	11	26	25.58	29.8068	36.2552	0	310	120.3	0.25	21.1	8.9
211	13	7	2	13	22	19.36	31.1137	35.4665	14.4	197	23.9	1.49	23.1	14.5

Num.	Date			Time			Latitude (° N)	Longitude (° E)	Depth (Km)	GAP (°)	Dmin (Km)	Rms (sec)	ERH (Km)	ERZ (Km)
	Y.	M.	D.	H.	M.	S.								
212	13	7	12	16	53	10.85	30.1065	35.0800	11.3	183	8.8	3.68	57	37.8
213	13	7	16	11	31	11.3	30.4892	35.9238	1	237	99	10.431	91.6	94.31
214	13	7	18	9	4	32.71	33.2623	35.5425	5.1	227	92.1	1.28	23.5	14.2
215	13	7	19	2	10	6.69	33.9603	35.7825	26.1	341	166	2.959	99.99	99.96
216	13	7	26	13	46	34.04	33.5955	35.6393	0	334	104.7	1.1	40.5	15.3
217	13	7	27	10	32	44.74	29.7887	36.2333	0	278	118.8	1.11	39.2	16.5
218	13	7	28	14	39	18.5	30.8690	34.8538	7.9	111	59.1	1.71	19	17.3
219	13	8	6	20	10	44.93	34.3067	35.7590	32.2	342	182.7	3.219	99.99	99.97
220	13	8	10	14	36	7.92	34.4140	35.7630	29.2	343	194.2	3.219	99.99	99.99
221	13	8	11	11	15	43.29	33.6283	35.7310	0	331	131.5	1.66	82.8	31.5
222	13	8	15	8	21	57.38	30.8288	34.9948	23.9	131	63.7	1.89	17.4	15.7
223	13	9	1	11	30	22.4	32.4403	35.4237	0	277	0.3	10.362	28.6	42.61
224	13	9	4	9	21	0.58	30.8082	36.5337	19.5	261	106.9	3.69	55.7	60.8
225	13	9	8	16	23	27.17	30.2437	35.8017	0	239	77.2	0.45	7.7	3.7
226	13	9	9	14	29	26.32	30.8788	34.9147	0	118	64	0.9	10.1	5.6
227	13	9	11	10	39	48.35	31.1818	35.4508	21.6	155	16.6	3.91	65.6	27
228	13	9	12	1	20	3.24	31.7568	35.5562	21.3	173	23.9	0.78	7.1	4.2
229	13	9	25	22	46	15.24	29.4985	34.7868	0	307	24.8	1.93	71	32.8
230	13	9	27	10	35	11.15	29.8870	36.2060	0	273	123.7	1.53	54	22.4
231	13	10	2	12	9	52.95	31.5835	34.7063	0	281	69.4	2.421	23.8	52.5
232	13	10	2	14	10	5.49	30.8755	34.7495	110.8	107	209.8	11.482	9.31	50.71
233	13	10	5	11	40	40.19	29.7962	36.2098	0	277	116.4	1.66	54.9	22
234	13	10	6	10	54	53.9	31.0508	36.2453	11.9	246	89.1	0.74	10.4	8.3
235	13	10	10	10	17	9.25	29.8180	36.3225	3.9	287	126.5	0.48	15.7	12.2
236	13	10	11	10	47	58.39	29.8805	36.4150	0	279	213.6	4.502	36.6	92.51
237	13	10	17	10	53	13.32	31.0713	36.2153	13.8	245	85.4	0.65	9.3	8
238	13	10	17	18	17	53.49	32.8630	35.5728	8.8	165	38.8	0.93	6.7	5.8
239	13	10	18	23	30	28.7	32.9012	35.6080	0.2	228	43.5	0.73	9.7	4.4
240	13	10	20	5	19	35.93	33.0810	35.4490	0	321	66.9	2.11	78	34.2
241	13	10	20	8	50	3.29	32.8718	35.6105	2	228	42.4	0.41	5	4.4
242	13	10	20	12	54	6.62	32.8768	35.5693	10.1	163	35.9	0.96	6.7	5.9
243	13	10	22	5	40	48.58	32.8930	35.6353	0.8	230	45.4	0.99	13.1	6
244	13	10	22	5	40	49.84	32.8462	35.5792	0	166	38.7	0.77	5.7	3
245	13	10	22	10	12	45.22	31.3232	36.5008	9.2	293	109.5	2.261	12.5	95.2
246	13	10	23	12	33	51.7	29.3922	34.8642	6.6	329	31.9	1.45	29.6	11.1
247	13	10	23	23	6	34.15	36.1080	36.2063	28.6	352	413.4	14.439	99.99	99.99
248	13	10	30	9	40	45.56	30.7038	33.7718	8.1	269	63.9	1.09	21.6	15.2
249	13	11	1	10	38	37.01	29.8625	36.1703	0.1	273	111.1	1.66	53.5	21.9
250	13	11	1	15	27	31.08	33.4700	35.5588	0.3	332	89	4.321	46.4	59.9
251	13	11	2	15	9	20.02	34.2205	35.5632	32.8	344	185.3	4.799	99.99	99.99
252	13	11	3	13	32	26.01	33.4500	35.3817	0	332	81.8	8.903	90.51	55.72
253	13	11	4	11	20	14.51	31.0350	36.2422	8.8	246	89.2	0.78	10.2	9
254	13	11	4	12	27	57.59	29.8052	36.7898	15	289	239.2	5.244	15.05	26.23

Num.	Date			Time			Latitude (° N)	Longitude (° E)	Depth (Km)	GAP (°)	Dmin (Km)	Rms (sec)	ERH (Km)	ERZ (Km)
	Y.	M.	D.	H.	M.	S.								
255	13	11	5	14	28	6.29	29.7792	36.2365	0	278	119.3	1.15	39.5	16.4
256	13	11	12	11	35	4.4	31.0642	36.2185	12	245	86	0.51	6.9	6
257	13	11	12	14	20	1.56	30.8845	35.0115	0.1	143	57.7	0.68	5.6	3.3
258	13	11	16	14	28	55.54	29.7850	36.2058	0	277	116.3	1.58	55.3	24.2
259	13	11	18	11	5	1.44	31.1000	36.2810	16.5	248	90.8	1.73	22.7	25.5
260	13	11	19	9	52	56.73	30.8700	34.9857	14.8	141	60.5	1	9.4	8.8
261	13	11	19	10	3	31.64	29.8680	36.2005	5.1	282	113.9	0.73	39.3	24.6
262	13	11	19	13	7	11.16	30.9773	35.9015	5	254	63.5	4.013	38.03	16.53
263	13	11	20	11	37	13.07	31.0420	36.2115	5.5	244	86.4	0.75	10.4	7.9
264	13	11	22	9	12	18.15	29.7182	36.3263	0	283	129.5	1.04	52.9	20.7
265	13	11	25	7	36	56.02	31.7233	35.0118	15.2	150	23.1	2.19	19.8	18.6
266	13	11	30	10	16	7.98	31.0623	36.2902	9.4	248	92.5	1.57	21	18.3
267	13	12	2	10	34	5.52	29.7467	36.2982	0	281	126	1.37	65.8	24.8
268	13	12	3	11	31	53.24	31.1778	36.2648	10.8	247	87.4	1.61	23.8	19.6
269	13	12	4	14	48	59.93	29.8463	36.2023	0	275	114.5	1.49	50.3	21.4
270	13	12	6	9	15	43.6	29.7820	36.3290	0	289	127.9	0.43	16.8	6.9
271	13	12	7	11	22	45.11	31.4223	35.0555	1.5	85	8.7	0.48	2.3	2.5
272	13	12	12	21	2	22.63	31.3472	35.1997	3.1	76	16.1	0.66	3.8	4.3
273	13	12	15	12	15	55.04	31.0622	36.2317	15.6	245	87.5	1.54	22.2	17.1
274	13	12	16	13	25	8.64	30.7897	33.4270	13.5	273	93.7	4.881	0.4	76.2
275	13	12	21	14	12	41.34	29.7908	36.3113	0	293	126	0.96	37.2	15.4
276	13	12	22	12	20	19.3	31.0807	36.1775	17.2	270	81.7	0.88	16	12.7
277	13	12	24	13	52	53.17	30.8413	36.0997	12.1	240	87.7	1.46	20.8	16.3
278	13	12	24	14	44	15.55	29.8230	36.1662	8.6	276	111.6	0.95	20	21.5
279	13	12	30	11	46	18.82	30.3650	33.3545	232.9	244	166.1	11.784	26.63	7.33
280	13	12	31	14	55	39.81	29.7528	36.2042	0	279	117	1.18	39.4	16
281	14	1	13	13	1	43.59	32.9620	35.5805	0.1	157	26.5	1.92	13.8	7.2
282	14	1	20	12	45	48.52	31.1215	35.1510	0	165	28.9	0.5	5.4	3
283	14	1	22	13	25	0.14	35.1547	35.8668	33.8	347	304.1	4.249	99.99	99.99
284	14	1	24	12	30	49.74	29.7418	34.5648	19.3	251	34.4	1.73	21.8	14.7
285	14	2	24	0	52	12.44	33.3527	35.4195	7.5	155	28.6	3.9	31.1	22.4
286	14	2	28	19	24	0.37	32.2262	35.5393	15	154	3.2	3.33	25.7	14.8
287	14	5	24	7	27	31.31	30.5222	34.9853	30.2	98	18.8	3.46	27.4	16.5
288	14	6	7	12	52	7.49	33.9085	35.7930	0	332	71.9	2.74	78.3	27.9
289	14	6	14	7	18	20.76	29.9150	35.0523	13.9	163	13.5	0.56	5.9	3.5
290	14	6	30	9	8	4.48	32.5000	35.5223	21.3	133	11.7	3.49	24	18.8
291	14	7	5	21	41	32.09	33.6883	35.5773	0	209	49.5	4.88	62.1	19.1
292	14	7	5	22	25	16.09	33.5347	35.6183	0	300	32.2	4.71	95.6	40.5
293	14	7	27	17	3	54.59	33.9648	35.9523	0	328	80.5	3.621	33	48.7
294	14	8	7	2	3	40.33	34.1805	35.6958	0	236	101.9	5.451	7.1	29
295	14	8	18	2	2	51.73	35.8398	36.5815	17.8	346	296.3	5.979	99.99	99.99
296	14	9	1	20	50	6.82	34.3242	36.0025	0	257	120.4	5.81	89.5	28.4
297	14	9	1	20	50	4.87	34.2377	36.4410	3.2	266	126.4	4.3	95.6	58.5

Num.	Date			Time			Latitude (° N)	Longitude (° E)	Depth (Km)	GAP (°)	Dmin (Km)	Rms (sec)	ERH (Km)	ERZ (Km)
	Y.	M.	D.	H.	M.	S.								
298	14	9	20	18	43	10.94	34.0553	36.0527	0	338	100.4	3.912	24.2	80.11
299	14	10	25	10	43	35.67	34.1358	36.9698	0	325	149.9	4.952	33.9	89.61
300	14	12	28	16	29	2.67	34.9992	36.4140	0	280	202.6	4.562	22.9	71.91
301	15	1	6	17	2	31.59	31.3078	35.5195	0	97	4.9	1.81	9.6	7.1
302	15	6	27	15	33	48.19	27.9935	34.5955	33.6	337	189	5.029	99.99	99.93
303	15	6	28	8	27	51.73	28.8878	34.7000	0	337	90.1	4.091	52.5	45.81
304	15	6	29	7	2	38.16	29.0622	34.7443	0	334	70.3	1.91	73.7	24.8
305	15	7	8	2	15	29.53	28.8603	34.5705	0	334	108.6	4.831	97.8	74.61
306	15	7	30	2	39	5.82	31.3972	35.4083	17.4	118	10.5	1.35	8.4	4.8
307	15	8	8	2	43	9.14	30.3602	33.8362	17.1	257	81	1.29	17.5	22.3
308	15	8	15	7	39	49.81	31.2943	35.3623	24.1	183	2.1	1.23	9.9	5
309	15	8	16	5	24	9.93	33.1593	36.9057	2.1	294	109.6	1.06	23	17.5
310	15	9	3	3	16	14.59	28.3705	34.6317	0	340	147.3	3.341	58.6	46.01
311	15	10	1	18	33	49.48	33.8368	36.1343	0	331	73.7	0.67	30.6	12.4
312	15	10	23	20	29	10.04	28.8928	34.7052	0	335	89.4	4.511	49.7	44.21
313	15	11	2	6	27	21.12	34.4715	35.8295	0	342	134.4	0.62	25	7.5
314	15	11	4	1	56	45.11	33.6365	35.5360	0	332	48.7	1.93	69.3	28.7
315	15	11	4	4	40	31.82	33.5517	35.5673	0	325	38.9	1.44	38	14.7
316	15	11	6	17	50	20.48	34.4453	36.1383	0	265	143.8	3.191	3.3	31
317	15	12	18	1	20	9.34	34.2185	35.6595	0	351	242.3	0.899	99.99	99.95
318	16	2	7	12	35	48.3	30.0375	35.1655	1.1	192	12.4	3.66	27.1	11.7
319	16	3	13	14	34	33.42	33.7142	35.7320	0	323	83.3	3.671	9.7	46.6
320	16	4	5	3	18	46.51	33.8377	35.9243	7	332	104.2	5.691	60.7	62.81
321	16	4	5	16	33	55.83	34.0450	35.7178	0	338	92.7	1.09	46	13.8
322	16	4	15	4	15	2.93	31.3093	35.1867	30.4	89	16.5	4.83	26.7	14.5
323	16	4	18	2	41	47.98	30.4837	34.4150	7.1	208	46.9	2.01	16.9	12.3
324	16	5	4	14	17	29.78	34.4625	35.2802	34.5	228	187.7	3.861	34.71	38.31
325	16	5	12	22	44	46.66	34.8905	33.8885	34.7	322	252.3	1.09	71.49	99.9
326	16	5	15	14	35	23.09	34.7222	35.8987	0	345	162.7	2.912	13.4	52.51
327	16	5	16	9	14	21.32	35.8195	38.1047	0	307	357.4	3.994	43.51	59.43
328	16	5	22	9	40	1.58	36.2413	37.0287	15	348	387.6	10.359	99.99	99.99
329	16	5	24	9	59	28.44	33.9922	35.7143	0	334	81	1.22	58.4	26.5
330	16	5	29	12	45	36.98	33.5643	35.4647	0	296	61.9	1.52	42.4	20.7
331	16	6	6	15	54	32.59	34.1313	35.8672	0	341	97.2	2.56	87.6	23.2
332	16	6	11	15	42	21.51	34.0838	35.8280	0	346	91.5	1.821	26.1	31.31
333	16	6	25	14	42	50.18	33.0532	35.7270	0	182	23.2	16.15	97	60.1
334	16	6	25	19	2	11.12	33.6882	35.8653	0	340	48.8	0.252	3.71	8.3
335	16	6	29	13	24	28.46	33.7930	35.5208	0	209	62.2	2.23	28.8	8.7
336	16	10	31	7	53	56.73	34.3453	35.9752	15.0*	342	156.5	4.111	54	0.01
337	16	11	19	23	37	23.21	33.3680	35.3855	5	156	31.2	1.38	11.8	12.3
338	16	11	22	3	9	39.41	34.3152	36.0258	15.0*	345	119.8	3.021	46.7	0.01
339	16	12	1	14	53	36.6	33.2815	35.4445	0	226	21.9	1.31	14.9	7.7
340	16	12	2	4	35	44.51	32.9520	35.6438	14.7	104	16	1.05	8.5	6.8

Num.	Date			Time			Latitude (° N)	Longitude (° E)	Depth (Km)	GAP (°)	Dmin (Km)	Rms (sec)	ERH (Km)	ERZ (Km)
	Y.	M.	D.	H.	M.	S.								
341	16	12	16	17	12	43.07	33.1955	35.4417	0	202	20.7	1.44	11.5	5.7

APPENDIX 6

ERROR PICKING

Date	Time (UTC)	Station Code	EMCS P arrival time		Our P arrival time		Diff. Time
			HR:MM	SECON	HR:MM	SECON	
2010-03-09	00:50:49.5	KSDI	00:51	5.3	00:51	5.37	0.07
		MMLI	00:51	10.4	00:51	10.79	0.39
		KZIT	00:51	30.8	00:51	30.77	-0.03
		HRFI	00:51	42.5	00:51	42.00	-0.5
		EIL	00:51	47.5	00:51	47.18	-0.32
2010-03-15	23:36:42.7	KSDI	23:36	47.1	23:36	47.04	-0.06
		MMLI	23:36	59.2	23:36	59.16	-0.04
2010-03-20	18:45:30.7	KSDI	18:45	35.8	18:45	35.75	-0.05
		MMLI	18:45	40	18:45	39.86	-0.04
		HRFI	18:46	16.1	18:46	16.47	0.37
2010-11-08	09:02:14.3	MMLI	09:02	41.2	09:02	41.38	0.18
2010-11-14	18:48:12.4	KSDI	18:48	16.8	18:48	16.83	0.03
		BLGI	18:48	21.3	18:48	21.15	-0.15
		OFRI	18:48	24.8	18:48	24.75	-0.05
		MMLI	18:48	25.5	18:48	25.54	0.04
		HMDT	18:48	28.8	18:48	28.87	0.07
		SLTI	18:48	30.3	18:48	30.30	0
		DSI	18:48	40.3	18:48	40.02	-0.28
		MZDA	18:48	44.6	18:48	44.66	0.06
		PRNI	18:48	58.7	18:48	58.29	-0.41
2010-11-16	02:32:01.5	KSDI	02:32	5.6	02:32	5.55	-0.05
		OFRI	02:32	13.6	02:32	13.62	0.02
		MMLI	02:32	14.3	02:32	14.22	-0.08
		SLTI	02:32	19.1	02:32	19.08	-0.02
		MZDA	02:32	33.3	02:32	33.33	0.03
		KZIT	02:32	41.5	02:32	41.47	-0.03
		ZFRI	02:32	43.9	02:32	43.99	0.09
		PRNI	02:32	47.1	02:32	46.94	-0.16
		KRMI	02:32	50.7	02:32	51.22	0.52
		MBRI	02:32	56.2	02:32	55.68	-0.52
		EIL	02:32	56.5	02:32	58.80	2.3
2010-11-25	10:17:36.0	KSDI	10:17	41	10:17	41.02	0.02
		HNTI	10:17	41.9	10:17	41.91	0.01
		BLGI	10:17	45.4	10:17	45.40	0
		OFRI	10:17	48.9	10:17	49.00	-0.01

		MMLI	10:17	49.6	10:17	49.66	0.06
		HMDT	10:17	53	10:17	53.04	0.04
		SLTI	10:17	54.4	10:17	54.52	0.12
		DSI	10:18	4	10:18	4.05	0.05
		MZDA	10:18	8.7	10:18	8.87	0.07
		PRNI	10:18	22.5	10:18	22.43	0.07
2010-12-01	05:08:49.0	SLTI	05:09	5.3	05:09	5.40	0.1
		PRNI	05:09	13	05:09	13.04	0.04
		BLGI	05:09	12.9	05:09	12.79	-0.11
		KRMI	05:09	17.2	05:09	17.41	0.21
		HRFI	05:09	17.5	05:09	17.30	-0.2
		KSDI	05:09	20.2	05:09	20.33	-0.13
		MBRI	05:09	20.8	05:09	20.87	0.07
2010-12-04	05:15:18.3	HNTI	05:15	23.9	05:15	23.58	-0.32
		MZDA	05:15	50.4	05:15	50.72	-0.32
		ZFRI	05:16	1.6	05:16	1.23	-0.37
		KRMI	05:16	8.2	05:16	9.19	0.99
		MBRI	05:16	12.1	05:16	12.19	0.09
2011-01-01	16:31:09.0	HRFI	16:31	51.7	16:31	51.69	-0.01
2011-01-20	38:50.0	BLGI	21:38	57.9	21:38	57.77	-0.13
		KZIT	21:39	30.4	21:39	29.30	-1.1
		ZFRI	21:39	32.3	21:39	32.33	0.03
		HRFI	21:39	39.1	21:39	38.93	-0.17
		MBRI	21:39	42.6	21:39	43.22	0.62
		EIL	21:39	44.1	21:39	47.44	3.34
2011-08-07	08:52:26.0	OFRI	08:52	35.5	08:52	35.58	0.08
		MBRI	08:53	9.2	08:53	9.19	-0.01
2011-12-04	20:55:21.0	KSDI	20:55	24.1	2055	24.16	0.06
		OFRI	20:55	35.5	2055	35.49	-0.01
		MMLI	20:55	35.2	2055	35.36	0.16
		HMDT	20:55	38.3	2055	38.18	-0.12
		SLTI	20:55	40.3	2055	40.44	0.14
		DSI	20:55	49.1	2055	49.00	-0.1
		AMAZ	20:55	51.8	2055	51.80	0
		MZDA	20:55	53.7	2055	53.69	-0.01
		KZIT	20:56	1.8	2056	1.97	-0.03
2012-02-09	11:11:56.0	MMLI	11:12	5.6	11:12	5.69	0.09
		HMDT	11:12	8.8	11:12	8.90	0.1
		DSI	11:12	20.3	11:12	20.30	0
		MZDA	11:12	25.2	11:12	25.19	-0.01

		PRNI	11:12	39.5	11:12	39.52	0.02
2014-05-24	07:27:29.8	ZFRI	07:27	35.2	07:27	35.2	0
		PRNI	07:27	37	07:27	37.50	0.5
		KRMI	07:27	42.5	07:27	42.52	0.02
		HRFI	07:27	40.6	07:27	40.55	-0.05
		KZIT	07:27	47	07:27	47.00	0
		MBRI	07:27	45	07:27	45.00	0
		AQBJ	07:27	45.7	07:27	45.77	0.07
		YTIR	07:27	46.7	07:27	46.69	-0.01
		EIL	07:27	46.5	07:27	46.52	0.02
		MDBI	07:27	45.2	07:27	45.52	0.32
		GHAJ	07:27	45.9	07:27	45.75	-0.15
		AMAZ	07:27	49.8	07:27	49.77	-0.03
		DRHJ	07:27	52.6	07:27	52.88	0.28
		UJAP	07:27	54.7	07:27	55.00	0.3
		SLTI	07:27	59.5	07:27	59.54	0.04
		MMLI	07:28	2.2	07:28	2.33	0.13
		OFRI	07:28	5	07:28	5.19	0.19
		BLGI	07:28	6.6	07:28	6.48	-0.12
		SHMJ	07:28	6.3	07:28	7.66	0.36
		HNTI	07:28	11.4	07:28	11.33	-0.07
		KSDI	07:28	13.2	07:28	12.93	-0.27
		GEM	07:28	12.9	07:28	12.94	0.04
		NATI	07:28	14	07:28	13.83	-0.17
2015-07-30	02:39:05.5	GHAJ	02:39	9.2	02:39	9.87	0.67
		DSI	02:39	10.6	02:39	10.80	0.2
		YTIR	02:39	12.6	02:39	12.69	0.09
		AMAZ	02:39	15.9	02:39	15.94	0.04
		HMDT	02:39	21.6	02:39	21.66	0.06
		ZFRI	02:39	22.1	02:39	22.16	0.06
		SLTI	02:39	22.6	02:39	22.61	0.01
		KZIT	02:39	25	02:39	25.25	0.25
		MMLI	02:39	24.5	02:39	24.37	-0.13
		PRNI	02:39	26.1	02:39	26.41	0.31
		OFRI	02:39	28.5	02:39	28.44	-0.06
		HRFI	02:39	30.4	02:39	30.19	-0.21
		MMA0B	02:39	33.4	02:39	33.54	0.14
2016-02-07	12:35:49.9	HRFI	12:35	54	12:35	53.94	-0.06
		MBRI	12:35	56.8	12:35	56.63	-0.17
		PRNI	12:35	57	12:35	57.11	0.11

		KRMI	12:35	57.5	12:35	57.47	-0.03
		EIL	12:35	57.9	12:35	57.97	0.07
		ZFRI	12:36	00	12:36	0.12	0.12
		KZIT	12:36	9.3	12:36	9.27	-0.03
		AMAZ	12:36	14.8	12:36	15.12	0.32
		DSI	12:36	15.8	12:36	15.62	-0.18
		HMDT	12:36	26	12:36	25.93	-0.07
2016-12-02	04:35:45.3	HNTI	04:35	53.6	04:35	53.55	-0.05
		MMLI	04:35	55.1	04:35	55.24	0.34
		AMAZ	04:36	12	04:36	12.12	0.12
		KZIT	04:36	22.2	04:36	22.47	0.27

جامعة النجاح الوطنية

كلية الدراسات العليا

تحديد السرعة النسبية للأمواج الأولية والثانوية من الزلازل المحلية على طول صدع البحر الميت خلال الفترة 2010 -2016

إعداد

أنس تيسير محمد عطاطري

إشراف

أ.د. جلال الدبيك

قدمت هذه الأطروحة استكمالاً لمتطلبات الحصول على درجة الماجستير في هندسة التخطيط الإقليمي والحضري، في كلية الدراسات العليا، في جامعة النجاح الوطنية، نابلس–فلسطين.

2018

تحديد السرعة النسبية للأمواج الأولية والثانوية من الزلازل المحلية على طول صدع البحر الميت خلال الفترة 2010 –2016

إعداد

أنس عطاطري

إشراف

أ.د. جلال الدبيك

الملخص

نظام صدع البحر الميت التحويلي من اهم التراكيب التكتونية في منطقة بلاد الشام وكذلك في الشرق الأوسط. تاريخيا، تسبب هذا النظام بزلازل مدمرة تسببت بخسائر بشرية ومالية. بدأ رصد النشاط الزلازل الخفيفة لهذا الصدع في ثمانينات القرن الماضي، حيث وضع محطات زلزالية مختلفة الحساسية على طول جناحي النظام الصدعي. هذه المحطات تعود الى عدد من المراصد المحلية والعالمية. تستخدم هذه المراصد معاملات مختلفة لتحديد المركز البؤري. من اهم هذه المعاملات النسبة بين تسارع الأمواج الأولية والثانوية (Vp/Vs ratio) ونماذج تسارع هذه الأمواج (1-D Velocity models)، والتي تؤثر بشكل مباشر على دقة تحديد البؤر الزلزالية. استخدم أكثر من 60 محطة لدراسة النشاط الزلزالي لهذا النظام الصدعي والتركيب المحيطة به خلال 2010–2016، وذلك باستخدام برنامج SEISAN. في حين هذه البيانات متوفرة في أرشيف الزلزال العالمي (GEOFON).

نسبة بين تسارع الأمواج الأولية والثانوية (Vp/Vs ratio) احدى العوامل التي تم التركيز عليها بهذه الدراسة باستخدام حوالي 190 زلزال والتي تمتلك على الأقل 5 قراءات واضحة لكل من الأمواج الأولية والثانوية. تراوحت قيمة هذه النسبة من 1.44 الى 2.14 بمعدل 1.75 ($\pm$ 0.08). طبق عدد من التحاليل الإحصائية للتأكد من دقة معدل هذه النسبة. معظم هذه الزلازل لها معامل ارتباط (correlation coefficient) $\leq$ 0.9.

تم اختبار ومقارنة عدد من نماذج تسارع الأمواج (1-D Velocity models) باستخدام عدد من معدلات قيم كل من بقايا وقت الوصول (RMS) والخطأ الافقي (ERH) والعمودي (ERZ) للمركز البؤري. هذه النماذج يتم استخدامها في كل من المراصد المحلية بالإضافة الى نموذج مرجعي بني على دراسة سيزمية (Seismic Refraction Method). من جهة أخرى تم تعديل النموذج المرجعي لتقليل الخطأ في تحديد موقع الزلازل. بلغ معدل كل من RMS و ERH 4.1 ثانية و45.59 كم على التوالي، التي تعتبر اقل القيم بين نماذج التسارع السابقة. في حين ERZ بلغ 42.26 كم. أظهرت الخريطة الزلزالية ان التراكيب التكتونية هي المسبب الرئيسي للزلازل في منطقة الدراسة. تتركز البؤر الزلزالية شمال منطقة الدراسة على طول الصدع التحويلي للبحر الميت والعمق البؤري لها ضحل جدا في الاغلب اقل من 10 كم. في حين البؤر الزلزالية تتوزع في جنوب منطقة الدراسة مع ملاحظة نشاط زلزالي معتبر على طول منطقة الصدع. أيضا، يزداد العمق البؤري في جنوب منطقة الدراسة ليصل الى حوالي اقل 40 كم.

تم تسليط الضوء على الخطأ في تحديد أوقات وصول الأمواج الأولية وتوزيع المحطات الزلزالية بالإضافة الى العوامل السابقة والتي تؤثر دقة الموقع البؤري. تمت مقارنة وقت وصول 120 قراءة للأمواج الأولية مع البيانات المنشورة لمركز الزلازل الارو-متوسطي (EMSC)، والذي يشمل بيانات المراصد المحلية. معظم فرق القراءات تراوح ما بين -0.7 الى 1 ثانية في حين تركزت الفروقات ما بين -0.2 الى 0.2 ثانية. كذلك توزيع المحطات حول المركز البؤري له دور مباشر في تقليل كل من الخطأ الافقي (ERH) والعمودي (ERZ) للمركز البؤري. حيث أن احتمالية كل من الخطأ الافقي (ERH) والعمودي (ERZ) للمركز البؤري تزداد بشكل كبير إذا وصلت فجوة الزاوية (The Azimuth Gap) الى 180° و160° على التوالي.